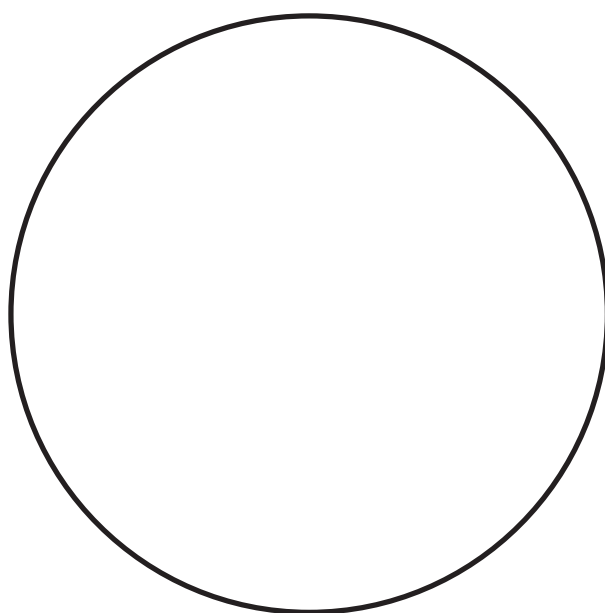


# IMPREGNATION AND SURFACE MODIFICATION OF POLYMERS IN LIQUID AND SUPERCRITICAL CARBON DIOXIDE

(COVERING INTERPENETRATING POLYMER NETWORKS)



DOCTORAL DISSERTATION  
MARTIN ALM

SUPERVISORS:  
PROFESSOR KJELD SCHAUMBURG  
DR. RER. NAT. MAIKE BENTER

19 JUNE 2007

DEPARTMENT OF LIFE  
SCIENCES AND CHEMISTRY  
ROSKILDE UNIVERSITY

NANO A/S  
PART OF THE NKT GROUP

© Martin Alm 2007

This work is typed with Computer Modern 11pt / 13.6pt  
Layout and typography by the author with assistance of L<sup>A</sup>T<sub>E</sub>X  
All figures are made by gnuplot, CorelDraw or METAPOST

## Abstract

Interpenetrating polymer networks (IPN) of silicone rubber and poly(2-hydroxyethyl methacrylate) (PHEMA) produced in supercritical carbon dioxide (scCO<sub>2</sub>) are studied. The purpose is to increase the hydrophilicity of silicone without losing transparency and make a suitable contact lens material. The compatibility between CO<sub>2</sub> and silicone is quantified by applying the Flory-Huggins interaction approach. The compatibility is modeled as a function of pressure and temperature revealing that liquid CO<sub>2</sub> is more compatible with silicone than scCO<sub>2</sub> is, resulting in a greater degree of swell. Free radical polymerization of 2-hydroxyethyl methacrylate (HEMA) in scCO<sub>2</sub> is examined. An insoluble cross-linked polymer material is formed. However, if ethanol is applied as co-solvent the cross-linking side-reaction can be suppressed. The kinetics of the free radical polymerization are determined by *in-situ* online FT-IR reaction monitoring. The tacticity of the produced polymers in terms of triads and pentads is analyzed by <sup>1</sup>H-NMR and <sup>13</sup>C-NMR. The experimental results are in fairly good agreement with those calculated statistically from Bernoullian and Markov first order statistics. Finally, the formation of IPNs of silicone and PHEMA is examined. It is found that the hydrophilicity of silicone can be increased by production of IPNs. However, the obtained effect is not enough for the produced IPNs to be suitable as contact lens material. This might be due to formation of an island-sea morphology. Furthermore, a self-assembly of silicone on the surface and PHEMA inside the IPN is observed. The produced IPNs with silicone and PHEMA are opaque due to a too large difference in refractive index between the substrate material and the guest polymer. However, when copolymers consisting of heptafluorobutyl acrylate (HFBA) and HEMA are used as guest polymer, transparent IPNs can be produced.

## Resumé

Interpenetrerende polymernetværk (IPN) af silikone gummi og poly(2-hydroxyethyl methacrylat) (PHEMA) produceret i superkritisk kuldioxid (scCO<sub>2</sub>) er undersøgt. Formålet er at forøge hydrofiliciteten af silikone uden at miste den optiske klarhed, hvilket vil gøre materialet egnet som kontaktlinsemateriale. Kompatibiliteten mellem CO<sub>2</sub> og silikone er modelleret som funktion af tryk og temperatur. Kvantificeringen viste, at flydende CO<sub>2</sub> er mere kompatibelt med silikone, end scCO<sub>2</sub> er. Fri-radikal polymerisation af 2-hydroxyethyl methacrylat (HEMA) i scCO<sub>2</sub> er undersøgt. Et uopløseligt tværbundet polymersystem bliver dannet. Hvis ethanol tilsættes som hjælpsolvent kan denne sidereaktion undgås. Kinetikken af denne polymerisation er bestemt ved brug af *in-situ* FT-IR online reaktionsovervågning. Takticiteten af de producerede polymerer er bestemt ud fra triader og pentader fra NMR spektra. De eksperimentelle resultater stemmer relativt godt overens med beregnede værdier fra Bernoullian og førsteordens Markov statistik. Til slut er dannelsen af IPN af silikone og PHEMA undersøgt. Hydrofiliciteten af silikone kan forøges ved at lave IPN, men den opnåede effekt er ikke tilstrækkelig til at de dannede IPN kan benyttes som kontaktlinse materiale. Dette kan skyldes dannelsen af en øhav-struktur. Desuden er det observeret, at der foregår en selvorganisering, hvilket betyder, at silikone diffunderer ud på overfladen og PHEMA er inde i IPNen. De producerede IPN er uklare, hvilket skyldes forskelle i refraktivt indeks mellem substrat materialet og gæstepolymeren. Det er vist at transparente IPN kan produceres, når copolymerer af heptafluorobutyl acrylat og HEMA bliver brugt som gæstepolymer.



# Contents

Abstract . . . . .	i
Resumé . . . . .	i
<b>Contents</b>	<b>iii</b>
<b>Preface</b>	<b>v</b>
<b>1 Introduction</b>	<b>1</b>
1.1 Silicone . . . . .	1
1.2 Interpenetrating polymer networks . . . . .	4
<b>2 Compatibility of silicone and carbon dioxide</b>	<b>7</b>
<b>3 Swelling and diffusion</b>	<b>37</b>
3.1 Swelling of gels . . . . .	37
3.2 Diffusion . . . . .	40
<b>4 2-hydroxyethyl methacrylate</b>	<b>45</b>
<b>5 Hydrophilicity</b>	<b>73</b>
5.1 Experimental . . . . .	73
5.2 Results and discussion . . . . .	74
5.3 Surface characterization . . . . .	75
<b>6 Transparency</b>	<b>85</b>
6.1 Scattering . . . . .	85
6.2 Reflection . . . . .	86
6.3 Free radical copolymerization . . . . .	86
6.4 Experimental . . . . .	91
6.5 Results and discussion . . . . .	91
<b>7 Conclusion</b>	<b>93</b>
<b>Appendices</b>	<b>97</b>
<b>A Phase diagram for carbon dioxide</b>	<b>99</b>
<b>B Molecular Interaction</b>	<b>103</b>
B.1 Solubility parameters . . . . .	106
<b>C List of abbreviations</b>	<b>111</b>
<b>Bibliography</b>	<b>119</b>



# Preface

The idea for the present dissertation was conceived during the work-up of the EU-financed THOR-project: Functional Composite Polymer Materials (FUCOMA), in which new applications for high pressure carbon dioxide (CO<sub>2</sub>) were investigated. NKT Research & Innovation / AdSphere (now Nanon A/S) joined the FUCOMA project to identify new opportunities for purifying polymeric materials and silicones. The FUCOMA project revealed that on a laboratory scale it was possible to extract impurities from injection moulded silicone elastomers by applying high pressure CO<sub>2</sub>. Furthermore, impregnating substances like color dyes into silicone elastomers was also found to be possible. This inspired the idea to apply high pressure CO<sub>2</sub> as an auxiliary solvent to impregnate chemistry into silicone elastomer materials, thereby changing the properties.[1]

The aim of this dissertation is to aid in understanding of the process and effect of different changeable parameters. Furthermore, the aim is to develop the approach to change the surface and bulk properties of silicone elastomers by impregnation and to make chemistry inside the matrix by applying high pressure CO<sub>2</sub>. The main focus is on the production of interpenetrating polymer networks (IPN). Throughout this text a case study concerning contact lenses is applied to exemplify the applied theories, but the objective is that the applied approaches and theories are generic and can be applied to any IPN system. During this study four patent applications and three scientific articles have been submitted.[2, 3, 4, 5, 6, 7, 8] In addition, seven oral presentations have been given at the following conferences:

- Medical Plastics 2005, 19th International Seminar And Conference, Copenhagen Denmark, 14–17 November 2005.
- 10th Meeting On Supercritical Fluids: Reactions, Materials and Natural Products Processing, Strasbourg (Colmar) France, 12–14 December 2005.
- International Silicone Conference, Dearborn, MI, USA, 4–5 April 2006.
- Nordic Polymer Days 2006, Copenhagen Denmark, 29–31 May 2006.
- Dansk Kemiingeniør Konference 2006 (Danish Chemistry Engineer Conference), Lyngby Denmark, 31 May – 2 June 2006.
- Possibilities With Lesser Known Polymers And Processes, Fredericia Denmark, 10 October 2006.
- 8th International Symposium on Supercritical Fluids (ISSF2006), Kyoto Japan, 5–8 November 2006.

Chapter 1 includes a general description of silicone, interpenetrating polymer networks and carbon dioxide. In chapter 2 and 3 thermodynamic models are applied in order to understand the behavior and compatibility between carbon dioxide and silicone and how it depends on pressure and temperature. Chapter 4 describes the free radical polymerization of 2-hydroxyethyl methacrylate in supercritical carbon dioxide. The kinetics of the polymerization is modeled and the tacticity in terms of pentads of the resulting polymers are determined by NMR and discussed. From chapter 5 forth the focus is given to interpenetration polymer networks. Chapter 5 and 6 include theories and experiments concerning the hydrophilicity and transparency respectively.

This dissertation is partly financed by the Danish Ministry of Science, Technology and Innovation, and is part of the Industrial PhD Initiative. The author would like to acknowledge:

- Kjeld Schaumburg—Department of Life Sciences and Chemistry, Roskilde University, and Maike Benter—Nanon, for their dedicated supervising and constructive discussions.
- Laurie L. Williams—Department of Physics and Engineering, Fort Lewis College, for supplying her dissertation.
- Roland Fromme—Woehlk, for discussion on the requirements for contact lenses.
- Helmut Steinberger—Momentive Performance Materials, and Gabriele Busler—Wacker Chemie AG, for discussions concerning silicone.
- Paul Charpentier—Department of Chemical and Biochemical Engineering, University of Western Ontario, for supplying the recipe for the applied initiator.
- Harald Behl—Mettler-Toledo AutoChem, and Nils Theyssen—Max-Planck-Institut für Kohlenforschung, for assisting in the *in-situ* FT-IR measurements.
- Annette Christensen—Department of Life Sciences and Chemistry, Roskilde University, for making the NMR measurements.
- Lene Hubert—Polymer Department, Risoe, for making the XPS measurements.
- Jakob B. Markussen—FORCE Technology, for making the FIB-SEM measurements.
- Lene V. Overby—NKT Flexibles, for making the DSC measurements.
- Lars Madsen—Department of Mathematical Sciences, University of Aarhus, for various hints and tricks using L<sup>A</sup>T<sub>E</sub>X.
- Employees at Nanon for they interest and support in the progress of this work.

To my beloved wife, Julie, and our son, Mathias, who make my world a lighter place to live.



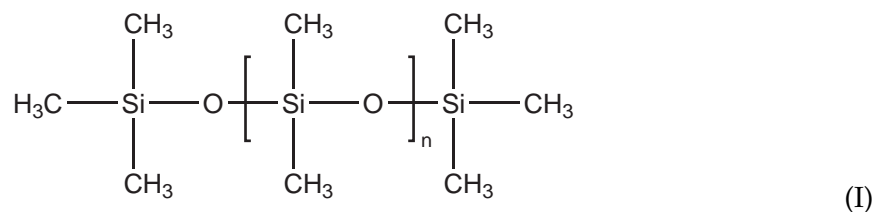
# Chapter 1

## Introduction

### 1.1 Silicone

Since its first industrial application in the 1940s, silicones have found usage in a vast number of products. Nowadays the main applications of silicone are within segments like: health care, automotive, sealants and colorants. Especially within health care many applications are found, like: contact lenses, catheters, implants, cosmetics and infant care such as for baby bottle nipples and pacifiers. It is estimated that in a typical modern car there is more than 50 potential applications for silicone based products, with a total usage of approx. 12 kg of silicones per car.[9, 10]

Silicones are a general category of synthetic polymers, whose backbone consist of repeating silicon (Si) to oxygen (O) bonds.[9] In addition to their bonds to O the Si-atoms are typically bonded to two organic groups. The most applied organic group is methyl (CH<sub>3</sub>), resulting in poly(dimethyl siloxane) (PDMS). Other organic groups may also be applied: phenyl, vinyl, flouro-containing compounds, etc.. The chemical structure of PDMS is shown in scheme (I):



The combination of organic side-groups and the inorganic backbone gives silicones a combination of unique properties.[9] The most significant characteristics of the PDMS chain are:[10]

- The extremely high energy of the Si–O-bond ( $461 \frac{\text{kJ}}{\text{mol}}$ ), which provides a high degree of stability to the PDMS structure:
  - High temperature stability
  - UV-stability
  - Weather-stability
  - Chemical resistance

- The high movability of the PDMS chain causes a low glass transition temperature ( $T_g \approx \sim 120^\circ\text{C}$ ) due to a low „package density“ of the molecular chains and low vibration energy, which leads to:
  - Low temperature
  - Durability
  - Mechanical flexibility
- The very strong hydrophobic character of the methyl groups due to the low rotational energy around the Si-O backbone, which leads:
  - Low surface free energy
  - Hydrophobicity
  - Moisture resistance

These properties make it possible to use silicones in different phases, as: fluids, emulsions, compounds, resins and elastomers in vast applications in diverse fields.[9] This dissertation concerns the alteration of bulk and surface properties of silicone elastomers, therefore only these will be considered further in this text. Under standard conditions ( $P = 1$  bar and  $T = 25^\circ\text{C}$ ) silicone polymers are fluids, due to the low  $T_g$ . In order to make silicone solid at standard conditions it is necessary to cross-link the polymer chains. The majority of silicone elastomers are cross-linked according to one of the following three reactions:[9]

**Condensation:** One-component room temperature vulcanization (1K RTV) silicone begins to cross-link when it comes in contact with moisture, typically from the humidity in the ambient air. Also a 2K RTV material exist which begins to cross-link when the two components are mixed and does not require moisture. 1K and 2K RTV eliminate acetic acid and alcohol during cross-linking respectively, resulting in shrinkage of 0.5–1%.

**Radicals:** high temperature vulcanization (HTV) silicone is cross-linked by free radical reaction of vinyl groups on the side-chains of the silicone. The cross-linking is initiated by thermal decomposition of organic peroxides. This cross-linking approach is used for high-consistency silicone rubbers (HCRs).

**Addition:** Cross-linking is achieved by reacting polymers with vinyl end-groups with Si-H groups on the silicone chains by applying a Platinum or Rhodium complex as catalyst. There are no by-products with this reaction and hence no shrinkage, which makes it suitable for injection moulding. The silicone used for injection moulding is called liquid silicone rubber (LSR).

Figure 1.1 shows a schematic partitioning of silicone elastomers. As can be seen on figure 1.1 another group is added to the HTV family: fluoro silicone elastomers, which are subdivided into a HCR and a LSR part. Fluor is incorporated into the silicone matrix to alter the silicone elastomers chemical and physical properties. Table 1.1 contains some general parameters for different types silicone elastomers.[10] In this work only LSR silicone elastomers will be considered further, but the applied techniques, theories and approached may be applied to the other silicone elastomer types as well.

# Silicone

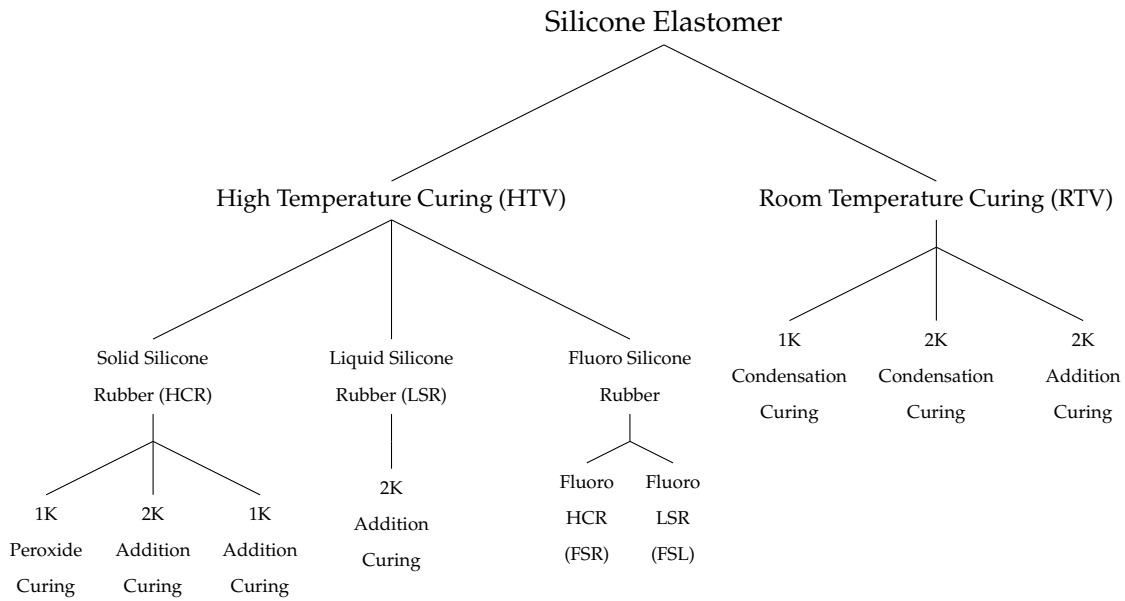


Figure 1.1: Schematic illustration of different types of silicone elastomers

Table 1.1: Comparison of different parameters for different silicone elastomer types.[10]

Properties	RTV-1	RTV-2	HTV (HCR)	LSR
Number of components	1	2	1	2
Mixing ratio	—	9 : 1	—	1 : 1
Chain length	200–1000	100–2000	300–10000	300–1000
Viscosity [Pas]	0.2–10	0.2–10	20000	5–100
Consistency	Flowable	Castable, liquid	Solid	High viscous, pasteous
Processing	Press, spray	Casting	Pressing, extrusion	Injection molding, casting
Pot life	Minutes	Hours	Months	Days
Curing $T$ [°C]	10–125	10–125	110–300	110–220
Cross-linking	Condensation	Addition, condensation	Organic peroxides	Addition
Reactive groups	Hydroxy	Hydroxy- or vinyl	Vinyl	Vinyl
Catalyst	Pt or Sn	Pt or Sn	—	Pt
Byproducts	Yes	Add: no, Cond: yes	Yes	No
Filler content	Low	Low	High	High
Filler types	HD silica	HD silica	HD silica, Quartz, ATH	HD silica

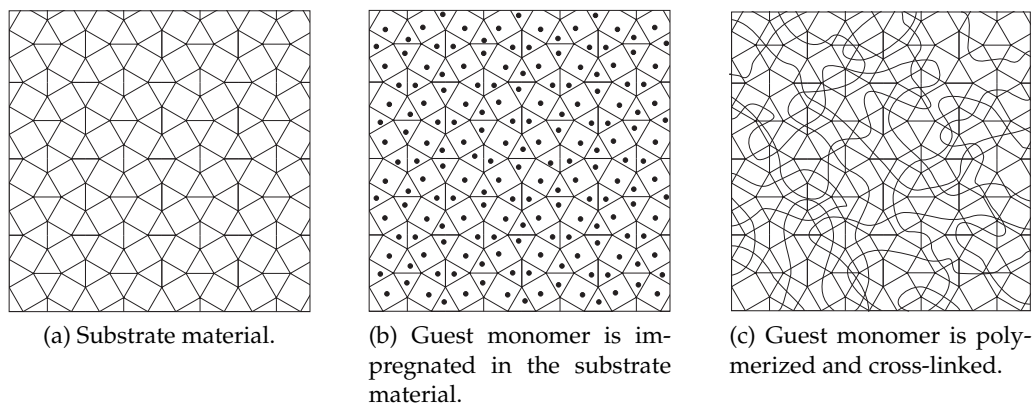


Figure 1.2: The three steps in producing an IPN. (a) A Cross-linked polymer is applied as substrate material, the lines represent the silicone polymers' backbone, which are chemical bond at the joints. (b) The substrate material is swollen with different monomer, the dots represent guest monomer-units. (c) Finally, the guest monomer is polymerized and cross-linked resulting in an interpenetrating polymer network.

For some applications some of the general properties of silicone elastomers are drawbacks or limiting factors. E.g. for contact lenses the high oxygen permeability and mechanical flexibility of silicones are desirable, but the low surface tension of silicone is a major drawback. Extensive efforts have been given in recent years for changing silicones properties in order to be able to apply it for this application. The low surface free energy of silicone elastomers can be altered by applying different techniques. In one approach hydrophilic groups like alcohols are incorporated in the side-chains on the silicone polymers before cross-linking.[11] In another approach silicone elastomers are exposed to first an Argon plasma then diatomic Oxygen and subsequently soaked in water and finally in hydrophilic monomers which are grafted to the surface.[12] In a third approach silicone-containing hydrophilic monomers are produced which can be used as cross-linking agents between a silicone elastomer and an organic hydrophilic network.[13] In this study yet another approach is taken, the production of interpenetrating polymer networks (IPN).[1] It is examined whether the IPN approach is suitable for changing the hydrophilicity of silicone elastomers.

## 1.2 Interpenetrating polymer networks

Interpenetrating polymer networks are defined as a polymer blend comprising two or more networks which are at least partially interlaced on a molecular scale but not covalently bonded to each other and cannot be separated unless chemical bonds are broken.[14] An IPN is made when a cross-linked polymer (the substrate material), cf. figure 1.2a, is swollen with a different monomer (the guest monomer), cf. figure 1.2b, then the monomer is polymerized and cross-linked, cf. figure 1.2c.[15]

Different morphologies of an IPN exists. The type of morphology is dependent on the phase separation during preparation of the IPN. Phase separation of multicomponent polymer systems can occur either by nucleation and growth which leads to a morphology of isolated guest polymer domains dispersed within the substrate material producing a sea-island morphology, or by spinodal decomposition which produces a bicontinuous structure of relative small, interconnected nodular domains of impreg-

nated polymer in the substrate material.[16] Typically at low guest monomer concentrations, a sea-island morphology is formed. As the concentration of the guest monomer is increased, a dual morphology is observed where both sea-island and interconnected nodular morphologies are formed. As the concentration of the guest monomer is further increased a strictly nodular interconnected morphology is formed.[16]

Different preparation approaches for producing IPNs are found in literature. In one study, the morphologies resulting from three different preparation approaches are examined.[16] In all three approaches a silicone elastomer is soaked in a mixture of monomer, cross-linker and initiator at standard conditions for 18 hours. Then the monomer-swollen silicone elastomer is purged with  $N_2$  and polymerized by UV radiation 1) in pure monomer, 2) in a  $N_2$  atmosphere and 3) between two glass slides, for 1 hour. With the latter two approaches IPNs with a morphology-spectrum ranging from dispersed hydrogel domains near the surface to a dual phase morphology, followed by a bicontinuous morphology indicative of spinodal decomposition are produced. The first approach, however, produced IPNs with phase morphologies indicative of spinodal decomposition, creating a uniform, bicontinuous morphology throughout the IPN.[16] In another study, the mechanical properties of silicone elastomers are improved by making IPNs with polystyrene.[17] Un-cross-linked silicone, catalyst, styrene, initiator and cross-linking agent are mixed and injected into a mould. Silicone is first cross-linked at  $25^\circ C$  for 8 h whereafter the mould is heated to  $80^\circ C$  for polymerization and cross-linking of the styrene. This method gave IPNs with a sea-island morphology.

Different industrial applications, where an IPN may solve the problem in concern or replace an existing product or process, are identified. The main focus is given to IPNs in which silicone elastomers are the substrate material. The reason for this choice is, that Nanon has experience in working with silicone elastomers from plasma treatment of silicone pads for the automotive industry. Furthermore, preliminary experiments have shown that it is possible to produce IPNs with PDMS as substrate material in  $scCO_2$ . The identified applications and requested effects are:

**Contact lenses:** Making silicone elastomers hydrophilic without losing transparency, mechanical properties and dimensional stability (optics).

**Automotive pads:** Making silicone elastomers white and hydrophilic to ease the subsequent painting process.

**Catheters:** Making silicone elastomers hydrophilic and bio-compatible to ease injection into bodily orifices and avoid bacteria adhesion and growth.

**Brain shunts:** Making silicone elastomers bio-compatible to avoid adhesion of blood, platelets, proteins etc..

**Barrier material:** Decrease the permeability of silicone elastomers.

The demands to an IPN depend on its final application. Some of these demands are however of a more or less general character. This means that the same theory can be applied to a multitude of systems. In this study contact lenses are chosen as a model system and will be applied as a case study. Mainly two different types of contact lenses exists on the world market; Disposable contact lenses, which are suitable for one-day usage, and extensive wear contact lenses, which are suitable for longer usages e.g. one month. Poly(2-hydroxyethyl methacrylate) (PHEMA) is a polymer which has found

extensive usage as disposable contact lens material. For extensive wear contact lenses especially surface modified silicone elastomers have been applied. The most important requirements to contact lenses are:

**Hydrophilic:** Contact lenses need to be hydrophilic in order to give a comfortable experience by the user. Lack of hydrophilicity is felt like burning or irritant to the eye, and the eye will try to repulse the contact lens. Furthermore the eye needs a water film beneath the contact lens in order to receive and remove nutrients, ions, proteins, etc..

**Transparent:** Contact lenses need to be transparent in order to look through them.

**Oxygen permeable:** Contact lenses need to be permeable to oxygen for the eye to breath. If the eye does not get enough oxygen blood vessels may growth into the cornea which may result in severe damage.

**Mechanical stable:** Contact lenses need to be mechanical stable. Ideally, a contact lens has the same properties before and after it is dropped on the floor and cleaned in water by rubbing it between the fingers.

The advantages of PHEMA is its hydrophilic nature, which makes it a hydrogel material. However, the main drawback is its relative low oxygen permeability, which is the reason why disposable contact lenses are recommended for only eight to ten hours of use per day. The opposite is true for silicone elastomers, which have a high permeability to oxygen but show a hydrophobic behavior. This drawback is overcome by different surface treatments of the silicone elastomer, like plasma treatment or grafting of hydrophilic groups on the silicone.

One approach would be to combine PHEMA and silicone elastomer into a new contact lens material using the advantages of each material. However, this is not possible by common available techniques, because PHEMA and silicone elastomers are immiscible and non-compatible. Hence the approaches to produce IPNs found in literature cannot be applied with success. Therefore another approach is taken. Injection moulded silicone elastomers (LSR) are applied as substrate material, a hydrophilic monomer is impregnated into the substrate material using supercritical carbon dioxide (scCO<sub>2</sub>) as an auxiliary solvent to assist the impregnation process. Then the guest monomer is polymerized and optionally cross-linked. The aim of this work is to examine whether it is possible to combine silicone elastomer and PHEMA by producing IPNs where scCO<sub>2</sub> is applied as an auxiliary solvent and obtain the given requirements for contact lenses. Two of the four major requirements are treated in more detail; the hydrophilicity and transparency. During the description, relevant theoretical approaches are identified and described. Before going into details about the different properties it will be convenient to understand some of scCO<sub>2</sub>'s properties, which makes it suitable as an auxiliary solvent for making IPNs where silicone elastomers are applied as substrate material. Therefore the compatibility between CO<sub>2</sub> and silicone elastomers is quantified.

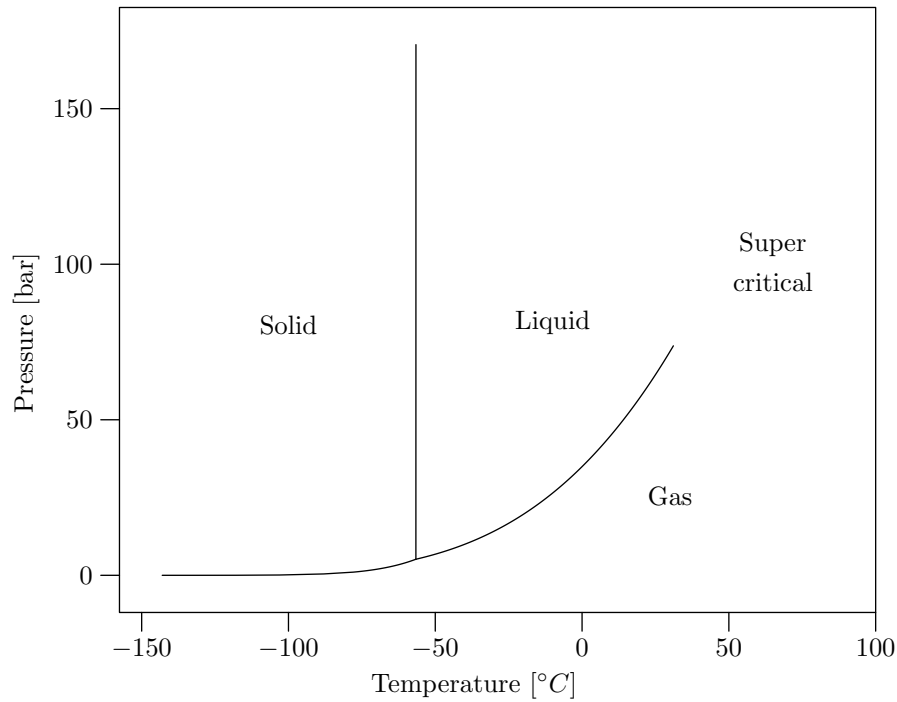
## Chapter 2

# Compatibility of silicone and carbon dioxide

Carbon dioxide ( $\text{CO}_2$ ) is a gas at standard conditions. The concentration of  $\text{CO}_2$  in the atmosphere is approx. 383 ppm, increasing every year with about 2 ppm, due to the burning of fossil fuels world-wide.[18] However,  $\text{CO}_2$  used for chemical processes is easier obtainable from the industry than from the atmosphere.  $\text{CO}_2$  is generated in large quantities in the industry and is recovered as byproduct from processes in ammonia, ethanol and hydrogen plants and in electrical power generation stations that burn fossil fuels. The  $\text{CO}_2$  used in chemical processes is therefore not contributing to the green house effect, but is postponing it.[19, 20]

Commercially,  $\text{CO}_2$  finds many applications such as a refrigerant, in beverage carbonation and in fire extinguishers. If the pressure is increased sufficiently  $\text{CO}_2$  becomes a liquid, and with simultaneous heating it enters the supercritical phase. The main application for liquid  $\text{CO}_2$  is dry-cleaning of clothes and for supercritical carbon dioxide ( $\text{scCO}_2$ ) decaffeination of green coffee beans and extraction of hop oil for beer production.  $\text{scCO}_2$  has furthermore been proven to be a viable and promising medium for a number of different polymerizations.[21, 22, 23, 24]  $\text{CO}_2$  has obvious advantages opposed to other organic solvents. In particular, it is nontoxic, nonflammable and has a threshold limit value (TLV) of 5000 ppm at  $25^\circ\text{C}$ . Furthermore  $\text{CO}_2$  is cheap (100-200 dollar/ton, year 2000), widely available and has a mild critical temperature ( $T_c = 31.1^\circ\text{C}$ ) and pressure ( $P_c = 73.8$  bar) and tunable solvating properties. In general  $\text{scCO}_2$  is a good solvent for many non-polar (and some polar) molecules with low molecular weights, whereas it is a poor solvent for most high molecular weight polymers under mild conditions ( $<100^\circ\text{C}$ ,  $<1000$  bar). Certain amorphous fluoropolymers and silicones of high molecular weight are shown to be soluble in  $\text{scCO}_2$ . Because of  $\text{scCO}_2$ 's special solvating properties, polymerization processes based on  $\text{scCO}_2$  most often lead to elimination of the polymer cleaning steps as the polymers can be isolated from the reaction media by simple depressurization, resulting in a dry polymer product. Likewise there is no need for disposal steps for removing residual monomers, since most monomers are soluble in  $\text{scCO}_2$  and can easily be removed from the polymer by  $\text{CO}_2$ -extraction. Furthermore there is no solvent to get rid of, and therefore no expensive wastewater treatment is necessary.[19, 20, 22]

One way to understand the phase behavior of  $\text{CO}_2$  is to go into details with its phase diagram. Appendix A contains a derivation of the phase diagram based on thermodynamics. The phase diagram describes the phase equilibrium as function of pressure ( $P$ )

Figure 2.1: Phase diagram for CO<sub>2</sub>.

and temperature ( $T$ ). Figure 2.1 shows the phase diagram for CO<sub>2</sub>.

This chapter includes the article "Compatibility of silicone and carbon dioxide", which is submitted to the Journal of Supercritical Fluids and is under review.[6] In the article the compatibility between silicone and CO<sub>2</sub> is quantified as function of  $P$  and  $T$  by applying Flory-Huggins (FH) theory and the lattice approach. In order to obtain data for the FH model the density ( $\rho$ ) of CO<sub>2</sub> as function of  $P$  and  $T$  is needed.  $\rho(P, T)$  is modeled by applying Huang's equation of state for CO<sub>2</sub> and verified experimentally.[25]

In order to determine the FH interaction parameter ( $\chi$ ) between PDMS and CO<sub>2</sub> Hansen's solubility parameter (HSP) approach is applied. More information on molecular interactions and the solubility approach can be found in appendix B. HSP is determined experimentally for PDMS and modeled as function of  $P$  and  $T$  by applying the derived models for HSP's dependence of  $P$  and  $T$  by considering the thermal expansion coefficient ( $\alpha$ ) and the isothermal compressibility coefficient ( $\beta$ ) for PDMS.

The FH model gives the free energy of mixing ( $F_m$ ). By modeling  $F_m$  for CO<sub>2</sub> and PDMS as function of  $P$  and  $T$  it is possible to map the compatibility of CO<sub>2</sub> and PDMS into two zones; spontaneous mixing and phase separation (non-mixing).

# Compatibility between Silicone and Carbon Dioxide

Martin Alm <sup>a,b,\*</sup>

<sup>a</sup>*Nanon A/S, Priorparken 878, 2605 Broendby, Denmark*

<sup>b</sup>*Roskilde University, Department of Life Sciences and Chemistry, Universitetsvej 1, 4000 Roskilde, Denmark*

---

## Abstract

That silicone and carbon dioxide is compatible is well described in literature. This article quantifies the compatibility between silicone rubber and carbon dioxide in the range from  $-55^{\circ}\text{C}$  to  $150^{\circ}\text{C}$  and 5 bar to 450 bar. Flory-Huggins theory is applied to determine the compatibility, and the Flory-Huggins interaction parameter ( $\chi$ ) is estimated from Hansen's solubility parameters (HSP). HSP are determined for silicone rubber at  $21^{\circ}\text{C}$  and 1 bar. Mathematical models for HSPs dependence on temperature and pressure are derived and applied on both silicone rubber and carbon dioxide. It is found that liquid carbon dioxide is compatible with silicone (the free energy of mixing is negative), whereas gaseous carbon dioxide is not (the free energy of mixing is positive). The supercritical phase is split in a compatible and a non-compatible part. The method described in this article is generic and may be applied for other materials as well.

*Key words:* Supercritical fluids, carbon dioxide, silicone, thermodynamics, solubility parameters

*PACS:*

---

## 1 Introduction

Silicone rubber has found widespread applications in health care due to properties such as hydrophobicity, low surface free energy and chemical and thermal stability.[1] One drawback of silicone rubber is that residual non-cross-linked

---

\* Corresponding author.

*Email address:* ma@nanon.dk (Martin Alm).

silicone oligomers and polymers migrate out of the silicone rubber. The industrial process to remove silicone oligomers is to heat the silicone rubber parts in an oven e.g. at 200°C for four hours. It would be convenient to identify a suitable solvent to remove the silicone oligomers and polymers.

For some applications e.g. contact lenses, the low surface free energy of silicone rubber is a drawback. To be able to use silicone rubber for such applications it is necessary to alter the surface chemistry of the silicone, e.g. by grafting hydrophilic polymers to the silicone network or by adding some hydrophilic groups by plasma treatment.[2–5] Another approach is to impregnate hydrophilic compounds into the silicone network.[6] It would be convenient to identify a suitable solvent to assist the impregnation of hydrophilic compounds into silicone rubber materials.

In general, polymers with a flexible backbone and a high free volume, and hence a low glass transition temperature ( $T_g$ ), such as silicones, have been found to exhibit high solubility in liquid and supercritical carbon dioxide ( $\text{CO}_2$ ).[7] Several advantages of applying  $\text{CO}_2$  for these applications exists:  $\text{CO}_2$  is a nonflammable, nontoxic, relative inert and cheap compared to organic solvents. Furthermore  $\text{CO}_2$  is a gas at standard conditions (21°C and 1 bar), which means that it is easy to remove after the process, simply by degassing.[8]

The scope of this article is to quantify the compatibility between silicone rubber and  $\text{CO}_2$  as function of pressure (P) and temperature (T) in order to decide if it is a suitable solvent for these applications.

## 2 Thermodynamics

### 2.1 Flory-Huggins

The compatibility between two substances (a polymer and a solvent) can be quantified by considering the thermodynamic properties of their interaction. One approach is the Flory-Huggins theory.[9,10] The Flory-Huggins theory is based on a lattice model, in which the volume of the total system is divided into small boxes each containing either a polymer segment or a solvent molecule. The volume fraction (or concentration) of polymer segments ( $\phi$ ) is given by equation (1):

$$\phi = \frac{n_p N}{\Omega} \tag{1}$$

where  $n_p$  is the number of polymer molecules in the mixture,  $N$  is the number of segments in each polymer molecule and  $\Omega$  is the total number of lattice sites. The Helmholtz total free energy of mixing ( $F_m$ ) is given by equation (2):

$$F_m = \Omega k_B T f_m(\phi) \quad (2)$$

where  $k_B$  is the Boltzmann constant,  $T$  is the absolute temperature and  $f_m(\phi)$  is the free energy of mixing per lattice site and is given by equation (3):

$$f_m(\phi) = \frac{1}{N} \phi \ln(\phi) + (1 - \phi) \ln(1 - \phi) + \chi \phi(1 - \phi) \quad (3)$$

The first two terms in equation (3) denotes the entropy of the system, which will always be negative, and the last term denotes the enthalpy of the system, which is positive or zero.  $\chi$  is the Flory-Huggins interaction parameter and is defined by equation (4):

$$\chi = \frac{z}{2k_B T} [\epsilon_{pp} + \epsilon_{ss} - 2\epsilon_{ps}] \quad (4)$$

where  $z$  is the lattice coordination number, which is 6 for a three dimensional lattice.  $\epsilon$  is the interaction energy between two neighbouring segments on the lattice. The subscripts pp, ss and ps denote the type of segments on the lattice; p denotes a polymer segment and s denotes a solvent molecule. It is very difficult if not impossible to determine the values of  $\epsilon_{pp}$ ,  $\epsilon_{ss}$  and  $\epsilon_{ps}$ , but since these three interaction energies originate from physical interactions it is possible to estimate  $\chi$  by applying the solubility parameter approach. If Hansen's solubility parameters (HSP) are used  $\chi$  is given by equation (5):[11]

$$\chi = \frac{V_m \left( (\delta_d^p - \delta_d^s)^2 + 0.25 (\delta_p^p - \delta_p^s)^2 + 0.25 (\delta_h^p - \delta_h^s)^2 \right)}{RT} \quad (5)$$

where  $V_m$  is the molar volume of the solvent,  $R$  is the gas constant and  $\delta_d^2$ ,  $\delta_p^2$  and  $\delta_h^2$  are the contribution to the total cohesive energy density from dispersion forces, dipole forces and hydrogen bonding respectively in the pure materials p and s.

## 2.2 HSP's dependence on pressure and temperature

It would be convenient to determine  $\chi$  as function of pressure and temperature in order to locate the best compatibility, and hence optimize the experimental

settings (pressure and temperature), between the two substances in concern, CO<sub>2</sub> and silicone. According to equation (5) it is necessary to know how  $\delta_d$ ,  $\delta_p$  and  $\delta_h$  depend on pressure and temperature in order to evaluate  $\chi(P, T)$ .

Only little information on HSP's dependence on pressure and temperature exist in literature.[11,12] Literature even states, that only very limited attempts have been made to calculate solubility parameters at higher temperature.[11] Generally solubility parameter correlations at higher temperatures have been found satisfactory when the parameters at 25°C have been used. In this work, however, the precise information is needed, therefore equations concerning HSP's dependence on pressure and temperature are derived. The unit  $\sqrt{\text{MPa}}$  is used for HSP throughout this text. The numeric value of  $\sqrt{\text{MPa}}$  is 2.0455 times larger than that in  $\sqrt{\frac{\text{Cal}}{\text{mL}}}$ , which sometimes is used in literature.[11]

### 2.2.1 $\delta_d$ 's dependence on pressure and temperature

$\delta_d^2$  is defined in equation (6):[11]

$$\delta_d^2 = \frac{E_d}{V_m} \quad (6)$$

where  $E_d$  is the contribution of the dispersion forces to the total cohesive energy ( $E_c$ ) and  $V_m$  is the molar volume.  $E_d$  is given by equation (7):[12,13]

$$E_d = -\frac{k}{V_m^{1.5}} \quad (7)$$

where  $k$  is a constant dependent upon the nature of the particular liquid. The value of the exponent is according to Hildebrand and Scott based on an examination of data on perfect liquids and hydrocarbons. Substituting equation (7) into equation (6) and isolating  $\delta_d$  yields equation (8):

$$\begin{aligned} \delta_d^2 &= \frac{1}{V_m} \cdot \left( -\frac{k}{V_m^{1.5}} \right) = -\frac{k}{V_m^{2.5}} \\ \Downarrow \\ \delta_d &= -\frac{\sqrt{k}}{V_m^{1.25}} \end{aligned} \quad (8)$$

Partial differentiation of equation (8) with respect to  $V_m$  at constant pressure and temperature and rearranging gives equation (9):

$$\begin{aligned} \left[ \frac{\partial \delta_d}{\partial V_m} \right]_{P,T} &= \frac{1.25\sqrt{k}}{V_m^{2.25}} = \frac{1.25}{V_m} \cdot \frac{\sqrt{k}}{V_m^{1.25}} = -\frac{1.25}{V_m} \delta_d \\ \Downarrow \\ \frac{\partial \delta_d}{\delta_d} &= -1.25 \frac{\partial V_m}{V_m} \end{aligned} \quad (9)$$

Equation (9) can now be differentiated for either temperature or pressure, or integrated. **The temperature dependence of  $\delta_d$**  can be determined by partial differentiation of equation (9) with respect to temperature at constant pressure. This is given by equation (10):

$$\frac{1}{\delta_d} \left[ \frac{\partial \delta_d}{\partial T} \right]_P = -1.25 \frac{1}{V_m} \left[ \frac{\partial V_m}{\partial T} \right]_P \quad (10)$$

The isobaric coefficient of thermal expansion ( $\alpha$ ) is defined in equation (11):

$$\alpha = \frac{1}{V_m} \left[ \frac{\partial V_m}{\partial T} \right]_P \quad (11)$$

Substituting  $\alpha$  into equation (10) gives the dependence of  $\delta_d$  on temperature at constant pressure, and is given in equation (12):

$$\left[ \frac{\partial \delta_d}{\partial T} \right]_P = -1.25\alpha\delta_d \quad (12)$$

**The pressure dependence of  $\delta_d$**  can be determined by partial differentiation of equation (9) with respect to pressure at constant temperature. This is given by equation (13):

$$\frac{1}{\delta_d} \left[ \frac{\partial \delta_d}{\partial P} \right]_T = -1.25 \frac{1}{V_m} \left[ \frac{\partial V_m}{\partial P} \right]_T \quad (13)$$

The isothermal compressibility ( $\beta$ ) is defined in equation (14):

$$\beta = -\frac{1}{V_m} \left[ \frac{\partial V_m}{\partial P} \right]_T \quad (14)$$

Substituting  $\beta$  into equation (13) gives the dependence of  $\delta_d$  on pressure at constant temperature, and is given in equation (15):

$$\left[ \frac{\partial \delta_d}{\partial P} \right]_T = 1.25\beta\delta_d \quad (15)$$

**The molar volume dependence of  $\delta_d$**  can be found by integrate equation (9) from known reference values ( $\delta_{d'}$  and  $V_{m'}$  at  $T'$  and  $P'$ ) to new unknown values ( $\delta_d$  and  $V_m$  at  $T$  and  $P$ ). This is given by equation (16):

$$\begin{aligned} & \int_{\delta_{d'}}^{\delta_d} \frac{\partial \delta_d}{\delta_d} = -1.25 \int_{V_{m'}}^{V_m} \frac{\partial V_m}{V_m} \\ \Downarrow & \\ & \left[ \ln \delta_d \right]_{\delta_{d'}}^{\delta_d} = -1.25 \left[ \ln V_m \right]_{V_{m'}}^{V_m}, \\ \Downarrow & \\ & \ln \frac{\delta_d}{\delta_{d'}} = -1.25 \ln \frac{V_m}{V_{m'}} = \ln \left[ \left( \frac{V_m}{V_{m'}} \right)^{-1.25} \right] \\ \Downarrow & \\ & \frac{\delta_d}{\delta_{d'}} = \left( \frac{V_m}{V_{m'}} \right)^{-1.25} \end{aligned} \quad (16)$$

### 2.2.2 $\delta_p$ 's dependence on pressure and temperature

$\delta_p$ 's dependence on pressure and temperature is determined in a similar manner as  $\delta_d$ 's.  $\delta_p$  is given by equation (17):[12,14]

$$\delta_p = \frac{18.3 \frac{\sqrt{\text{Cal}}}{\text{Debye}} \cdot 2.0455 \frac{\sqrt{\text{MPa}}}{\sqrt{\frac{\text{Cal}}{\text{mL}}}}}{\sqrt{V_m}} \mu = \frac{37.4 \frac{\sqrt{\text{MPa} \cdot \text{mL}}}{\text{Debye}}}{\sqrt{V_m}} \mu \quad (17)$$

where  $\mu$  is the dipole moment of the considered molecule expressed in Debye unit.  $V_m$  is expressed in mL unit. The partial derivative of  $\delta_d$  with respect to  $V_m$  at constant pressure and temperature is given by equation (18):

$$\begin{aligned} \left[ \frac{\partial \delta_p}{\partial V_m} \right]_{P,T} &= -\frac{37.4 \frac{\sqrt{\text{MPa} \cdot \text{mL}}}{\text{Debye}} \mu}{2\sqrt{V_m^3}} = -\frac{\delta_p}{2V_m} \\ \Downarrow \\ \frac{\partial \delta_p}{\delta_p} &= -\frac{\partial V_m}{2V_m} \end{aligned} \quad (18)$$

**The temperature dependence of  $\delta_p$**  can be determined by partial differentiation of equation (18) with respect to temperature at constant pressure. This is given in equation (19):

$$\frac{1}{\delta_p} \left[ \frac{\partial \delta_p}{\partial T} \right]_P = -\frac{1}{2V_m} \left[ \frac{\partial V_m}{\partial T} \right]_P \quad (19)$$

By substituting  $\alpha$  into equation (19) and rearranging gives equation (20):

$$\begin{aligned} \frac{1}{\delta_p} \left[ \frac{\partial \delta_p}{\partial T} \right]_P &= -\frac{\alpha}{2} \\ \Downarrow \\ \left[ \frac{\partial \delta_p}{\partial T} \right]_P &= -0.5\alpha\delta_p \end{aligned} \quad (20)$$

**The pressure dependence of  $\delta_p$**  can be determined by partial differentiation of equation (18) with respect to pressure at constant temperature. This is given in equation (21):

$$\frac{1}{\delta_p} \left[ \frac{\partial \delta_p}{\partial P} \right]_T = -\frac{1}{2V_m} \left[ \frac{\partial V_m}{\partial P} \right]_T \quad (21)$$

By substituting  $\beta$  into equation (21) and rearranging gives equation (22):

$$\begin{aligned} \frac{1}{\delta_p} \left[ \frac{\partial \delta_p}{\partial P} \right]_T &= \frac{\beta}{2} \\ \Downarrow \\ \left[ \frac{\partial \delta_p}{\partial P} \right]_T &= 0.5\beta\delta_p \end{aligned} \quad (22)$$

**The molar volume dependence of  $\delta_p$**  can be found by integrate equation (18) from known reference values ( $\delta_p'$  and  $V_m'$  at  $T'$  and  $P'$ ) to new unknown values ( $\delta_p$  and  $V_m$  at  $T$  and  $P$ ). This is given by equation (23):

$$\begin{aligned}
& \int_{\delta_p'}^{\delta_p} \frac{\partial \delta_p}{\delta_p} = \int_{V_m'}^{V_m} -\frac{\partial V_m}{2V_m} = -0.5 \int_{V_m'}^{V_m} \frac{\partial V_m}{V_m} \\
& \Downarrow \\
& \left[ \ln \delta_p \right]_{\delta_p'}^{\delta_p} = -0.5 \left[ \ln V_m \right]_{V_m'}^{V_m}, \\
& \Downarrow \\
& \ln \frac{\delta_p}{\delta_p'} = -0.5 \ln \frac{V_m}{V_m'} = \ln \left[ \left( \frac{V_m}{V_m'} \right)^{-0.5} \right] \\
& \Downarrow \\
& \frac{\delta_p}{\delta_p'} = \left( \frac{V_m}{V_m'} \right)^{-0.5} = \sqrt{\frac{V_m'}{V_m}} \tag{23}
\end{aligned}$$

### 2.2.3 $\delta_h$ 's dependence on pressure and temperature

$\delta_h$ 's dependence on  $V_m$  is given by the definition of  $\delta_h^2$ , which is given in equation (24):[12,11]

$$\begin{aligned}
& \delta_h^2 = \frac{E_h}{V_m} \\
& \Downarrow \\
& E_h = V_m \delta_h^2 \tag{24}
\end{aligned}$$

where  $E_h$  is the hydrogen bonding contribution to the total cohesion energy. **The temperature dependence of  $\delta_h$**  can be determined by partial differentiation of equation (24) with respect to temperature at constant pressure. This is given in equation (25):

Table 1

Values for  $E_h$  and  $\partial E_h/\partial T$  for different functional groups according to literature.[12]

Functional group	$E_h$	$\partial E_h/\partial T$	$C_h^a$
Aliphatic	[cal/mol]	[cal/mol · K]	[K <sup>-1</sup> ]
-OH	4650 ± 400	-10	2.15 · 10 <sup>-3</sup>
-NH <sub>2</sub>	1350 ± 200	-4.5	3.33 · 10 <sup>-3</sup>
-CN	500 ± 200	-7.0	14 · 10 <sup>-3</sup>
-COOH	2750 ± 250	-2.9	1.05 · 10 <sup>-3</sup>
Average	2312.5 ± 262.5	-6.1	2.64 · 10 <sup>-3</sup>

$$^a C_h = -\frac{1}{E_h} \left[ \frac{\partial E_h}{\partial T} \right]_P$$

$$\begin{aligned}
& \left[ \frac{\partial E_h}{\partial T} \right]_P = V_m(2\delta_h) \left[ \frac{\partial \delta_h}{\partial T} \right]_P + \delta_h^2 \left[ \frac{\partial V_m}{\partial T} \right]_P \\
\Downarrow & \\
2V_m\delta_h \left[ \frac{\partial \delta_h}{\partial T} \right]_P &= \left[ \frac{\partial E_h}{\partial T} \right]_P - \delta_h^2 \left[ \frac{\partial V_m}{\partial T} \right]_P \\
\Downarrow & \\
\left[ \frac{\partial \delta_h}{\partial T} \right]_P &= \frac{\left[ \frac{\partial E_h}{\partial T} \right]_P - \delta_h^2 \left[ \frac{\partial V_m}{\partial T} \right]_P}{2V_m\delta_h} \\
\Downarrow & \\
\left[ \frac{\partial \delta_h}{\partial T} \right]_P &= \frac{1}{2V_m\delta_h} \left[ \frac{\partial E_h}{\partial T} \right]_P - \frac{\delta_h}{2V_m} \left[ \frac{\partial V_m}{\partial T} \right]_P \quad (25)
\end{aligned}$$

By extending the fraction of the first term with  $\delta_h$  and substitute  $\alpha$  into the second term of equation (25) gives equation (26):

$$\left[ \frac{\partial \delta_h}{\partial T} \right]_P = \frac{\delta_h}{2V_m\delta_h^2} \left[ \frac{\partial E_h}{\partial T} \right]_P - \frac{\delta_h}{2} \alpha \quad (26)$$

By substituting  $V_m\delta_h^2$  with  $E_h$  gives equation (27):

$$\left[ \frac{\partial \delta_h}{\partial T} \right]_P = \frac{\delta_h}{2} \left( \frac{1}{E_h} \left[ \frac{\partial E_h}{\partial T} \right]_P - \alpha \right) \quad (27)$$

Values for  $E_h$ ,  $\partial E_h/\partial T$  for different functional groups can be found in literature and are listed in table 1.[12]

Substituting  $-\frac{1}{E_h} \left[ \frac{\partial E_h}{\partial T} \right]_P$  with  $C_h$  in equation (27) gives equation (28):

$$\left[ \frac{\partial \delta_h}{\partial T} \right]_P = -\frac{\delta_h}{2} (C_h + \alpha) \quad (28)$$

**The pressure dependence of  $\delta_h$**  is determined by first combining the definitions of  $\alpha$  and  $\beta$  and then applying the chain rule to  $\partial \delta_h / \partial P$ . Combining equation (11) and (14) is given by equation (29):

$$\begin{aligned} \alpha &= \frac{1}{V_m} \left[ \frac{\partial V_m}{\partial T} \right]_P \wedge \beta = -\frac{1}{V_m} \left[ \frac{\partial V_m}{\partial P} \right]_T \\ \Downarrow \\ V_m &= \frac{1}{\alpha} \left[ \frac{\partial V_m}{\partial T} \right]_P \wedge V_m = -\frac{1}{\beta} \left[ \frac{\partial V_m}{\partial P} \right]_T \\ \Downarrow \\ & \frac{1}{\alpha} \left[ \frac{\partial V_m}{\partial T} \right]_P = -\frac{1}{\beta} \left[ \frac{\partial V_m}{\partial P} \right]_T \\ \Downarrow \\ & -\frac{\beta}{\alpha} = \frac{\left[ \frac{\partial V_m}{\partial P} \right]_T}{\left[ \frac{\partial V_m}{\partial T} \right]_P} = \frac{\partial T}{\partial P} \end{aligned} \quad (29)$$

The chain rule suggests equation (30):

$$\frac{\partial \delta_h}{\partial P} = \frac{\partial \delta_h}{\partial T} \cdot \frac{\partial T}{\partial P} \quad (30)$$

By substituting equation (28) and (29) into equation (30) gives equation (31):

$$\left[ \frac{\partial \delta_h}{\partial P} \right]_T = -\frac{\delta_h}{2} (C_h + \alpha) \cdot \left( -\frac{\beta}{\alpha} \right) = \frac{\delta_h}{2} \left( \frac{C_h \beta}{\alpha} + \beta \right) \quad (31)$$

**The molar volume dependence of  $\delta_h$**  can be determined by inserting  $\alpha$  into equation (28), rearranging and subsequently integrate it from known reference values ( $\delta_h'$ ,  $V_m'$  and  $T'$  at  $P'$ ) to new unknown values ( $\delta_h$ ,  $V_m$  and  $T$  at  $P$ ). This is given by equation (32):

$$\begin{aligned}
& \left[ \frac{\partial \delta_h}{\partial T} \right]_P = -\frac{\delta_h}{2} \left( C_h + \frac{1}{V_m} \left[ \frac{\partial V_m}{\partial T} \right]_P \right) \\
& \Downarrow \\
& \frac{\partial \delta_h}{\delta_h} = - \left( \frac{C_h}{2} + \frac{1}{2V_m} \cdot \frac{\partial V_m}{\partial T} \right) \partial T \\
& \Downarrow \\
& \frac{\partial \delta_h}{\delta_h} = - \left( \frac{C_h}{2} \partial T + \frac{\partial V_m}{2V_m} \right) \\
& \Downarrow \\
& \int_{\delta_h'}^{\delta_h} \frac{\partial \delta_h}{\delta_h} = - \left( \int_{T'}^T \frac{C_h}{2} \partial T + \int_{V_m'}^{V_m} \frac{\partial V_m}{2V_m} \right) \\
& \Downarrow \\
& \left[ \ln \delta_h \right]_{\delta_h'}^{\delta_h} = - \left( \frac{C_h}{2} [T]_{T'}^T + 0.5 \left[ \ln V_m \right]_{V_m'}^{V_m} \right) \\
& \Downarrow \\
& \ln \frac{\delta_h}{\delta_h'} = - \left( \frac{C_h}{2} (T - T') + 0.5 \ln \frac{V_m}{V_m'} \right) \\
& \Downarrow \\
& \ln \frac{\delta_h}{\delta_h'} = \frac{C_h}{2} (T' - T) + \ln \sqrt{\frac{V_m'}{V_m}} \\
& \Downarrow \\
& \frac{\delta_h}{\delta_h'} = \exp \left[ \frac{C_h}{2} (T' - T) + \ln \sqrt{\frac{V_m'}{V_m}} \right] \\
& \Downarrow \\
& \delta_h = \delta_h' \sqrt{\frac{V_m'}{V_m}} \exp \left[ \frac{C_h}{2} (T' - T) \right] \tag{32}
\end{aligned}$$

#### 2.2.4 Summary of section 2.2

The temperature dependence of  $\delta_d$ ,  $\delta_p$  and  $\delta_h$  is given by equation (12), (20) and (28) respectively. The pressure dependence of  $\delta_d$ ,  $\delta_p$  and  $\delta_h$  is given by equation (15), (21) and (31) respectively. The molar volume dependence of  $\delta_d$ ,  $\delta_p$  and  $\delta_h$  is given by equation (16), (23) and (32) respectively.

In order to model HSP as function of pressure and temperature it is convenient to solve the partial differential equations by numerical method. Equations (33) - (38) lists the Euler-Cauchy numerical solutions of the pressure and temperature dependence of HSP:

$$\begin{aligned}
& \left[ \frac{\partial \delta_d}{\partial T} \right]_P = -1.25\alpha \delta_d' \\
& \Downarrow \\
& \frac{\Delta \delta_d}{\Delta T} = -1.25\alpha \delta_d' \\
& \Downarrow \\
& \frac{\delta_d - \delta_d'}{\Delta T} = -1.25\alpha \delta_d' \\
& \Downarrow \\
& \delta_d = -1.25\alpha \delta_d' \Delta T + \delta_d' \\
& \Downarrow \\
& \delta_d(T) = (1 - 1.25\alpha \Delta T) \delta_d' \quad (33) \\
& \delta_p(T) = (1 - 0.5\alpha \Delta T) \delta_p' \quad (34) \\
& \delta_h(T) = \left[ 1 - \left( \frac{C_h}{2} + \frac{\alpha}{2} \right) \Delta T \right] \delta_h' \quad (35) \\
& \delta_d(P) = (1 + 1.25\beta \Delta P) \delta_d' \quad (36) \\
& \delta_p(P) = (1 + 0.5\beta \Delta P) \delta_p' \quad (37) \\
& \delta_h(P) = \left[ 1 + \left( \frac{C_h \beta}{2\alpha} + \frac{\beta}{2} \right) \Delta P \right] \delta_h' \quad (38)
\end{aligned}$$

$\delta_d$ ,  $\delta_p$  and  $\delta_h$  at any pressure and temperature can be estimated from known HSP at a given pressure and temperature by combining equation (33) with (36), equation (34) with (37) and equation (35) with (38) respectively, since any change in pressure and temperature can be understood as first an isothermal pressure alteration followed by an isobaric temperature alteration or visa versa.  $\delta_d$ ,  $\delta_p$  and  $\delta_h$  at any pressure and temperature are given by equation (39) to (41):

$$\delta_d(P, T) = (1 + 1.25\beta(P - P')) (1 - 1.25\alpha(T - T')) \delta_d' \quad (39)$$

$$\delta_p(P, T) = \left( 1 + \frac{\beta(P - P')}{2} \right) \left( 1 - \frac{\alpha(T - T')}{2} \right) \delta_p' \quad (40)$$

$$\delta_h(P, T) = \left[ 1 + \left( \frac{C_h \beta}{2\alpha} + \frac{\beta}{2} \right) (P - P') \right] \left[ 1 - \left( \frac{C_h}{2} + \frac{\alpha}{2} \right) (T - T') \right] \delta_h' \quad (41)$$

### 3 HSP for carbon dioxide

To determine how HSP change for CO<sub>2</sub> as function of pressure and temperature Huang's equation of state is applied (EoS).[15] Huang et al. developed an empirical EoS that yield high accuracy in  $PVT$  calculations over wide ranges of temperatures (216–423 K) and pressures (to 310.3 MPa).[15] The EoS is a combination of an analytical part and a nonanalytical part, and is given by equation (42):

$$\begin{aligned}
 Z = \frac{P}{\rho RT} = & 1 + b_2\rho' + b_3\rho'^2 + b_4\rho'^3 + b_5\rho'^4 + b_6\rho'^5 \\
 & + b_7\rho'^2 \exp[-c_{21}\rho'^2] + b_8\rho'^4 \exp[-c_{21}\rho'^2] \\
 & + c_{22}\rho' \exp[-c_{27}(\Delta T)^2] \\
 & + c_{23}\Delta\rho/\rho' \exp[-c_{25}(\Delta\rho)^2 - c_{27}(\Delta T)^2] \\
 & + c_{24}\Delta\rho/\rho' \exp[-c_{26}(\Delta\rho)^2 - c_{27}(\Delta T)^2]
 \end{aligned} \tag{42}$$

where  $\rho$  is the density. The reduced temperatures and densities are  $T' = \frac{T}{T_c}$ ,  $\rho' = \frac{\rho}{\rho_c}$ ,  $\Delta T = 1 - T'$ , and  $\Delta\rho = 1 - \frac{1}{\rho'}$ .  $b_i$  are functions of temperature are given by equation (43) to (49).  $c_i$  are constants listed in table 2.

$$b_2 = \left( c_1 + \frac{c_2}{T'} + \frac{c_3}{T'^2} + \frac{c_4}{T'^3} + \frac{c_5}{T'^4} + \frac{c_6}{T'^5} \right) \tag{43}$$

$$b_3 = \left( c_7 + \frac{c_8}{T'} + \frac{c_9}{T'^2} \right) \tag{44}$$

$$b_4 = \left( c_{10} + \frac{c_{11}}{T'} \right) \tag{45}$$

$$b_5 = \left( c_{12} + \frac{c_{13}}{T'} \right) \tag{46}$$

$$b_6 = \left( \frac{c_{14}}{T'} \right) \tag{47}$$

$$b_7 = \left( \frac{c_{15}}{T'^3} + \frac{c_{16}}{T'^4} + \frac{c_{17}}{T'^5} \right) \tag{48}$$

$$b_8 = \left( \frac{c_{18}}{T'^3} + \frac{c_{19}}{T'^4} + \frac{c_{20}}{T'^5} \right) \tag{49}$$

The three last terms in equation (42) are nonanalytical terms used to reproduce the critical isotherm. The term nonanalytical is used to denote the critical fluctuations exhibited by the scaled variables  $\Delta\rho$  and  $\Delta T$  in the exponentials.

Table 2

Constants  $c_i$  to be used in equation (42) to (49).

$i$	$c_i$	$i$	$c_i$
1	0.376194	15	-2.79498
2	0.118836	16	5.62393
3	-3.04379	17	-2.93831
4	2.27453	18	0.988759
5	-1.23863	19	-3.04711
6	0.250442	20	2.32316
7	-0.115350	21	1.07379
8	0.675104	22	$-0.599724 \cdot 10^{-4}$
9	0.198861	23	$0.885339 \cdot 10^{-4}$
10	0.216124	24	$0.316418 \cdot 10^{-2}$
11	-0.583148	25	10
12	$0.119747 \cdot 10^{-1}$	26	50
13	$0.537278 \cdot 10^{-1}$	27	80,000
14	$0.265216 \cdot 10^{-1}$		

The constants in table 2 are determined through a nonlinear regression subroutine by fitting equation (42) to available vapour pressure and thermal data.[15] Equation (42) cannot be more accurate than the available experimental data. Therefore density calculation is reliable to within 0.1-0.2% outside the critical region and to within 1% near the critical point. Figure 1 shows the density of CO<sub>2</sub> as function of pressure and temperature based on equation (42).

Three different regions are found in figure 1: The gas phase at low pressures where the density is low. The liquid phase, at low temperatures and higher pressure the density is high. The supercritical state at high pressures and high temperatures (above  $T_c = 31.1^\circ\text{C}$  and  $P_c = 73.8$  bar), in this region the density can be varied from gas-like to liquid-like. Especially near the critical point the density varies much, this behavior describes the tunability of the solubility properties of CO<sub>2</sub>.

The density behavior has been examined experimentally, by production of PVT data and curves. An 11 ml high-pressure stainless steel reactor was equipped with a thermocouple and a digital pressure transmitter. The reactor was placed in an oven at  $20.4^\circ\text{C}$  and loaded with CO<sub>2</sub> to a pressure of 100 bar. The oven was then heated to  $70^\circ\text{C}$  and the temperature and the pressure in the reactor was read every minute. From equation (42) the density of CO<sub>2</sub> at

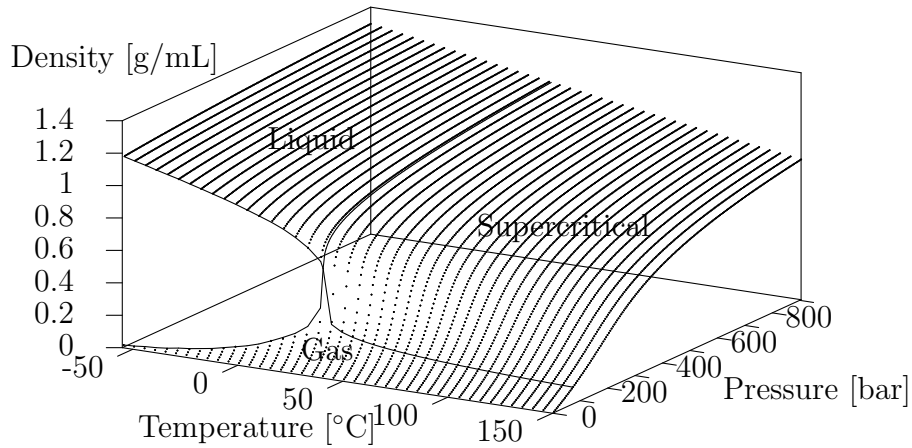


Fig. 1. Density of CO<sub>2</sub> as function of pressure and temperature.

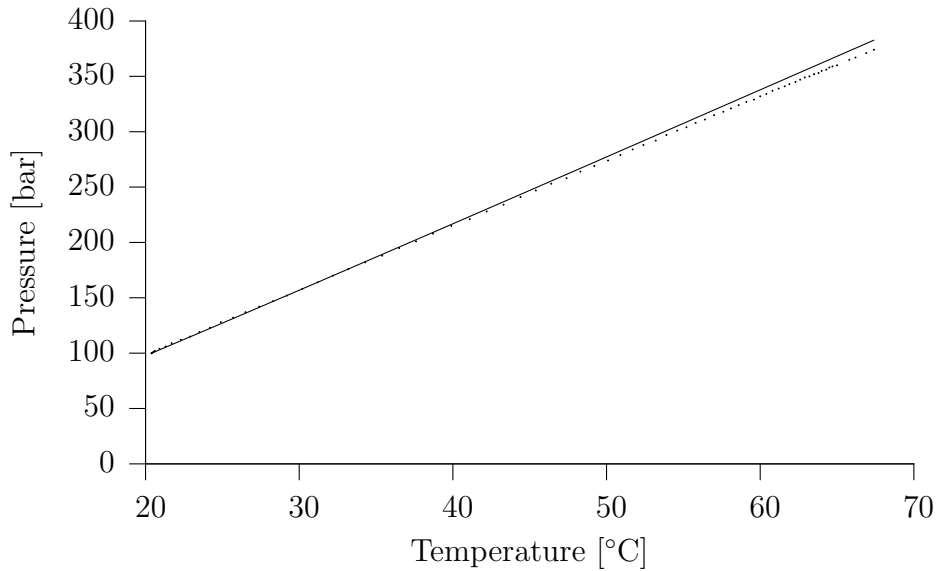


Fig. 2. Validation of Huang's EoS. Solid line is the modeled values and the dots are the experimental data.

100 bar and 20.4°C is estimated to 0.856 g/ml. Since the system is closed the density will remain constant throughout the experiment, and equation (42) can be applied to make a theoretical P(T) curve. Figure 2 shows the pressure as function of temperature, the experimental data is presented as dots and the model as a solid line. The reason for the divergence of the experimental data from the model might be that the system is not completely closed. The divergence correspond to a loss of approx 50 mg of CO<sub>2</sub>.

Since equation (42) yields the molar volume dependence on pressure and tem-

Table 3

Values for HSP for CO<sub>2</sub>. Reference values are found in literature.[12] Calculated values are based on equation (42), (16), (23) and (32).

values	$T$	$P$	$V_m$	$\delta_d$	$\delta_p$	$\delta_h$
	[°C]	[bar]	[ml/mol]	[MPa <sup>1/2</sup> ]	[MPa <sup>1/2</sup> ]	[MPa <sup>1/2</sup> ]
reference	25	905	39.13	15.6	5.2	5.8
calculated	75	300	57.34	9.7	4.3	4.5

perature, equation (16), (23) and (32) and be applied to determine how  $\delta_d$ ,  $\delta_p$  and  $\delta_h$  depend on pressure and temperature. Suitable reference values are found in literature and listed in table 3.[12] Table 3 further lists the modeled values at 300 bar and 75°C.

At first sight, it appears peculiar that  $\delta_h$  is not zero for CO<sub>2</sub>, because pure CO<sub>2</sub> would not contain hydrogen bonds. At least two explanations why  $\delta_h$  is not zero exist. Firstly, the method of determining HSP is not based on CO<sub>2</sub> itself, but on how it mixes with other materials with known HSP. Therefore there is a possibility that CO<sub>2</sub> would make hydrogen bonds to the solvent it is mixed with, e.g. alcohols. Secondly, it must be emphasized that in the solubility parameter approach the term *hydrogen bonding* is defined rather loosely, and some more ambiguous term such as weak chemical bonds or association bonds might be better.[14] However, historical considerations favor continuation of this loose usage, with the understanding that some  $\pi$ -bonds, quadrupole and octapole interactions, and probably other yet unnamed forces are included in  $\delta_h$ . CO<sub>2</sub> is known for showing quadrupole interactions.[8]

## 4 HSP for silicone

No suitable reference values for HSP for silicone rubber is found in literature. Therefore it is necessary to determine a set of HSP before determining the changes as function of pressure and temperature.

### 4.1 Reference values

Slides with a thickness of 1.00 mm of Elastosil LR 3003/10 shore A, supplied by Wacker Silicones (Germany) are used as model material, denoted Elastosil in the following. HSP for this silicone rubber material is determined by the conventional experimental method of placing a piece of material (0.50 g) in 42 different solvents (10 ml) with known HSP and observing the solubility behaviour at 21°C and 1 bar.[11] Table 4 lists the experimentally obtained

solubility data and HSP values for the 42 solvents. Table 5 describes the different solubility grades (SG).

Table 4: Result from solubility determination experiment. The solubility grades (SG) are listed in table 5.

Name	$\delta_d$ [ $\sqrt{\text{MPa}}$ ]	$\delta_p$ [ $\sqrt{\text{MPa}}$ ]	$\delta_h$ [ $\sqrt{\text{MPa}}$ ]	$V_m$ [ $\frac{\text{mol}}{\text{L}}$ ]	SG
Acetone	15.5	10.4	7.0	74.0	6
Acetophenone	19.6	8.6	3.7	117.4	6
Aniline	19.4	5.1	10.2	91.5	6
Benzene	18.4	0.0	2.0	89.4	4
1-Butanol	16.0	5.7	15.8	91.5	6
n-Butyl acetate	15.8	3.7	6.3	132.5	4
$\gamma$ -Butyrolactone	19.0	16.6	7.4	76.8	6
Carbon tetrachloride	17.8	0.0	0.6	97.1	4
Chlorobenzene	19.0	4.3	2.0	102.1	4
Cyclohexanol	17.4	4.1	13.5	106.0	6
Diacetone alcohol	15.8	8.2	10.8	124.2	6
o-Dichlorobenzene	19.2	6.3	3.3	112.8	5
Diethyl ether	14.5	2.9	5.1	104.8	6
Diethylene glycol	16.6	12.0	20.7	94.9	6
N,N-Dimethylformamide	17.4	13.7	11.3	77.0	6
Dimethylsulfoxide	18.4	16.4	10.2	71.3	6
1,4-Dioxan	19.0	1.8	7.4	85.7	6
Ethanol	15.8	8.8	19.4	58.5	6
Ethanolamine	17.0	15.5	21.2	59.8	6
Ethylacetate	15.8	5.3	7.2	98.5	5
1,2-Dichloroethane	19.0	7.4	4.1	79.4	6
Ethylene glycol	17.0	11.0	16.0	55.8	6

*continues ...*

Table 4: (continued)

Name	$\delta_d$ [ $\sqrt{\text{MPa}}$ ]	$\delta_p$ [ $\sqrt{\text{MPa}}$ ]	$\delta_h$ [ $\sqrt{\text{MPa}}$ ]	$V_m$ [ $\frac{\text{mol}}{\text{L}}$ ]	SG
Ethylene glycol monobutyl ether	16.0	5.1	12.3	131.6	6
Ethylene glycol monoethyl ether	16.2	9.2	14.3	97.8	6
Ethylene glycol monomethyl ether	16.2	9.2	16.4	79.1	6
Formamide	17.2	26.2	19.0	39.8	6
n-Hexan	14.9	0.0	0.0	131.6	4
Isophorone	16.6	8.2	7.4	150.5	6
Methanol	15.1	12.3	22.3	40.7	6
Methyl ethyl ketone	16.0	9.0	5.1	90.1	6
Methyl isobutyl ketone	15.3	6.1	4.1	125.8	4
N-Methyl-2-pyrrolidone	18.0	12.3	7.2	96.5	6
Methylene dichloride	18.2	6.3	6.1	63.9	4
Nitroethane	16.0	15.5	4.5	71.5	6
Nitromethane	15.8	18.8	5.1	54.3	6
2-Nitropropane	16.2	12.1	4.1	86.9	NA
Propylene carbonate	20.0	18.0	4.1	85.0	6
Propylene glycol	16.8	9.4	23.3	73.6	6
Tetrahydrofuran	16.8	5.7	8.0	81.7	4
Toluen	18.0	1.4	2.0	106.8	4
Trichloroethylene	18.0	3.1	5.3	90.2	4
o-Xylene	17.8	1.0	3.1	121.2	4

The solubility grade is evaluated by denoting the 42 different solvents as either *good* or *bad* solvents. For Elastosil, solvents with a SG value of 1 to 5 are denoted as good solvents and only solvents with a SG value of 6 are denoted as bad solvents. This interpretation is chosen because Elastosil is an elastomer (a chemical gel) and the specimen will hence never be dissolved. Furthermore all solvents that give a physical change of the specimen are then attributed

Table 5  
Description of solubility grade (SG).

SG	Description
1	Totally dissolved - No residue
2	Almost totally dissolved - Small amount of residue
3	Not dissolved - Strongly gelled (large volume expansion) or partly dissolved
4	Not dissolved - Partly gelled (small volume expansion) or very slightly dissolved
5	Not dissolved - Whitens (no visible volume expansion)
6	Not dissolved - Remains clear

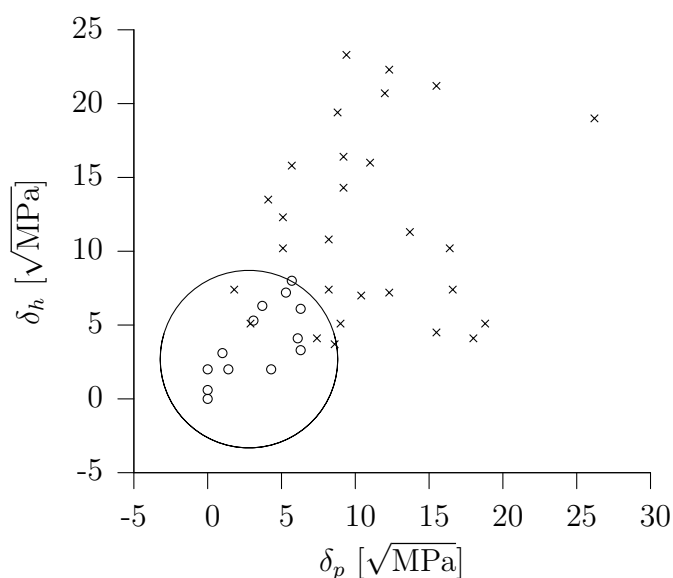


Fig. 3. Principle of experimental estimation of HSP. (o) are good solvents, (x) are bad solvents. The line is the calculated boundary between good and bad solvents.

properties similar to those of Elastosil.

A three dimensional HSP plot using  $\delta_d$ ,  $\delta_h$  and  $\delta_p$  as the three dimensions is made. Each solvent is plotted using its HSP and a symbol indicating whether it is a good (o) or a bad (x) solvent. The good solvents will tend to cluster on such a plot and therefore the plot can be separated into two zones. One zone containing the good solvents and one zone containing the bad solvents. The principle is illustrated in figure 3 where only the  $\delta_p$ -axis and  $\delta_h$ -axis are shown.

Ideally a sphere with radius  $R$  containing only good solvents can be drawn. The HSP for the compound is then given as the parameters at the center of the

Table 6  
Experimentally determined HSP values for Elastosil.

Parameter	Value
$\delta_d$ [ $\sqrt{\text{MPa}}$ ]	17.0
$\delta_p$ [ $\sqrt{\text{MPa}}$ ]	2.9
$\delta_h$ [ $\sqrt{\text{MPa}}$ ]	2.6
$R$ [ $\sqrt{\text{MPa}}$ ]	5.7
Data fit	0.9951

sphere. Often however there will be some bad solvents inside the sphere and some good solvents outside the sphere. To indicate the amount of failures of the system and to place the sphere where the amount of failures is minimized, a mathematical method is used.  $\delta_d$ ,  $\delta_p$ ,  $\delta_h$  and the solubility sphere radius ( $R$ ) can be found by optimizing the Data fit function given in equation (50) to approach 1 by changing  $\delta_d$ ,  $\delta_p$ ,  $\delta_h$  and  $R$ .

$$\text{Data fit} = \left( \prod_{i=1}^n A_i \right)^{\frac{1}{n}} \quad (50)$$

where  $A_i$  is Data fit for the  $i$ 'th solvent, given by equation (51)

$$A_i = \begin{cases} 1 & \text{if good solvent} \wedge \text{Ra} \leq R \\ \exp[R - \text{Ra}] & \text{if good solvent} \wedge \text{Ra} > R \\ \exp[\text{Ra} - R] & \text{if bad solvent} \wedge \text{Ra} < R \\ 1 & \text{if bad solvent} \wedge \text{Ra} \geq R \end{cases} \quad (51)$$

where  $\text{Ra}$  is the solubility parameter distance between two materials given by equation (52):

$$\text{Ra}^2 = 4(\delta_{ds} - \delta_{dp})^2 + (\delta_{ps} - \delta_{pp})^2 + (\delta_{hs} - \delta_{hp})^2 \quad (52)$$

The constant 4 in equation (52) is applied because if the  $\delta_d$  scale is doubled compared to the other two parameters, essential spherical rather than spheroidal regions of solubility are found.[14]

By applying this model  $\delta_d$ ,  $\delta_p$ ,  $\delta_h$  and  $R$  are determined to 17.0, 2.9, 2.6 and 5.7  $\sqrt{\text{MPa}}$  respectively, with a Data fit of 0.9951. The values are listed in table 6. The data represented in figure 3 are those obtained for Elastosil.

## 4.2 Pressure and temperature effects

According to section 2.2 HSP are highly dependent on  $V_m$ . In order to determine how HSP for Elastosil change with pressure and temperature, it is necessary to consider the isobaric coefficient of thermal expansion ( $\alpha$ ) and the isothermal compressibility ( $\beta$ ).

According to the supplier all Elastosil silicone materials have an  $\alpha$  of about  $3 \cdot 10^{-4} \text{ K}^{-1}$ . [16]

No literature value of the isothermal compressibility of Elastosil exist. A way to determine  $\beta$  is by using the relationship in equation (53): [17,18]

$$k_u \approx 11 \frac{E_c}{V_m} \quad (53)$$

where  $k_u$  is the bulk modulus. The relationship between  $\beta$  and  $k_u$  is given by equation (54):

$$\beta = \frac{1}{k_u} \quad (54)$$

According to literature this is probably the simplest and most accurate way of determining the cohesive energy density. [18] The constant 11 was determined by plotting  $k_u$  as function of the total cohesive energy density ( $\frac{E_c}{V_m}$ ) and fitting the best linear line. [17]

From the definition of the solubility parameters, cf. equation (55), and equation (53) and (54)  $\beta$  is given by equation (56):

$$\delta_c^2 = \frac{E_c}{V_m} = \frac{E_d}{V_m} + \frac{E_p}{V_m} + \frac{E_h}{V_m} = \delta_d^2 + \delta_p^2 + \delta_h^2 \quad (55)$$

$$\begin{aligned} k &\approx 11\delta_c^2 \\ \Downarrow \\ k &\approx 11(\delta_d^2 + \delta_p^2 + \delta_h^2) \\ \Downarrow \\ \beta &\approx \frac{1}{11(\delta_d^2 + \delta_p^2 + \delta_h^2)} \end{aligned} \quad (56)$$

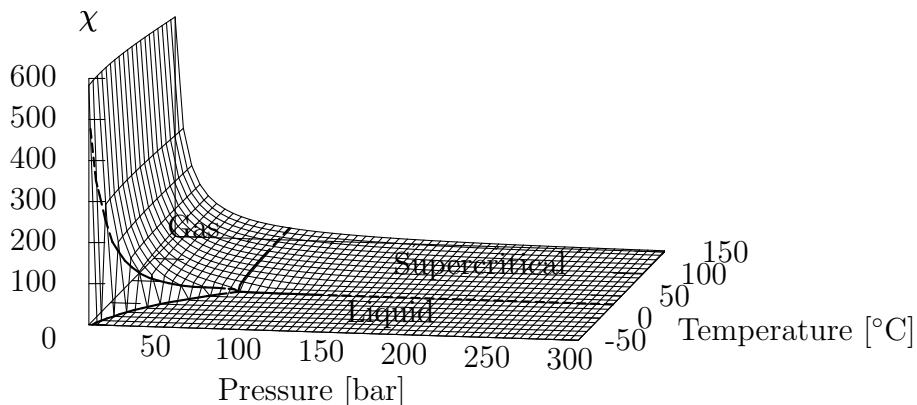


Fig. 4. Flory-Huggins interaction parameter ( $\chi$ ) between  $\text{CO}_2$  and Elastosil LR 3003/10 (silicone) as function of temperature and pressure.

By inserting the values for HSP for Elastosil listed in table 6 into equation (56)  $\beta$  can be estimated to  $2.9 \cdot 10^{-5} \text{ bar}^{-1}$ .

$\delta_d$ ,  $\delta_p$  and  $\delta_h$  for Elastosil can be modeled as function of pressure and temperature by applying equations (39) - (41). Reference values for  $\delta_d$ ,  $\delta_p$  and  $\delta_h$  at 21°C and 1 bar are determined and listed in table 6.

## 5 The compatibility between $\text{CO}_2$ and Elastosil LR 3003/10

In sections 3 and 4 it was shown how to model how HSP change for  $\text{CO}_2$  and Elastosil respectively as function of pressure and temperature. The enthalpic interaction between  $\text{CO}_2$  and Elastosil can be determined by applying these models to equation (5) giving the Flory-Huggins interaction parameter ( $\chi$ ). Figure 4 and 5 illustrate  $\chi$  as function of pressure and temperature.

In order to achieve a spontaneous mixing, the free energy of mixing ( $f_m$ ) must be negative. The enthalpy of mixing ( $\chi\phi(1-\phi)$ ) will always be positive or zero. This means that the smaller the  $\chi$  the more compatible are the two matters in concern.

The development of  $\chi$  in the supercritical phase is easily seen on figure 5. Furthermore it is seen that  $\text{CO}_2$  and Elastosil are the most compatible when  $\text{CO}_2$  is in its liquid state. In general both an increase in pressure and a decrease in temperature will enhance the compatibility. Figure 5 furthermore illustrates the tunability of the solvent properties of  $\text{scCO}_2$ , because  $\chi$  can be varied

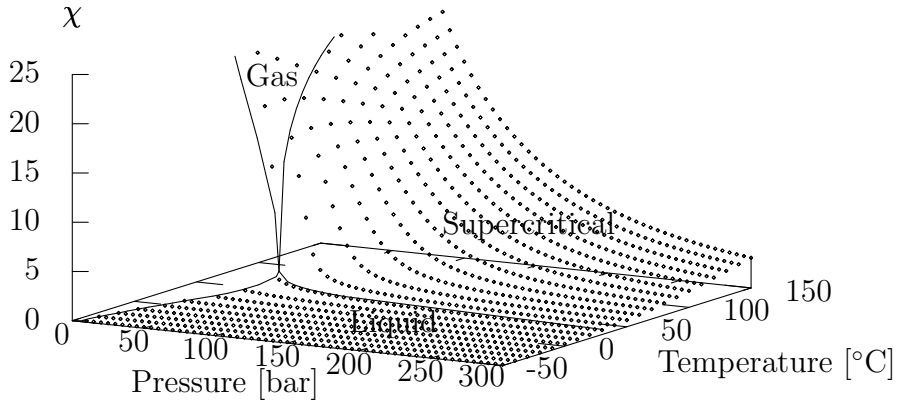


Fig. 5. Flory-Huggins interaction parameter ( $\chi$ ) between CO<sub>2</sub> and Elastosil with focus on the behavior in the supercritical phase.

simply by changing the pressure and temperature.

From equation (3) it is seen that  $\phi$  highly effects the entropy of the system. Figure 6 shows how the entropy changes with  $\phi$  when the number of polymer segments in a polymer chain ( $N$ ) is set to 100. The contribution from entropy (the shape of the curve in figure 6) does not change much when  $N$  is above 30 and practically not at values above 100. Therefore it is not crucial to know the true value of  $N$ . Figure 6 shows that in order to get the highest contribution to the free energy of mixing from entropy 63% of the volume should consist of Elastosil.

By applying a  $\phi$  value of 0.63 and the values for  $\chi$  given in figure 4 on equation (2) and (3) it is possible to determine how the free energy of mixing is changing as function of pressure and temperature. The curve in figure 7 shows where the free energy of mixing equals zero. Under the curve the free energy of mixing is positive and above it is negative. In the area where the free energy of mixing is negative, CO<sub>2</sub> and Elastosil are compatible. The curve in figure 7 have a characteristic shape. From -55°C to near  $T_c$  the curve follows the liquid-gas equilibrium, meaning that liquid CO<sub>2</sub> is compatible with Elastosil, whereas gaseous CO<sub>2</sub> is not. From near  $T_c$  the slope of the curve becomes steeper, splitting the supercritical phase of CO<sub>2</sub> into a compatible and a non-compatible part. This illustrates the tunability of near-critical and supercritical CO<sub>2</sub>.

When optimizing the experimental settings and choosing the best suited parameters of pressure and temperature, the compatibility between the two matters is only one thing to consider. The compatibility approach presented in this

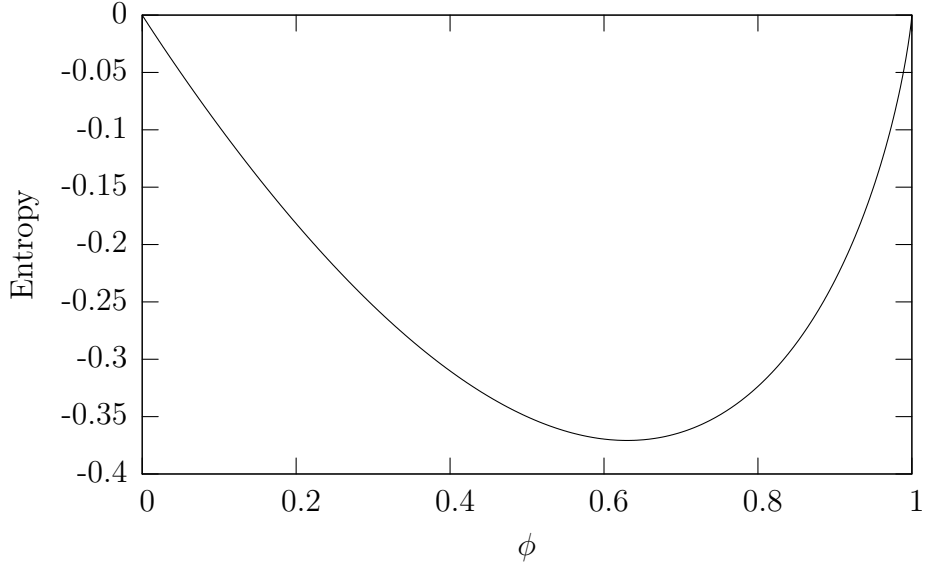


Fig. 6. The entropy contribution to the free energy of mixing, cf. the two first terms in equation (3).  $N$  is set to 100.

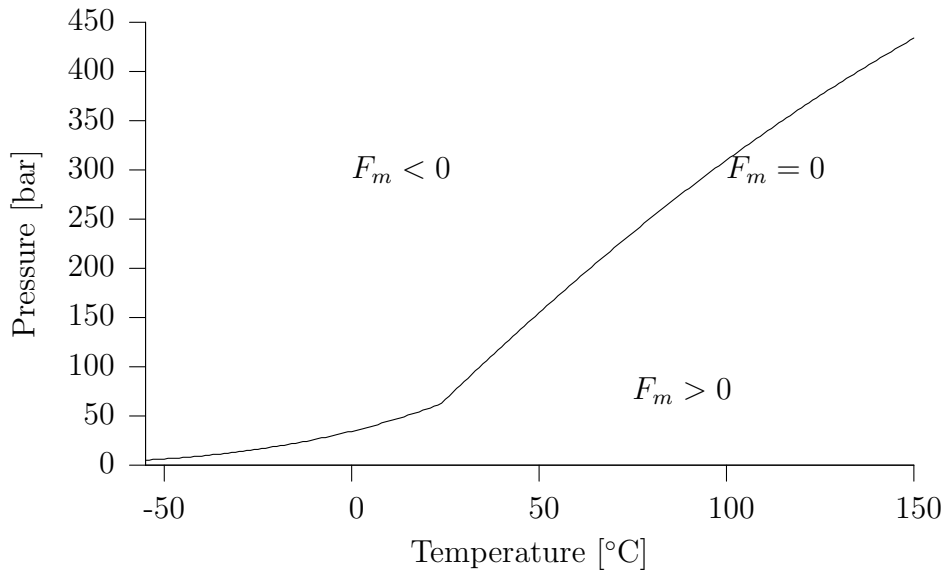


Fig. 7. The curve represents the pressure and temperature values where the free energy of mixing ( $F_m$ ) is zero for  $\text{CO}_2$  and Elastosil. Above the curve  $F_m$  is negative resulting in mixing, below the curve  $F_m$  is positive resulting in phase separation.  $N$  is set to 100, and  $\phi$  is set to 0.63.

article does not include a time scale dependence, it only tells if the *reaction* will occur, not how long time it takes. Therefore it is necessary to consider dependence of pressure and temperature on the considered *reaction*. The dependence of temperature on diffusion constants ( $D$ ) and chemical reaction rate constants ( $k$ ) are known to follow an Arrhenius type of behavior.[19,20] This means that both diffusion constants and chemical reaction rates increase with

an increase in temperature, and hence in general a temperature increase will speed up the considered process. The speed of the process should be considered in order to choose optimal experimental settings.

In the case of extracting free silicone oligomers from a cross-linked silicone matrix, liquid CO<sub>2</sub> would apparently be the best choice due to the better compatibility between silicone and CO<sub>2</sub>, c.f. figure 7. The diffusion constant ( $D_{\text{CO}_2}$ ) at approx. 51 bar and 15°C has been estimated by applying Fick's second law of diffusion in one dimension to be approx.  $8.9 \cdot 10^{-12} \frac{\text{m}^2}{\text{s}}$ . Industrially the free silicone oils are removed by heating the samples in an oven e.g. at 200°C for four hours.  $D_{\text{heat}}$  for the heat treatment has been estimated by applying Fick's second law of diffusion in one dimension to be in the size of  $1.0 \cdot 10^{-13} \frac{\text{m}^2}{\text{s}}$ . Comparing these values it is obvious that the removal of free silicone oils can be speeded up significantly by changing the traditional heat treatment with a treatment in liquid CO<sub>2</sub>. Since the positive effect of changing from heat treatment to liquid CO<sub>2</sub> is so large, there is at the moment, no incentive to use supercritical CO<sub>2</sub>. Whereas the temperature changes the speed of the process, the pressure changes the concentration (and hence  $\phi$ ) of the species in the mixture.

## 6 Conclusion

In this study the compatibility of CO<sub>2</sub> and silicone was quantified by applying the Flory-Huggins theory. It was shown that liquid and liquid-like supercritical CO<sub>2</sub> is compatible with silicone, whereas gaseous and gas-like supercritical CO<sub>2</sub> is non-compatible. It was shown that Hansen's solubility parameters (HSP) can be applied to determine the enthalpic interactions. Mathematical equations to model HSP's dependence of pressure and temperature were derived and applied. Furthermore HSP were determined for silicone to be  $\delta_d = 17.0\sqrt{\text{MPa}}$ ,  $\delta_p = 2.9\sqrt{\text{MPa}}$  and  $\delta_h = 2.6\sqrt{\text{MPa}}$ . The method presented in this article is generic and may be applied to other materials than silicone. From knowing HSP or the chemical structure of the material it is possible to estimate the compatibility with CO<sub>2</sub> as function of pressure and temperature.

## References

- [1] A. Colas, J. Curtis, Biomaterials science—An introduction to materials in medicine, 2nd Edition, Elsevier Academic Press, 525 B Street, Suite 1900, San Diego, California 92101–4495, USA, 2004, Ch. Application of materials in medicine, biology, and artificial organs: Medical applications of silicone, pp. 697–707.
- [2] A. R. LeBoeuf, Hydrophilic silicone compounds and contact lenses containing polymers thereof, Patent US004294974A.
- [3] R. A. Janssen, E. M. Ajello, R. D. Auten, G. S. Nomura, T. E. Shank, Process for graft polymerization of surfaces of preformed substrates to modify surface properties, Patent US005805264A.
- [4] D. G. Vanderlaan, I. M. Nunez, M. Hargiss, Silicone hydrogel polymers, Patent US006020445.
- [5] J. F. Kunzler, A. W. Martin, Contact lens material, Patent WO01/07523A1.
- [6] J. Karthausser, A method of producing an interpenetrating polymer network (ipn), the ipn and use thereof, Patent WO2005/003237 (2005) 1–35.
- [7] M. F. Kemmere, T. Meyer, Supercritical carbon dioxide - In polymer reaction engineering, Wiley-VCH, Weinheim, Germany, 2005.
- [8] E. J. Beckman, Supercritical and near-critical CO<sub>2</sub> in green chemical synthesis and processing, Journal of Supercritical Fluids 28 (2004) 121–191.
- [9] M. Doi, Introduction to polymer physics, Oxford science publications, Great Clarendon Street, Oxford OX2 6DP, New York, 2004.
- [10] A. F. M. Barton, Handbook of solubility parameters and other cohesion parameters, CRC press, Boca Raton Florida 33431, 1991.
- [11] C. M. Hansen, Hansen solubility parameters-A users handbook, CRC press, New York, 2000.
- [12] L. L. Williams, Removal of polymer coating with supercritical carbon dioxide, Ph.D. thesis, Colorado State University, Fort Collins, Colorado (2001).
- [13] J. H. Hildebrand, R. L. Scott, The solubility of nonelectrolytes, 3rd Edition, Vol. 17 of Monograph Series, Journal of the American Chemical Society, 350 West Forty-second Street, New York, USA, 1950.
- [14] C. M. Hansen, Solubility in the coatings industry, Farg och lack (1971) 69–77.
- [15] F.-H. Huang, M.-H. Li, L. L. Lee, K. E. Starling, F. T. H. Chung, An accurate equation of state for carbon dioxide, Journal of Chemical Engineering of Japan 18 (6) (1985) 490–496.

- [16] WackerSilicones, Processing elastosil  
lr liquid silicone rubber, <http://www.wacker.com>, Hanns-Seidel-Platz 4, 81737  
Mnchen, Germany (2006).
- [17] E. Morel, V. Bellenger, M. Bocquet, J. Verdu, Structure-properties relationships  
for densely cross-linked epoxide-amine systems based on epoxide or amine  
mixtures - part 3 elastic properties, *Journal of Materials Science* 24 (1989)  
69–75.
- [18] J.-P. Pascault, H. Sautereau, J. Verdu, R. J. J. Williams, *Thermosetting  
Polymers*, Marcel Dekker Inc., Basel, Switzerland, 2002.
- [19] J. Crank, G. S. Park, *Diffusion in polymers*, Academic press inc., Berkeley  
Square House, Berkeley Square, London, 1968.
- [20] R. Chang, *Physical chemistry—for the chemical and biological sciences*,  
University science books, 55D Gate Five Road Sausalito California, 2000, third  
edition.



## Chapter 3

# Swelling and diffusion

In chapter 2 the compatibility between CO<sub>2</sub> and PDMS was quantified.[6] In this chapter these results are applied to model the degree of swell of silicone in CO<sub>2</sub>. Furthermore the experiments that provide the basis for determining the diffusion constants for the extraction of un-cross-linked silicone oligomers out of silicone elastomer in liquid CO<sub>2</sub> and in heat treatment at 200°C, mentioned in chapter 2 are described.

The substrate material in an IPN is a three-dimensional network of polymer chains jointed at a number of connection sites, a gel.[26] In chemical gels these connections are due to chemical bonds (covalent) and in physical gels they are due to physical interactions such as the Van der Waal's forces. There are basically two ways to make a chemical gel; If the polymer contains a functional group a cross-linking agent reacting with the functional group, can be added to a system of polymer chains, causing them to form a network. The other approach is to form the network during the polymerization step, here a trivalent (or higher valency) segment (-B<) can be mixed with the divalent monomer (-A-), which result in cross-linking. Injection moulded silicone elastomers (LSR) are prepared by the first approach of reacting functional groups. As the cross-linking process proceeds the molecular weight increases, resulting in one giant polymer spanning the entire system. This gives an extremely high molecular weight and that is why gels are not soluble.

### 3.1 Swelling of gels

When producing IPNs the degree of swell of the substrate material is important. If a dried gel is placed in a solvent, it absorbs the solvent and its volume increases. This phenomenon is called gel swelling. The driving force in gel swelling is the free energy of mixing of the solvent and polymer ( $F_m$ ), which is quantified in chapter 2. If the polymer molecules were not joint together in a gel, they would be dissolved in the solvent to decrease the free energy of mixing. Swelling is however hindered by the change in elastic energy of the gel ( $F_{el}$ ) when the volume is increased. The free energy of mixing seeks to increase the volume of the gel, whereas the elastic energy seeks the unstressed state, i.e. decreasing the volume of the swelled gel. If there is enough solvent available the swelling establishes an equilibrium where these two forces compete to determine the volume of the gel. This is mathematically given by equation (3.1):[26]

$$F = F_m + F_{el} \quad (3.1)$$

where,  $F$  is the total Hemholtz free energy of the system,  $F_m$  is the free energy of

mixing and  $F_{el}$  is the elastic energy.  $F_m$  is estimated from the Flory-Huggins theory and is giving by equation (3.2):

$$F_m = \frac{V}{v_c} f_m(\phi) k_B T \quad (3.2)$$

where,  $V$  is the volume of the gel,  $v_c$  is the volume of a lattice site, thus  $\frac{V}{v_c}$  is the number of lattice sites occupied by the gel,  $f_m(\phi)$  is the free energy of mixing for one lattice site,  $\phi$  is the volume fraction of the gel and  $k_B$  is Boltzmanns constant. According to chapter 2  $f_m(\phi)$  is given by equation (3.3):

$$f_m(\phi) = \frac{1}{N} \phi \ln(\phi) + (1 - \phi) \ln(1 - \phi) + \chi \phi(1 - \phi) \quad (3.3)$$

where  $N$  is the number of repeating units in the gel and  $\chi$  is the Flory-Huggins interaction parameter. The first two terms in equation (3.3) are a measure of the entropy of the system whereas the last term is a measure of the enthalpy. The molecular weight of a gel is huge ( $N \sim 10^{20}$ ), therefore the first term in equation (3.3) can be neglected.  $F_{el}$  from equation (3.1) is given by equation (3.4):[26]

$$F_{el} = \frac{1}{2} n_c k_B T (E_{\alpha\beta})^2 \quad (3.4)$$

where  $n_c$  is the number of partial chains in the gel and  $E_{\alpha\beta}$  is the deformation gradient tensor, which is given by the type of deformation. Mathematical  $E_{\alpha\beta}$  is a 3x3 matrix where  $\alpha$  and  $\beta$  are the entries. Assuming that swelling of the gel gives an isotropic deformation,  $E_{\alpha\beta}$  is given by equation (3.5):[26]

$$\begin{aligned} E_{\alpha\beta} &= \left( \frac{V}{V_0} \right)^{1/3} \delta_{\alpha\beta} \\ &= \left( \frac{\phi_0}{\phi} \right)^{1/3} \delta_{\alpha\beta} \end{aligned} \quad (3.5)$$

where  $V_0$  and  $\phi_0$  are the volume and the volume fraction of the gel before expansion respectively, and  $\delta_{\alpha\beta}$  is a delta function which is 1 if  $\alpha = \beta$  and zero otherwise. Note that  $V\phi = V_0\phi_0$ . Substituting equation (3.5) into equation (3.4) gives equation (3.6):

$$\begin{aligned} F_{el} &= \frac{1}{2} n_c k_B T \left[ \left( \frac{\phi_0}{\phi} \right)^{1/3} \delta_{\alpha\beta} \right]^2 \\ \Downarrow \quad \delta_{\alpha\beta}^2 &= 3 \\ F_{el} &= \frac{3}{2} n_c k_B T \left( \frac{\phi_0}{\phi} \right)^{2/3} \end{aligned} \quad (3.6)$$

Substituting  $F_m$  (equation (3.2)) and  $F_{el}$  (equation (3.6)) into the total free energy of the system given by equation (3.1) and rearranging gives equation (3.7):

$$\begin{aligned}
F &= \frac{V}{\nu_c} f_m(\phi) k_B T + \frac{3}{2} n_c k_B T \left( \frac{\phi_0}{\phi} \right)^{2/3} \\
\Downarrow \quad V &= V_0 \frac{\phi_0}{\phi} \\
F &= \frac{V_0}{\nu_c} k_B T \left[ \frac{\phi_0}{\phi} f_m(\phi) + \frac{3}{2} \frac{n_c \nu_c}{V_0} \left( \frac{\phi_0}{\phi} \right)^{2/3} \right] \\
\Downarrow \quad \omega_c &= \frac{n_c}{V_0} \nu_c \\
F &= \frac{V_0}{\nu_c} k_B T \left[ \frac{\phi_0}{\phi} f_m(\phi) + \frac{3}{2} \omega_c \left( \frac{\phi_0}{\phi} \right)^{2/3} \right] \tag{3.7}
\end{aligned}$$

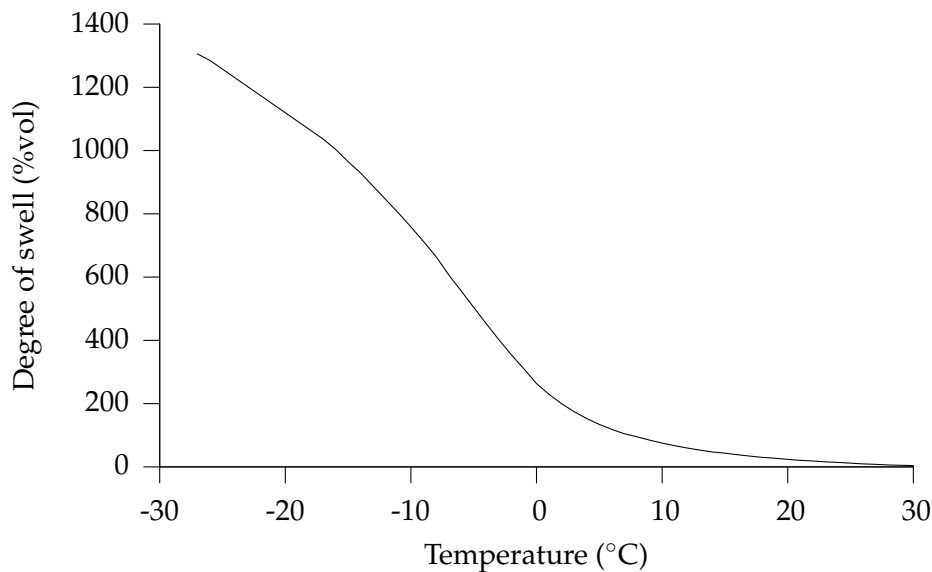
$\omega_c$  is the probability that a given lattice site is an entanglement, since it is the ratio of the number of partial chains in the gel ( $n_c$ ) (i.e. the number of entanglements) to the total number of lattice sites occupied by the gel ( $\frac{V_0}{\nu_c}$ ). Therefore  $\frac{1}{\omega_c}$  is a measure for the degree of cross-linking or entanglement, i.e. the number of lattice sites between entanglements.  $\frac{1}{\omega_c}$  for different types of silicone elastomers are listed in table 1.1. For LSR  $\frac{1}{\omega_c}$  is between 300 and 1000. The volume of the gel at equilibrium swell is given by the  $\phi$  that minimizes equation (3.7), i.e. where the partial differential of  $F$  with respect to  $\phi$  is zero. This is given by equation (3.8):

$$\begin{aligned}
\frac{\partial F}{\partial \phi} &= \frac{\partial}{\partial \phi} \left[ \frac{\phi_0}{\phi} f_m(\phi) + \frac{3}{2} \omega_c \left( \frac{\phi_0}{\phi} \right)^{2/3} \right] = 0 \\
\Downarrow \\
\frac{\partial F}{\partial \phi} &= \frac{\partial}{\partial \phi} \left[ \frac{\phi_0}{\phi} ((1 - \phi) \ln(1 - \phi) + \chi \phi(1 - \phi)) + \frac{3}{2} \omega_c \left( \frac{\phi_0}{\phi} \right)^{2/3} \right] = 0 \\
\Downarrow \\
\frac{\partial F}{\partial \phi} &= \phi + \ln(1 - \phi) + \chi \phi^2 + \omega_c \left( \frac{\phi}{\phi_0} \right)^{1/3} = 0 \tag{3.8}
\end{aligned}$$

Equation (3.8) can be used to determine the equilibrium  $\phi$  and hence the equilibrium degree of swelling. When the equilibrium  $\phi$  is determined, the volume of the swelled gel is given by  $V = \frac{V_0 \phi_0}{\phi}$ . The swell is then  $\frac{V - V_0}{V_0} \cdot 100\%$ . Table 3.1 lists the degree of swell in terms of %vol of silicone elastomer in CO<sub>2</sub> at different pressures and temperatures. Figure 3.1 shows the degree of swell of silicone elastomer in liquid CO<sub>2</sub> as function of temperature at the gas-liquid equilibrium. It is seen that a decrease in temperature increases the degree of swell of the silicone. Figure 3.2 shows the degree of swell of silicone elastomer as function of pressure at 75°C. It is seen that the degree of swell increases with pressure, and that the pressure needs to be above approx. 200 bar in order to swell silicone elastomer in CO<sub>2</sub> at 75°C. Elastosil LR 3003/10 shore A, which is

Table 3.1: Degree of swell of a silicone elastomer in CO<sub>2</sub> at different pressures and temperatures according to thermodynamics.

$P$ (bar)	$T$ (°C)	$\chi$	Swell (%vol)
46	10	0.84	75
52	15	1.02	43
200	75	2.17	5.9
300	75	1.10	35

Figure 3.1: Degree of swell of silicone elastomer in liquid CO<sub>2</sub> as function of temperature at the liquid gas interphase. Note the pressure is not constant, but varies with temperature according to the phase diagram, cf. figure 2.1.

used as a model material, has an elongation at break of 660% and would be destroyed if wrong experimental settings are used.[27] From figure 3.1 it is seen that the temperature should not be lower than approx -8°C at the gas-liquid equilibrium, and from figure 3.2 the pressure should not be above approx. 585 bar at 75°C in order not to break the silicone elastomer network. Destroying of the silicone elastomer network is observed experimentally when too cold liquid CO<sub>2</sub> is applied; after depressurization the silicone elastomers are swelled and fractures in the texture, depending on the silicone type, are observed.

## 3.2 Diffusion

One of the disadvantages with silicone elastomers for many applications is the presence of un-cross-linked silicone oligomers, further denoted as silicone oils. The silicone oils migrate to the surface and contaminate the surroundings. Unfortunately no common, available method to remove all of the silicone oils exists. Traditionally, silicone oils are removed by heat curing, a method including heating the injection moulded silicone elas-

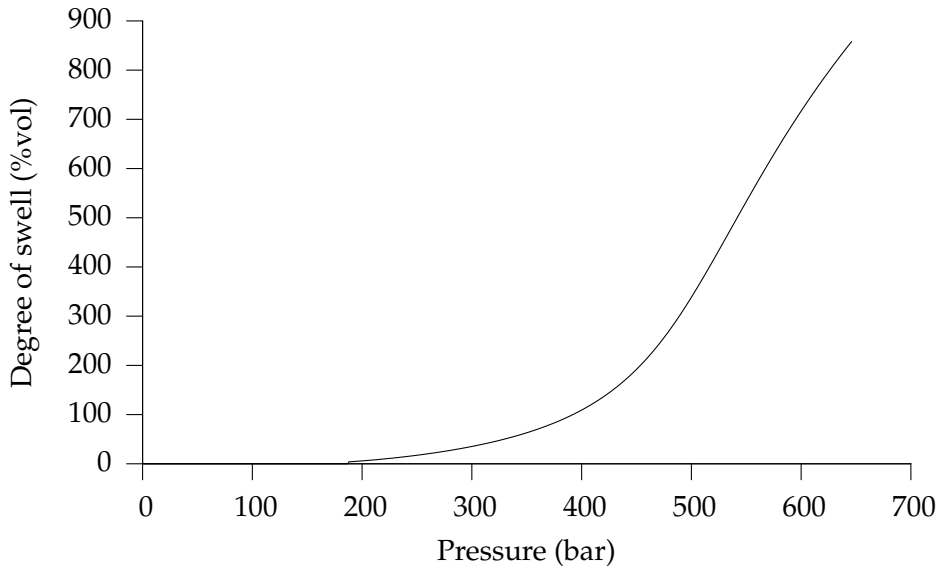


Figure 3.2: Degree of swell of silicone elastomer in scCO<sub>2</sub> as function of pressure at 75°C.

tomers in an oven at e.g. 200°C for 4 hours. Another approach could be to remove the silicone oils by extraction in liquid CO<sub>2</sub>. [2] In this section the diffusion of silicone oils out of the silicone elastomer is modeled. The diffusion constants in liquid CO<sub>2</sub> ( $D_{CO_2}$ ) and in heat treatment ( $D_{heat}$ ) are determined. The driving force in the removal of silicone oils from the matrix arises from differences in concentration and Fick's second law of diffusion can be applied to model the diffusion and determine the diffusion constants. Fick's second law of diffusion is given by equation (3.9): [28]

$$\frac{\partial C}{\partial t} = D \frac{\partial^2 C}{\partial x^2} \quad (3.9)$$

where  $C$  is the relative concentration of silicone oil,  $t$  is time and  $x$  is distance. In order to model the concentration of silicone oils throughout the silicone matrix as function of time and estimate  $D$ , equation (3.9) is solved by a numerical method, this is given by equation (3.10):

$$C_{t,x} = D \frac{C_{t-1,x-1} - 2C_{t-1,x} + C_{t-1,x+1}}{\Delta x^2} \Delta t + C_{t-1,x} \quad (3.10)$$

For the treatment in liquid CO<sub>2</sub> 25 discs of Elastosil LR 3003/10 shore A (diameter 10 mm, thickness 1 mm) are run in an industrial Wascator Liquid CO<sub>2</sub> machine supplied by Electrolux (Sweden). The Wascator run for one hour at parameters on the liquid-gas equilibrium at temperatures of 10–15°C, giving pressures in the range of approx. 46–52 bar, c.f. figure 2.1, and the degree of swell is between 43–75%vol, c.f. table 3.1 and figure 3.1. The Elastosil discs are weighed between each treatment, the obtained results are listed in table 3.2.

The diffusion of silicone oil occur in all directions, but since the ratio between the radius and half the thickness of the silicone elastomer is relative large radial diffusion can be neglected and it is only necessary to model the diffusion in one dimension. Half the height of the specimen is subdivided into 10 boxes giving a  $\Delta x$  of 50  $\mu\text{m}$ . The time step ( $\Delta t$ ) is set to 1 s. The concentration of silicone oil in bulk CO<sub>2</sub> is set to zero at all time

since the ratio of the initial silicone oil content in the silicone elastomer (approx. 7%wt of 25 g) to the amount of CO<sub>2</sub> (50 L) is very small. At time  $t = 0$  the relative concentration of silicone oil is 1 in all silicone boxes, and the total relative concentration of silicone oil in the silicone elastomer ( $C_{t,\text{silicone,model}}$ ) is given by equation (3.11):

$$C_{t,\text{silicone,model}} = \frac{\sum_{i=1}^{10} C_{t,i}}{i_{\text{max}}} \quad (3.11)$$

where  $i$  is an index denoting the boxes in the model. The weight loss as function of time has to be transferred into concentration, however the content of silicone oil in the silicone elastomer and the mass of the silicone elastomer are not known, hence the theoretical max weight loss is unknown. The measured masses are the sum of the silicone elastomer and the silicone oil. Since no changes (degradation, chemical reaction, etc.) of the silicone elastomer take place, the mass of the silicone elastomer is constant over time. The relative concentration of silicone oil in the silicone elastomer at all times ( $C_{t,\text{silicone,real}}$ ) can then be estimated from the measured masses and the initial silicone oil content in the silicone elastomer ( $\phi_{0,\text{silicone}}$ ) by equation (3.12):

$$C_{t,\text{silicone,real}} = \frac{m_t - m_0(1 - \phi_{0,\text{silicone}})}{m_0\phi_{0,\text{silicone}}} \quad (3.12)$$

The concentration of silicone oil in the silicone elastomer as function of time can now be modeled by knowing  $\phi_{0,\text{silicone}}$  and  $D$ . However, they are not known, but can be estimated by minimizing the root mean square error (RMSE) by changing  $\phi_{0,\text{silicone}}$  and  $D_{\text{CO}_2}$ . By setting  $\phi_{0,\text{silicone}}$  to 10%wt of the silicone matrix and  $D_{\text{CO}_2}$  to  $10^{-10} \frac{\text{m}^2}{\text{s}}$  and applying Microsoft Excel Solver function to minimize RMSE by changing  $\phi_{0,\text{silicone}}$  and  $D_{\text{CO}_2}$ , they are estimated to 7.3%wt and  $8.9 \cdot 10^{-12} \frac{\text{m}^2}{\text{s}}$  respectively, with a RMSE of 0.0045. The experimental and modeled values for  $\phi_{0,\text{silicone}}$  are shown in figure 3.3.

For the heat treatment a 250x250x1 mm<sup>3</sup> sheet of Elastosil LR 3003/10 Shore A is weighed and placed in a preheated oven at 200°C perpendicular to the flow in the oven. Each hour the sheet is weighed, table 3.2 include the obtained data. The method, assumptions and boundary conditions in the model are the same as for the liquid CO<sub>2</sub> treated samples.  $D_{\text{heat}}$  is optimized to  $1.0 \cdot 10^{-13} \frac{\text{m}^2}{\text{s}}$  with a RMSE of 0.0023. Figure 3.3 includes experimental and modeled values for  $\phi_{0,\text{silicone}}$  for heat treatment. By comparing  $D_{\text{CO}_2}$  and  $D_{\text{heat}}$  or looking at figure 3.3 it is obvious that the extraction of silicone oils is much faster and more efficient in liquid CO<sub>2</sub> than the traditional heat curing at 200°C. The ratio between  $D_{\text{CO}_2}$  and  $D_{\text{heat}}$  is approx. 85.

Table 3.2: Mass of silicone elastomer for determination of diffusion constants for extraction of silicone oil from the silicone elastomer in liquid CO<sub>2</sub> ( $m_{\text{CO}_2}$ ) and heat-treatment at 200°C ( $m_{\text{heat}}$ ).

Time (h)	$m_{\text{CO}_2}$ (g)	$m_{\text{heat}}$ (g)
0	25.7868	45.1800
1	25.0937	45.1050
2	24.7562	45.0620
3	24.5619	45.0380
4	24.4279	45.0210
5	24.3055	45.0072
6	24.2238	44.9895
7	24.1560	
8	24.0758	
9	24.0105	
10	23.9490	

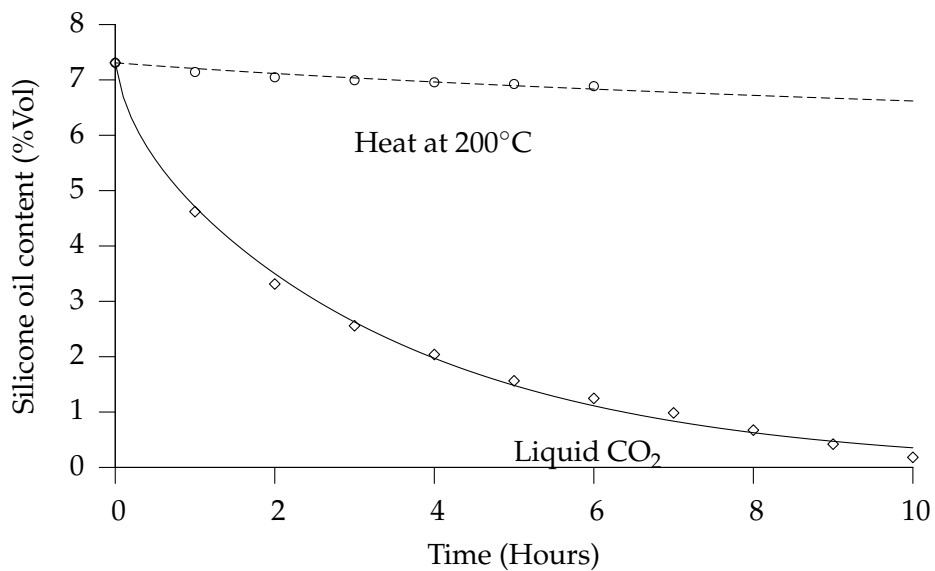


Figure 3.3: Experimental and modeled silicone oil content (%vol) in silicone elastomer during extraction in liquid CO<sub>2</sub> ( $\diamond$  (exp) and solid line (model)) and heat treatment at 200°C ( $\circ$  (exp) and dashed line (model)).



## Chapter 4

# 2-hydroxyethyl methacrylate

In chapter 2 and 3 the compatibility between CO<sub>2</sub> and silicone is quantified. It would therefore be convenient to examine how the other component of the IPN—2-hydroxyethyl methacrylate (HEMA), behaves in CO<sub>2</sub>. This chapter includes a characterization of the free radical polymerization of HEMA in scCO<sub>2</sub>. Two articles are included: "Free radical polymerization of 2-hydroxyethyl methacrylate in supercritical carbon dioxide" and "Kinetics of the free radical polymerization of 2-hydroxyethyl methacrylate in supercritical carbon dioxide".[7, 8]

One of the troublesome aspects of IPNs is, that it is rather difficult to analyze/test the result directly. Many of the analysis that can be made on IPNs give derivative results, that is information on the (physical) properties of the IPN. In order to get information on the polymerization progress experiments without silicone are run to make polymers suitable for analyzes like NMR, GPC and DSC. These analyzes are treated in the article "Free radical polymerization of 2-hydroxyethyl methacrylate in supercritical carbon dioxide", which further describes the development of the method to prepare polymers suitable for interpenetrating polymer networks. The kinetics of this polymerization is modeled in the article "Kinetics of the free radical polymerization of 2-hydroxyethyl methacrylate in supercritical carbon dioxide".

Two different initiators are considered for the polymerization: 2,2'-azobis(isobutyronitrile) (AIBN) and diethyl peroxydicarbonate (DEPDC). Both AIBN and DEPDC decompose in scCO<sub>2</sub> and are well described in literature.[19, 20, 29, 30] Due to transport and upscale issues of AIBN combined with the relative easy preparation of DEPDC, DEPDC is chosen as initiator. DEPDC is prepared as described in the article "Free radical polymerization of 2-hydroxyethyl methacrylate in supercritical carbon dioxide" and is applied as initiator.

# Free radical polymerization of 2-hydroxyethyl methacrylate in supercritical carbon dioxide

Martin Alm <sup>a,b,\*</sup>, Anne Marie Jensen <sup>a</sup>, Maike Benter <sup>a</sup>, and Kjeld Schaumburg <sup>b</sup>

<sup>a</sup>*Nanon A/S, Priorparken 878, 2605 Broendby, Denmark*

<sup>b</sup>*Roskilde University, Department of Life Sciences and Chemistry, Universitetsvej 1, 4000 Roskilde, Denmark*

---

## Abstract

This article describes the free radical polymerization of 2-hydroxyethyl methacrylate in supercritical carbon dioxide. It is found that an auto-acceleration takes place which in turn results in a chain-transfer to monomer leading to chemical cross-linking. This can be suppressed by addition of a co-solvent to ensure a homogeneous polymerization. Two different co-solvents are applied: ethanol and ethylene glycol. The tacticity of the produced polymers in terms of triads and pentads are analyzed by <sup>1</sup>H-NMR and <sup>13</sup>C-NMR. From analysis of the  $\alpha$ -CH<sub>3</sub> resonance signals from <sup>1</sup>H-NMR it is found that the produced polymers have approx. 6% isotactic, 37% heterotactic and 57% syndiotactic triads. The carbonyl carbon group give resonance signals with different chemical shifts sensitive to sequences of tactic pentads. The experimental results are in fairly good agreement with those calculated statistically from Bernoullian and Markov first order statistics.

*Key words:* Supercritical fluids, carbon dioxide, free radical polymerization, poly(2-hydroxyethyl methacrylate), tacticity

*PACS:*

---

## 1 Introduction

Polymers containing the 2-hydroxyethyl methacrylate (HEMA) unit have been widely used as biomaterials due to their ability to form hydrogels and hence reduce e.g. protein adsorption by minimizing the hydrophobic hydration.[1,2]

---

\* Corresponding author.

*Email address:* ma@nanon.dk (Martin Alm).

PHEMA hydrogels have been used, or suggested for use, in a wide range of biomedical applications: In contact lenses, as corneal replacement, as synthetic dural prosthesis, as artificial skin wound dressing, as artificial articulating surface for joint prostheses or osteochondral defect repair grafts, as cement to stabilize implants, as intervertebral disc prosthesis and as drug delivery system.[3]

Supercritical carbon dioxide (scCO<sub>2</sub>) has been proven to be a viable and promising medium for a number of polymerizations.[4-7] CO<sub>2</sub> has obvious advantages opposed to organic solvents. In particular, it is nontoxic, non-flammable and has a threshold limit value of 5000 ppm at 25°C. Furthermore CO<sub>2</sub> is relative cheap, widely available and has a mild critical temperature ( $T_c = 31.1^\circ\text{C}$ ) and pressure ( $P_c = 73.8$  bar) and tunable solvating properties.

The scope of this article is to develop a polymerization method which may be suitable for producing interpenetrating polymer networks of silicone and PHEMA in scCO<sub>2</sub>. [8] Different approaches to polymerize HEMA are found in literature. Bulk and solution polymerization of HEMA to produce porous polymeric bio-materials are described.[9] In another approach infrared laser is applied to introduce hydrogen peroxide groups on the surface of a silicone rubber substrate, which in turn can be decomposed thermally to initiate grafting of PHEMA on silicone.[10] Also living polymerizations (atom transfer free radical polymerization, ATRP) of HEMA is described in literature resulting in polymers with low polydispersities.[11,12] In a study of different stabilizers for the dispersion polymerization of HEMA in scCO<sub>2</sub> diblock-copolymers of polystyrene and poly(1,1-dihydroperfluorooctyl acrylate) is found to be the most effective.[13]

## 2 Experimental part

### 2.1 Methods and materials

98% 2-hydroxyethyl methacrylate (HEMA) with 200 ppm monomethyl ether hydroquinone (MEHQ) as inhibitor supplied by Acros Organics (Belgium) is passed through an inhibitor remover disposable column (Cat no. 306312) supplied by Aldrich (USA) for removal of inhibitor. HEMA is then purified by distillation at reduced pressure, and the fraction at 67°C and 3.5 mbar is collected and stored at 5°C under an N<sub>2</sub> atmosphere. 99.9% ethanol supplied by Merck (Germany), 99.9% ethylene glycol supplied by Acros Organics (Belgium), 98% ethyl chloroformate and molecular sieve UOP type 13X supplied by Fluka Chemie (Switzerland), NaOH pellets and 30% H<sub>2</sub>O<sub>2</sub> supplied by Bie & Berntsen (Denmark) and CO<sub>2</sub> N48 supplied by Air Liquide Denmark A/S

(Denmark) are all used as received.

## 2.2 Initiator synthesis

Diethyl peroxydicarbonate[14,15] (DEPDC) is synthesized by reacting 12 mL ethyl chloroformate with 6.64 mL 30%  $\text{H}_2\text{O}_2$  and 24 mL 5M NaOH in 100 mL pre-cooled demineralized water under stirring. The reactants are added in the given order drop by drop to ensure that the temperature never exceed  $10^\circ\text{C}$ . After stirring for another 10 min 50 mL of pre-cooled hexane is added to extract DEPDC under increased stirring speed for 5 min. The mixture is transferred to a separation funnel and the organic phase is collected. The extraction and separation are done twice. Traces of water are removed by adding molecular sieves. The produced DEPDC is stored in hexane with molecular sieves at  $-18^\circ\text{C}$ . The concentration of DEPDC in hexane is measured to 0.2 M by titration with iodine.[16] The initiator mixture is regularly examined by semi-quantitative peroxide test stick Quantofix supplied by Macherey-Nagel (Germany). Iodine titrations showed that DEPDC is stable at  $-18^\circ\text{C}$  for several months.

## 2.3 Polymerizations

A 16 mL stainless steel high-pressure reactor is used for the experiments. A Thar P-50 electrical driven high pressure pump from Thar Designs Inc. (USA) is applied for assuring the operation pressure. The pump is equipped with a heat exchanger and is supplied with cooling water at  $5^\circ\text{C}$ .

### 2.3.1 Polymerization method without co-solvent

In a typical experiment 0.64 mL HEMA and 0.05 mL 0.2 M DEPDC are added by syringe to the 16 mL stainless steel reactor equipped with a magnetic stirrer. Then the reactor is closed, placed in an oil bath at  $25^\circ\text{C}$  and pressurized with  $\text{CO}_2$  to approx. 60 bar under stirring. The oil bath is heated to  $75^\circ\text{C}$ , and  $\text{CO}_2$  is added to ensure a pressure of approx. 300 bar. After the polymerization (2 min – 24 h) the reactor is removed from the oil bath, and when the temperature returns to ambient temperature the pressure is released during 20–30 min.

## 2.4 Polymerization method with co-solvent

The experiments with co-solvent are carried out similar to those without, except for addition of 3.2 mL of either ethanol or ethylene glycol, which are added to the reactor before HEMA.

The polymers produced when ethanol is used as co-solvent, further denoted PHEMA(EtOH), are precipitated in diethyl ether, filtrated and redissolved in ethanol three times. The purified polymers are placed in a vacuum desiccator.

The polymers produced when ethylene glycol is used as co-solvent, further denoted PHEMA(EtGly), require an additional purification step. Ethylene glycol and diethyl ether are immiscible, therefore it is necessary to remove ethylene glycol before the produced polymers can be precipitated. Therefore, ethylene glycol is first removed by rotary evaporation at approx. 6 mbar, then the polymers are dissolved in ethanol and precipitated in diethyl ether and filtered three times. The purified polymers are placed in a vacuum desiccator.

## 2.5 Characterization

All molecular weights are determined by gel permeation chromatography (GPC) on a system consisting of a Knauer HPLC pump 64 and a Linear(2) and a 100 Å Phenomenex Phenogel 5 $\mu$  columns in series. Data are collected with a Knauer Differential-Refractometer. Dimethyl formamide (DMF) containing 5.0 mM LiBr is used as eluent with a flow rate of 0.5  $\frac{\text{mL}}{\text{min}}$ . The column temperature is 25°C. A series of near-monodisperse poly(methyl methacrylates) supplied by Polymer Standards Service (Germany) are used as calibration standard.

300 MHz  $^1\text{H}$  and 75 MHz  $^{13}\text{C}$  nuclear magnetic resonance spectra (NMR) are recorded in 99.9% ethanol( $\text{D}_6$ ) using a Varian Mercury Spectrometer.

Differential scanning calorimetry (DSC) measurements are carried out on a Mettler Toledo Star<sup>e</sup> thermal analysis modules DSC822<sup>e</sup>. The samples are heated from -60°C to 200°C with a heating speed on 10  $\frac{^\circ\text{C}}{\text{min}}$ , then quenched from 200°C to -60°C at -40  $\frac{^\circ\text{C}}{\text{min}}$  and then reheated from -60°C to 200°C with a heating speed of 10  $\frac{^\circ\text{C}}{\text{min}}$ . Melting points ( $T_m$ ) are taken from the first warm up and glass transition temperatures ( $T_g$ ) are determined for the second warm up.

### 3 Results

#### 3.1 Polymerization without co-solvent

All experiments without addition of co-solvent result in white insoluble polymers. Different pressure and temperature profiles are examined. The reactor is pressurized to approx. 100 bar at 25°C, so no refilling of CO<sub>2</sub> is needed, then placed in an oil-bath at 75°C. When the temperature of the oil-bath returns to 75°C (within a few minutes) the reactor is removed from the oil-bath and placed in an ice-bath for quenching. Even these polymerizations result in white insoluble polymers. Polymer samples placed in known solvents for PHEMA (methanol and ethanol) are not even dissolved after two years. The reason for this is discussed in section 4.1. To avoid to produce insoluble polymers, it is chosen to apply a co-solvent. Ethanol and ethylene glycol are chosen as co-solvents due to their ability to make homogeneous free radical polymerization of HEMA, furthermore ethanol is a solvent for PHEMA.

#### 3.2 Polymerization with co-solvent

Typical GPC profiles of PHEMA(EtOH) and PHEMA(EtGly) are shown in figure 1. Two peaks are seen on the profiles. For PHEMA(EtOH) the first peak is assigned a  $M_n$  of approx. 92.0 kDa and the second peak is assigned a value of approx. 21.0 kDa, according to the PMMA standard curve. For PHEMA(EtGly) the first peak is assigned a  $M_n$  of approx. 25.6 kDa and the second peak is assigned a value of approx. 11.3 kDa. PHEMA is known to give two peaks or one peak with a shoulder at either the high-molecular-weight side or the low-molecular-weight side, even when the polymerization is termed controlled or living.[11,12]

$T_g$  for PHEMA(EtGly) is determined to 86.2°C. Furthermore a melting endotherm is starting at 145°C with a peak max at 148.4°C. According to literature PHEMA has a  $T_g$  of 85°C.[17,18] However,  $T_g$  for PHEMA has been reported to depend on the tacticity.[19]

In figure 2 and 3 the <sup>1</sup>H-NMR spectra of PHEMA(EtOH) and PHEMA(EtGly) are illustrated. Figure 4 is a <sup>13</sup>C-NMR spectrum of PHEMA(EtOH). Table 1 lists the observed and expected chemical shifts and integrals of the peaks for the produced polymers. The expected values are found by applying the predict <sup>1</sup>H-NMR shifts function on a HEMA quadromer in ChemDraw Ultra 10.0 software from CambridgeSoft (USA).

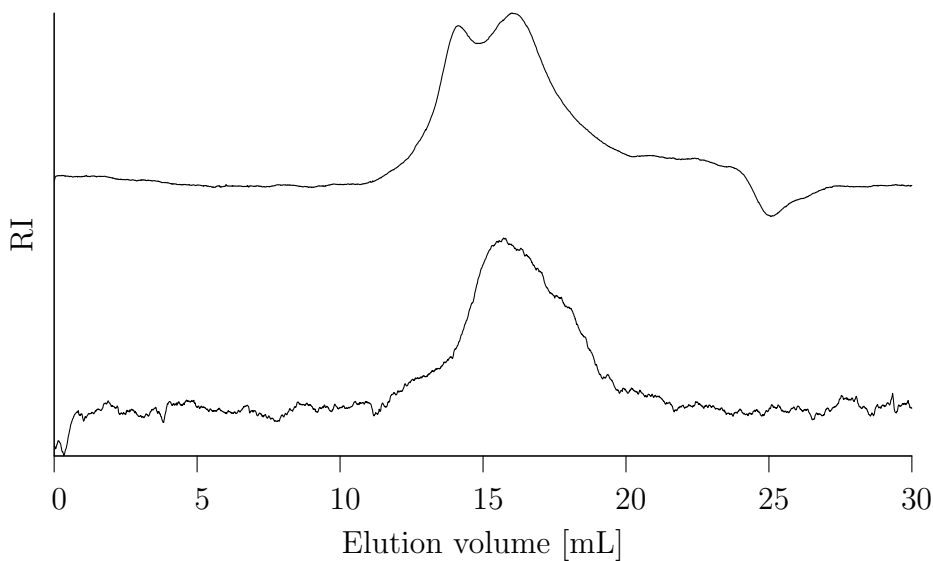


Fig. 1. GPC profiles of PHEMA(EtOH) (top) and PHEMA(EtGly) (bottom).

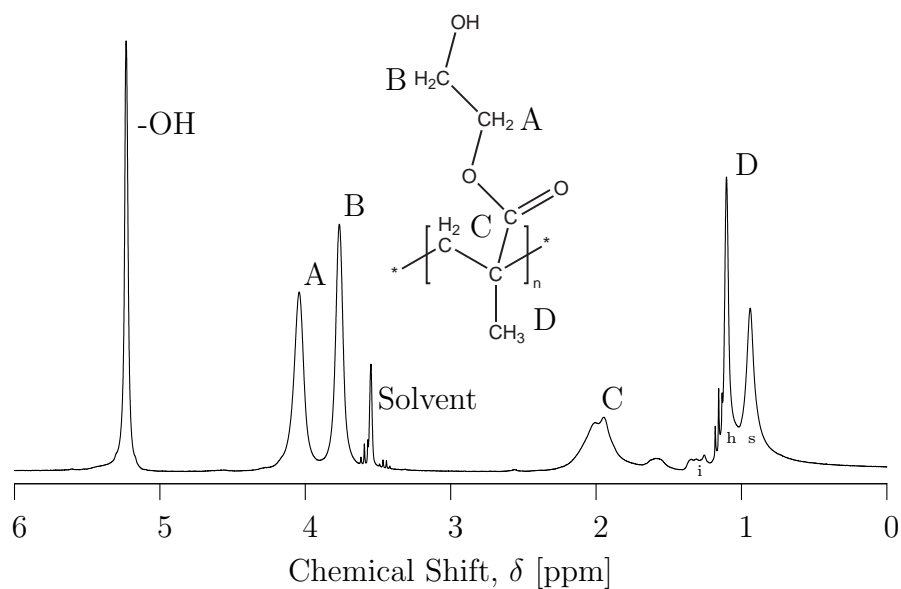


Fig. 2.  $^1\text{H}$ -NMR spectra of PHEMA(EtOH). i, h and s denote the isotactic (*mm*), heterotactic (*mr*) and syndiotactic (*rr*) triads respectively. The spectrum is recorded in ethanol( $\text{D}_6$ ).

## 4 Discussion

### 4.1 Polymerization without co-solvent

The produced polymers without addition of a co-solvent could not be dissolved in methanol and ethanol, even after two years. This strongly indicates that some kind of cross-linking has taken place during the polymerization.

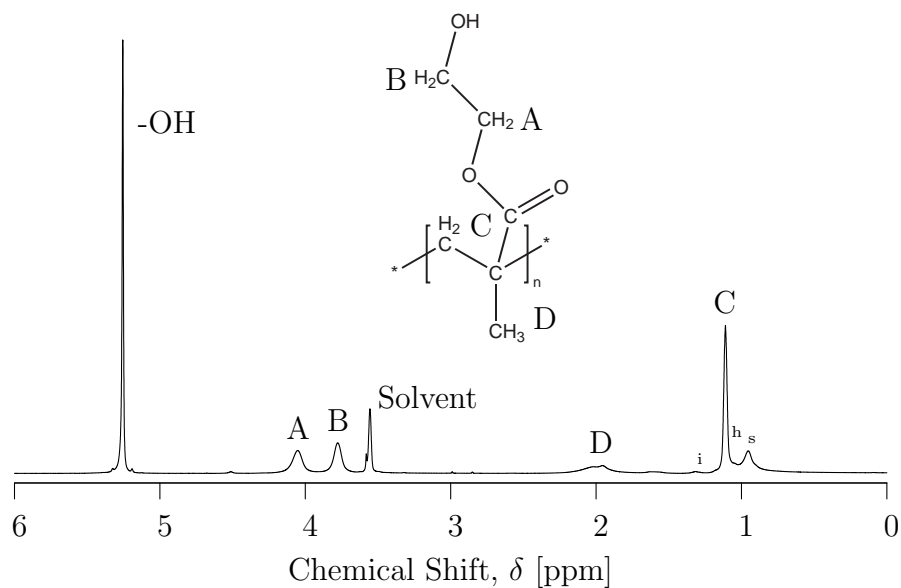


Fig. 3.  $^1\text{H-NMR}$  spectra of PHEMA(EtGly). i, h and s denote the isotactic ( $mm$ ), heterotactic ( $mr$ ) and syndiotactic ( $rr$ ) triads respectively. The spectrum is recorded in ethanol( $\text{D}_6$ ).

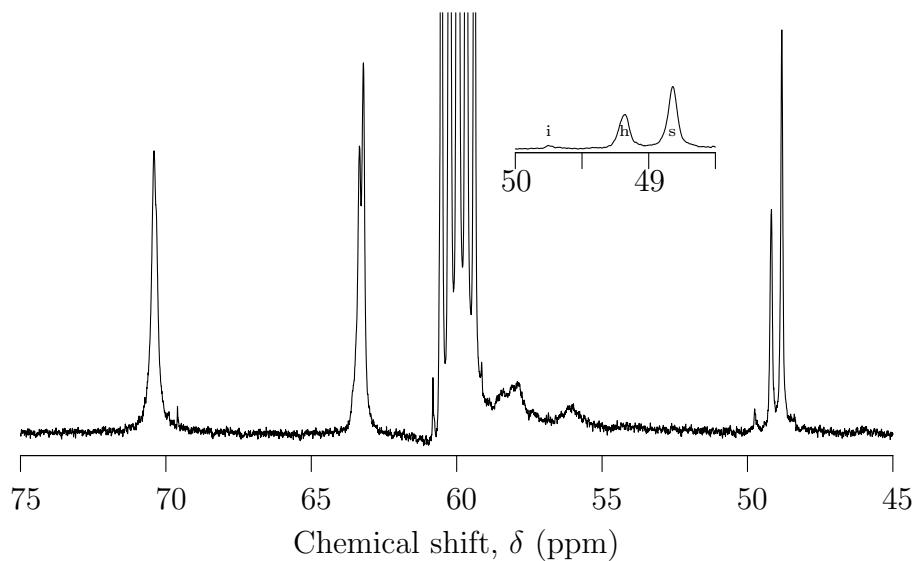


Fig. 4.  $^{13}\text{C-NMR}$  spectra of PHEMA(EtOH). The spectra is recorded in ethanol( $\text{D}_6$ ).

A central problem encountered in free radical polymerization of certain monomer types is an auto-acceleration in the rate of polymerization.[20] This phenomenon is known as the Trommsdorff effect, gel effect or Norris-Smith effect,[21] and occurs in bulk or concentrated solution polymerizations when the medium viscosities becomes too high, or in solution polymerization when the polymer precipitates.[22,23] Two propagating chains first undergo trans-

Table 1

Observed and calculated  $^1\text{H-NMR}$  resonance chemical shifts and integrals for the produced polymers.

Peak	PHEMA(EtOH)		PHEMA(EtGly)		Calculated <sup>a</sup>	
	$\delta$	Int	$\delta$	Int	$\delta$	Int
A	4.0	2.0	4.0	2.0	4.27	2
B	3.8	2.1	3.8	2.2	3.56	2
C	2.2–1.5	1.9	2.2–1.5	1.4	1.99	2
D	1.3–0.8	3.0	1.3–0.8	3.0	1.38	3

<sup>a</sup> Estimated values from the predict  $^1\text{H-NMR}$  shifts function on a HEMA quadromer in ChemDraw Ultra 10.0 software from CambridgeSoft (USA).

lational diffusion<sup>1</sup> until they are within proximity of one another. Next, the chain-end radicals come within a given reaction radius via segmental diffusion<sup>2</sup>. Finally, the two radicals react.[20,21,23]

Precipitated polymer has a reduced chain mobility, with the result that the chain-end radicals have a lower probability of being in a position to terminate. Because smaller monomer molecules can still diffuse to the active chain-ends even when the rate of termination decreases, there is a marked increase in the rate of polymerization and hence an auto-acceleration.[22] Because polymerization is exothermic the temperature increases, this further enhances initiation, and may result in an uncontrolled process, sometimes even an explosion.[23]

The Trommsdorff effect is known to take place in free radical polymerization of methacrylates.[20] If enough energy is present a side reaction may occur. The side reaction shown in figure 5 is suggested in literature.[24] A free radical reacts with the methyl group on the methacrylate instead of the vinyl group and makes a methylene radical by chain-transfer to monomer. The structure of the formed radical is based on electron spin resonance (ESR) experiments.[24] These experiments further showed, that the presence of the methyl group is necessary to observe the formation of the radical. The formed radical may lead to a chemical gel since it has two binding sites.

The chain-transfer to monomer reaction shown in figure 5 can proceed due

<sup>1</sup> Diffusion of center-of-mass of the individual macroradical coils toward each other through the reaction medium.

<sup>2</sup> Rearrangement of the two chains so that the two radical ends are sufficiently close for a chemical reaction. This process happens by rouse or reptation kinetics depending of the length of the polymer chains and concentration.

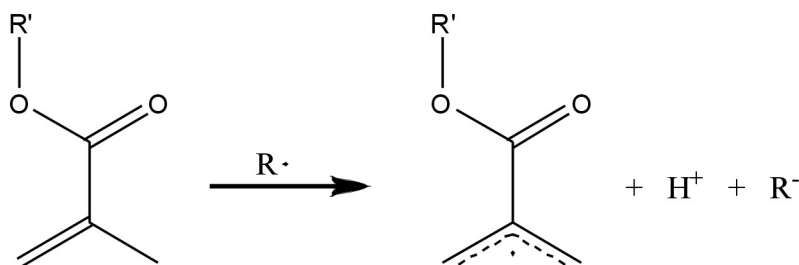


Fig. 5. Reaction scheme for the chain-transfer to monomer, in which a methylene radical is formed.[24]

to the excess energy produced by the auto-accelerated exothermic polymerization. This may be realized by considering the homolytic bond dissociation energies.[25] The excess energy makes it possible to break a H-C single bond on a methyl group on the HEMA unit.

Three things can be done to hinder or even avoid the Trommsdorff effect, and hence suppress production of insoluble polymer materials:

- Addition of a stabilizer (block-copolymer) to prevent precipitation by making emulsion polymerization.[13]
- Addition of (co-)solvent to prevent precipitation.[20]
- Addition of a chain transfer agent.[20]

When polymerizing in  $scCO_2$  a stabilizer is often applied in order to obtain higher molecular weights and avoid precipitation.[26,27] However, that approach is not feasible in the scope of preparing interpenetrating polymer networks, since it is very difficult if not impossible to control emulsions inside a swelled substrate material. Dispersion polymerizations are governed by a delicate interplay that includes the partitioning and interactions of all of the reaction mixture components.[13] In this work the addition of a co-solvent to prevent a precipitation is chosen. Two different solvents are chosen as co-solvents: ethanol and ethylene glycol.

#### 4.2 Polymerization with co-solvent

To overcome the Trommsdorff effect ethanol or ethylene glycol are applied as co-solvents. In a typical experiment 20%Vol of co-solvent in respect to the reactor volume is used, this is enough to avoid the Trommsdorff effect and cross-linking side-reaction.

The tacticity of the produced polymers can be determined from the  $^1H$ - and  $^{13}C$ -NMR spectra.[28] Due to the pseudo-asymmetric nature of a methacrylate backbone, two adjacent repeating units (a diad) can be placed in two different ways: *meso* (*m*) and *racemic* (*r*) configurations. If the chemical structure is

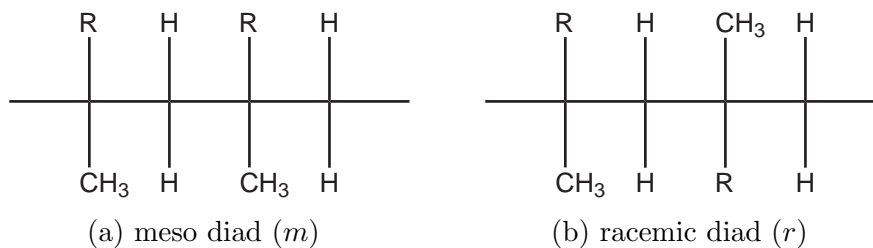


Fig. 6. R is the 2-hydroxyethyl ester ( $\text{COOCH}_2\text{CH}_2\text{OH}$ ) group on HEMA. In figure (a) and (b) are shown a meso and a racemic diad respectively.

Table 2

Mole fractions of the isotactic ( $mm$ ), heterotactic ( $mr$ ) and syndiotactic ( $rr$ ) triads on the produced polymers predicted by  $^1\text{H-NMR}$  analysis of the  $\alpha$ -methyl group.

	i	h	s	
Polymer	( $mm$ )	( $mr$ )	( $rr$ )	$B^a$
PHEMA(EtOH)	0.064	0.366	0.570	1.08
PHEMA(EtGly)	0.052	0.388	0.560	0.77

$$^a B = \frac{4(mm)(rr)}{(mr)^2}.$$

represented by a rotated Fisher projection, the side groups are placed on the same side of the polymer backbone in a meso diad. In a racemic diad they are placed on opposite sides. The meso and racemic diads for PHEMA are illustrated in figure 6.

There are three distinctive triads: isotactic ( $i = mm$ ), heterotactic ( $h = mr = rm$ ) and syndiotactic ( $s = rr$ ). The  $\alpha$ -methyl group (peak D) on the  $^1\text{H-NMR}$  spectra splits into these three triads, as can be seen on figure 2 and 3. The mole fraction of each triad is determined from the distribution of the integrals of the three peaks, and are listed in table 2.

Generally free radical polymerization of acrylates have been found to follow Bernoullian statistics.[29–31]<sup>3</sup> If the polymerization can be described by Bernoullian statistics,  $B$ , listed in table 2, should be between 0.5 and 2.[31] As can be seen in table 2 the obtained  $B$  values are within these limits.

The analysis of the carbonyl carbon ( $\text{C=O}$ )  $^{13}\text{C-NMR}$  resonances is interesting because of the sensitivity of this group to the stereochemical configuration of surrounding units in terms of pentads. Figure 7 shows the spectrum of the  $\text{C=O}$  resonances for PHEMA(EtOH). The assignment of the signals for

<sup>3</sup> If a polymerization is Bernoullian, the type of diad already existing in the growing chain does not influence on the stereochemistry of the addition of the new monomer unit, only the configuration of the ultimate tertiary (or quaternary) carbon atom in the chain has an influence.

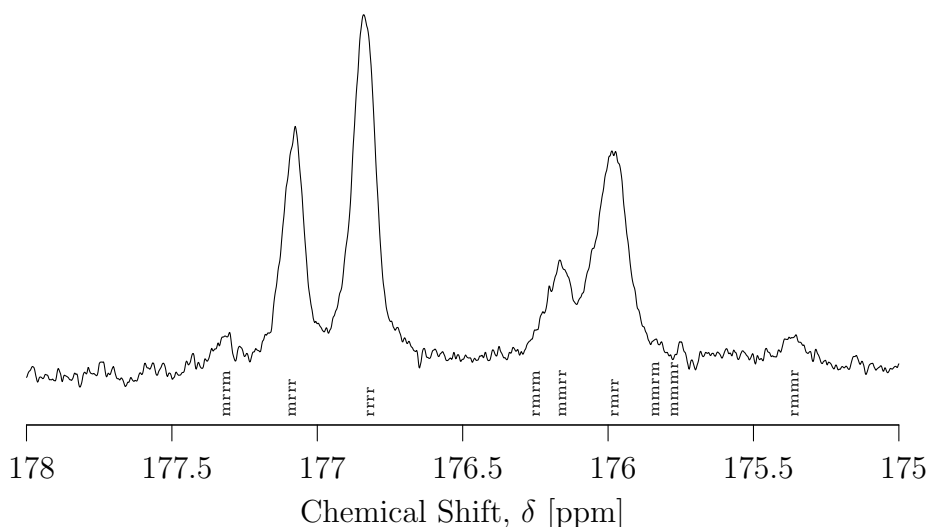


Fig. 7.  $^{13}\text{C}$ -NMR spectra of the C=O resonances for PHEMA(EtOH).

PHEMA has been reported in literature.[30]

The mole fractions of the ten different pentad sequences can be determined from the measured triad mole fractions, listed in table 2, by applying the equations listed in table 3. Table 3 includes both the equations for Bernoullian and Markov first order statistics. Furthermore table 3 lists the observed and modeled mole fractions of the pentads determined from the carbonyl carbon.

There is a rather good fit between the modeled and measured mole fractions, which is illustrated in figure 8 where the measured and calculated mole fractions for each pentads are plotted. As can be seen from figure 8 Markov first order statistics gives a better fit than the Bernoullian. This suggest that the penultimate repeating unit might have some influence on the tacticity of the addition of a new monomer unit to the propagating polymer chain. There is a good agreement with the mole fractions obtained in this study with reported values in literature.[29,30,32,33]

## 5 Conclusion

The free radical polymerization of 2-hydroxyethyl methacrylate in supercritical carbon dioxide has been examined. It is found that if no co-solvent is used, an auto-acceleration occurs, which facilitates a side-reaction that leads to a highly cross-linked polymer material. Ethanol and ethylene glycol are used as co-solvents.

The tacticity of the produced polymers with co-solvent have been analyzed.

Table 3

Equations to model the pentad mole fractions from triad mole fractions. Equations for both Bernoullian statistics and Markov first order statistics are included. Furthermore the measured and calculated mole fractions are listed.

Pentad	Measured		Bernoullian <sup>a</sup>		Markov <sup>b,c</sup>	
	$\delta$ (ppm)	Int	model	cal	model	cal
<i>mrrm</i>	177.3	0.015	$\sigma^2(1 - \sigma)^2$	0.037	$\frac{uw^2(1-w)}{(u+w)}$	0.034
<i>mrrr</i>	177.1	0.199	$2\sigma(1 - \sigma)^3$	0.211	$\frac{2uw(1-w)^2}{(u+w)}$	0.210
<i>rrrr</i>	176.8	0.354	$(1 - \sigma)^4$	0.303	$\frac{u(1-w)^3}{(u+w)}$	0.326
<i>rmrm</i>	176.3	0.034	$2\sigma^2(1 - \sigma)^2$	0.073	$\frac{2u^2w^2}{(u+w)}$	0.066
<i>mmrr</i>	176.2	0.071	$2\sigma^2(1 - \sigma)^2$	0.073	$\frac{2uw(1-u)(1-w)}{(u+w)}$	0.071
<i>rmrr</i>	176.0	0.284	$2\sigma(1 - \sigma)^3$	0.211	$\frac{2u^2w(1-w)}{(u+w)}$	0.206
<i>mmrm</i>	175.8	0.017	$2\sigma^3(1 - \sigma)$	0.025	$\frac{2uw^2(1-u)}{(u+w)}$	0.023
<i>mmmr</i>	175.7	0.005	$2\sigma^3(1 - \sigma)$	0.025	$\frac{2uw(1-u)^2}{(u+w)}$	0.024
<i>rmmr</i>	175.4	0.021	$\sigma^2(1 - \sigma)^2$	0.037	$\frac{u^2w(1-u)}{(u+w)}$	0.035
<i>mmmm</i>	—	—	$\sigma^4$	0.004	$\frac{w(1-u)^3}{(u+w)}$	0.004

<sup>a</sup>  $\sigma = \sqrt{(mm)}$  is the probability for a *m* diad and  $1 - \sigma$  is the probability for an *r* diad.

<sup>b</sup>  $w = P_{r/m} = 1 - P_{r/r} = \frac{(mr)}{2(rr)+(mr)}$  is the probability that an *r* diad is followed by an *m* diad.

<sup>c</sup>  $u = P_{m/r} = 1 - P_{m/m} = \frac{(mr)}{2(mm)+(mr)}$  is the probability that an *m* diad is followed by an *r* diad.

The good agreement between statistical and experimental results supports the assignment of peaks and the validity of the statistical parameters considered, according to the model of stereochemical distribution described above. Furthermore it is found that supercritical carbon dioxide does not change the stereochemical distribution of the produced polymers, compared to conventional solvent polymerizations of HEMA.

## Acknowledgements

The authors would like to thank Annette Christensen for making the <sup>1</sup>H-NMR measurements, and Lene V. Overby for making the DSC measurements. Paul Charpentier for supplying the recipe for producing the initiator (DEPDC).

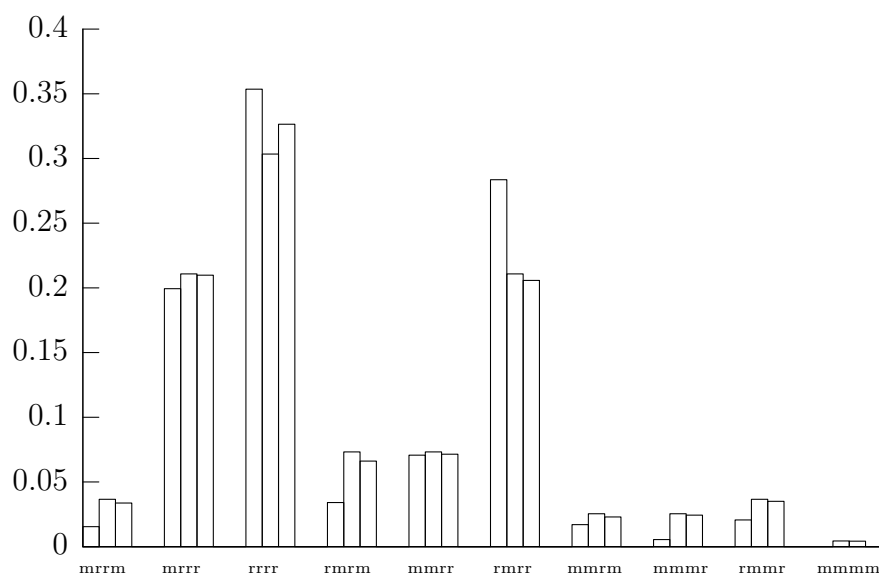


Fig. 8. Measured and calculated mole fractions of the ten different pentads from  $^{13}\text{C}$ -NMR spectra of the C=O resonances for PHEMA(EtOH). The first pillar is the measured mole fraction. The middle and the right pillars are calculated values from Bernoullian and Markov first order statistics respectively.

## References

- [1] C. Tanford, *The hydrophobic effect*, 2nd edition, Wiley-Interscience, John Wiley and Sons, Inc., Heboken, New Jersey, USA, **1980**.
- [2] Ishihara, K.; Nomura, H.; Kurita, K.; Iwasaki, Y.; Nakabayashi, N. *Journal of Biomedical Materials Research*, **1998**, *39*, 323.
- [3] Meakin, J. R.; Hukins, D. W. L.; Aspden, R. M.; Imrie, C. T. *Journal of Materials Science: Materials in Medicine*, **2003**, *14*, 783.
- [4] Kendall, J. L.; Canelas, D. A.; Young, J. L.; DeSimone, J. M. *Chemical Review*, **1999**, *99*, 543.
- [5] Kemmere, M. F.; Meyer, T., *Supercritical carbon dioxide - In polymer reaction engineering*, Wiley-VCH, Weinheim, Germany, **2005**.
- [6] Beckman, E. J. *Journal of Supercritical Fluids*, **2004**, *28*, 121.
- [7] Cooper, A. I. *Journal of Materials Chemistry*, **2000**, *10*, 207.
- [8] Karthausser, J. *A method of producing an interpenetrating polymer network (IPN), the IPN and use thereof*, Patent:WO2005/003237, **2005**.
- [9] Seidel, J. M.; Malmonge, S. M. *Materials Research*, **2000**, *3*, 79.
- [10] Khorasani, M. T.; Mirzadeha, H.; Sammes, P. G. *Radiation Physics and Chemistry*, **1999**, *55*, 685.

- [11] Ishizu, K.; Khan, R. A.; Ohta, Y.; Furo, M. *Journal of Polymer Science: Part A: Polymer Chemistry*, **2004**, *42*, 76.
- [12] Weaver, J. V. M.; Bannister, I.; Robinson, K. L.; Bories-Azeau, X.; Armes, S. P.; Smallridge, M.; McKenna, P. *Macromolecules*, **2004**, *37*, 2395.
- [13] Shiho, H.; DeSimone, J. M. *Journal of Polymer Science; Part A: Polymer Chemistry*, **2000**, *38*, 3783.
- [14] Charpentier, P. A. *Preparation of DEPDC*, Personal communication, **2004**.
- [15] Xu, W. Z.; Li, X.; Charpentier, P. A. *Polymer*, **2007**, *48*, 1219.
- [16] American Standard Methods *Standard test methods for assay of organic peroxides: E298-01*, 100 Barr Harbor Drive, West Conshohocken, PA USA, **2001**.
- [17] SigmaAldrich, *Poly(2-hydroxyethyl methacrylate)*, webpage: <http://www.sigmaaldrich.com/catalog/search/ProductDetail/ALDRICH/529265>, **2007**.
- [18] Brandrup, J.; Immergut, E. H.; Grulke, E. A. *Polymer handbook*, 4th edition, Wiley-Interscience, John Wiley and Sons, USA, **1999**.
- [19] Sung, Y. K.; Gregonis, D. E.; Russell, G. A.; Andrade, J. D. *Polymer*, **1978**, *19*, 1362.
- [20] O'Neil, G. A.; Wisnudel, M. B.; Torkelson, J. M. *Macromolecules*, **1996**, *29*, 7477.
- [21] Odian, G. *Principles of polymerization*, 4th edition, Wiley-Interscience, John Wiley and Sons, Hoboken, New Jersey, USA, **2004**.
- [22] Stevens, M. C. *Polymer chemistry, an introduction*, Oxford university press, 198 Madison Avenue, New York 10016, **1999**.
- [23] Matyaszewski, K.; Davis, T. P. *Handbook of radical polymerization*, 1st edition, Wiley-Interscience, John Wiley and Sons, 605 third avenue, New York, USA, **2002**.
- [24] Billaud, C.; Sarakha, M.; Bolte, M. *European Polymer Journal*, **2000**, *36*, 1401.
- [25] Morrison, R. T.; Boyd, R. N. *Organic Chemistry*, 5th edition, Allyn and Bacon, Inc., 7 Wells Avenue, Newton, Massachusetts, USA, **1987**.
- [26] Wang, W.; Griffiths, R. M. T.; Giles, M. R.; Williams, P.; Howdle, S. M. *European Polymer Journal*, **2003**, *39*, 423.
- [27] Giles, M. R.; Griffiths, R. M. T.; Irvine, D. J.; Howdle, S. M. *European Polymer Journal*, **2003**, *39*, 1785.
- [28] Hatada, K.; Kitayama, T. *NMR spectroscopy of polymers*, Springer-Verlag, Berlin, Germany, **2004**.
- [29] Gallardo, A.; Roman, J. S. *Polymer*, **1994**, *35*, 2501.

- [30] Roman, J. S.; Gallardo, A. *Polymer Engineering and Science*, **1996**, *36*, 1152.
- [31] Pino, P.; Suter, U. W. *Polymer*, **1976**, *17*, 977.
- [32] Gregonis, D. E.; Russell, G. A.; Andrade, J. D. *Polymer*, **1978**, *19*, 1279.
- [33] Verhoeven, J.; Peschier, L. J. C.; van Det, M. A.; Bouwstra, J. A.; Junginger, H. E. *Polymer*, **1989**, *30*, 1942.

# Kinetics of the free radical polymerization of 2-hydroxyethyl methacrylate in supercritical carbon dioxide

Martin Alm <sup>a,c,\*</sup>, Harald Behl <sup>b</sup>, and Kjeld Schaumburg <sup>c</sup>

<sup>a</sup>*Nanon A/S, Priorparken 878, 2605 Broendby, Denmark*

<sup>b</sup>*Mettler-Toledo AutoChem, Inc., 7075 Samuel Morse Drive, Columbia, MD 21046, USA*

<sup>c</sup>*Roskilde University, Department of Life Sciences and Chemistry, Universitetsvej 1, 4000 Roskilde, Denmark*

---

## Abstract

The kinetics of the free radical polymerization of 2-hydroxyethyl methacrylate (HEMA) in supercritical carbon dioxide (scCO<sub>2</sub>), in which ethylene glycol is applied as a co-solvent, is examined by *in-situ* FT-IR online reaction monitoring. The method has been shown feasible and it is possible to model the polymerization progress. It is found that the free radical polymerization follows steady state kinetics and the ratio between the rate of propagation and the square root of rate of termination ( $\frac{k_p}{\sqrt{k_t}}$ ) has been determined to  $0.23 \frac{1}{\sqrt{M s}}$ .

*Key words:* online reaction monitoring, FT-IR, PHEMA, supercritical fluids, carbon dioxide, polymerization kinetics

*PACS:*

---

## 1 Introduction

Most biological processes require a wide variety of ions and molecules to move about in proximity, i.e. being soluble in a common solvent. Water serves as the universal intracellular and extracellular medium. This arises primarily from water's tendency to form hydrogen bonds and its dipolar character.[1]

---

\* Corresponding author.

*Email address:* ma@nanon.dk (Martin Alm).

Many synthetic polymers which have been shown to be bio-compatible contains groups capable of forming hydrogen bonds, such as poly(2-hydroxyethyl methacrylate) (HEMA), poly(N-vinyl pyrrolidone) (PVP), poly(ethylene oxide) and poly(ether urethane).[2,3] Soft contact lenses are an application in which hydrogels containing PHEMA has found extensive use.[1,4]

Supercritical carbon dioxide (scCO<sub>2</sub>) has been demonstrated to be a promising alternative reaction medium for free radical polymerizations.[5,6] Particular advantages of CO<sub>2</sub> are associated with a pronounced lowering of viscosity, facilitating separation of CO<sub>2</sub> from the polymeric product and with the inertness of CO<sub>2</sub>. In a recent article the free radical polymerization of HEMA in scCO<sub>2</sub> was described.[7] It was found that addition of a co-solvent was necessary in order to avoid an auto-acceleration and a subsequent cross-linking side reaction. Addition of 20%Vol ethanol or ethylene glycol was found sufficient to suppress this side reaction. Furthermore it was found that the tacticity could be described by Bernullian statistics. In this article the kinetics of this polymerization is determined. The kinetics is described by high pressure *in-situ* ATR-FTIR online reaction monitoring.

The kinetics of the free radical polymerization of HEMA in bulk and in 1-butanol has been described in literature.[8,9] The propagation rate coefficient ( $k_p$ ) was determined by pulsed laser polymerization (PLP)/size-exclusion chromatography (SEC) technique.[9] It is reported that  $k_p$  values for polymerization in 1-butanol are slightly below those obtained in bulk, but the deviations are within the limits of experimental accuracy.  $k_p$ 's dependence of temperature (at ambient pressure) is given by equation (1):[9]

$$\ln k_p = A - \frac{E_a}{RT} \quad (1)$$

where  $A$  is the pre-exponential factor,  $E_a$  is the activation energy,  $R$  is the gas constant and  $T$  is the absolute temperature.  $A$  is 16.1 and  $\frac{E_a}{R}$  is 2677 K at ambient pressure giving an  $E_a$  of 22.3  $\frac{\text{kJ}}{\text{mol}}$ .  $k_p$ 's dependence of pressure (at 30°C) is given by equation (2):[9]

$$\ln k_p = C + \frac{\Delta V^\ddagger \cdot P}{RT} \quad (2)$$

where  $C$  is the pre-exponential factor,  $\Delta V^\ddagger$  is the activation volume and  $P$  is the pressure.  $C$  is 7.37 at 30°C and  $\frac{\Delta V^\ddagger}{RT}$  is  $6.03 \cdot 10^{-4}$  giving a  $\Delta V^\ddagger$  of 15.2  $\frac{\text{mL}}{\text{mol}}$  at 30°C.[9] Unfortunately no value for  $k_t$  is given by Buback and Kurz.

The rate coefficients for propagation ( $k_p$ ) and termination ( $k_t$ ) for the free radical bulk photo-polymerization of HEMA have been determined at 30°C and

ambient pressure to  $k_p = 1000 \frac{1}{\text{M s}}$  and  $k_t = 1.1 \cdot 10^6 \frac{1}{\text{M s}}$  respectively by differential scanning calorimetry (DSC).[8] However, Buback and Kurz[9] notes that  $k_p$  from ref.[8] is determined by a conventional procedure [DSC] which may be associated with significant uncertainty. Moreover  $k_t/k_p$  calculated from the individual  $k_p$  and  $k_t$  values in ref.[8] is stated to be in conflict with the  $k_t/k_p$  value directly measured for HEMA by SP-PLP technique.[9,10]

It might be expected that chemically controlled reaction steps such as initiation and propagation is only moderately affected by the presence of CO<sub>2</sub>, whereas CO<sub>2</sub> might have a strong impact on the diffusion-controlled termination step.[5]  $k_p$  is moderately influenced by CO<sub>2</sub>. Reductions up to 40% compared to values obtained in bulk polymerizations have been found.[5] Modeling of polymerizations where the polymer is soluble in scCO<sub>2</sub> may be carried out using  $k_p$  values from bulk polymerizations.[5]

In contrast to chemically controlled propagation, the termination reaction is diffusion controlled. It is to be expected that the termination rate constant may increase upon addition of CO<sub>2</sub>, as the viscosity is lowered and diffusion is increased. For methacrylates an enhancement of  $k_t$  by a factor of 4 upon addition of CO<sub>2</sub> compared to bulk is typical found.[5]

In this study diethyl peroxydicarbonate (DEPDC) has been applied as initiator. The kinetics of the decomposition of DEPDC in supercritical CO<sub>2</sub> has been reported in literature.[11,12] The decomposition of DEPDC is illustrated in figure 2a. Two different methods have been used to describe the decomposition kinetics of DEPDC, a radical scavenger in the temperature range of 65–85°C,[11] and *in-situ* ATR-FTIR in the temperature range of 40–60°C.[12] The activation energy ( $E_a$ ) and pre-exponential factor ( $A_d$ ) for the decomposition of DEPDC in scCO<sub>2</sub> is found to be slightly higher when the radical scavenger approach is used compared to the *in-situ* ATR-FTIR approach. This might be due to not all the free radicals from the decomposition reacting with the radical scavenger.[12] Table 1 lists values for the rate of decomposition ( $k_d$ ) and the initiator efficiency ( $f$ ) found in literature.[11,12]

## 2 Experimental

### 2.1 Methods and materials

98% 2-hydroxyethyl methacrylate (HEMA) with 200 ppm monomethyl ether hydroquinone (MEHQ) as inhibitor supplied by Acros Organics (Belgium) is passed through an inhibitor remover disposable column (Cat no. 306312) supplied by Aldrich (USA) for removal of inhibitor. HEMA is then purified

Table 1

Diethyl peroxydicarbonate decomposition parameters in supercritical carbon dioxide.[11,12]

Temperature	Pressure	$k_d$	$f$
[°C]	[bar]	[s <sup>-1</sup> ]	[-]
40	105	$8.7 \cdot 10^{-6}$	NA <sup>a</sup>
45	121	$2.0 \cdot 10^{-5}$	NA
50	137	$3.4 \cdot 10^{-5}$	NA
55	152	$7.0 \cdot 10^{-5}$	NA
60	168	$1.4 \cdot 10^{-4}$	NA
65	300	$2.4 \cdot 10^{-4}$	0.58
70	300	$4.3 \cdot 10^{-4}$	0.69
75	300	$9.9 \cdot 10^{-4}$	0.60
70	300	$33 \cdot 10^{-4}$	0.63

<sup>a</sup> NA: not available.

by distillation at reduced pressure, and the fraction at 67°C and 3.5 mbar is collected and stored at 5°C under an argon atmosphere over molecular sieves. 99.9% ethylene glycol supplied by Acros Organics (Belgium), 98% ethyl chloroformate and molecular sieve UOP type 13X supplied by Fluka Chemie (Switzerland), NaOH pellets and 30% H<sub>2</sub>O<sub>2</sub> supplied by Bie & Berntsen (Denmark) and CO<sub>2</sub> N48 supplied by Air Liquide Denmark A/S (Denmark) are all used as received.

## 2.2 Initiator synthesis

Diethyl peroxydicarbonate[12,13] (DEPDC) is synthesized by reacting 12 mL ethyl chloroformate with 6.64 mL 30% H<sub>2</sub>O<sub>2</sub> and 24 mL 5M NaOH in 100 mL pre-cooled demineralized water under stirring. The reactants are added in the given order drop by drop to ensure that the temperature never exceed 10°C. After stirring for another 10 min 50 mL of pre-cooled hexane is added to extract DEPDC under increased stirring speed for 5 min. The mixture is transferred to a separation funnel and the organic phase is collected. The extraction and separation are done twice. Traces of water are removed by adding molecular sieves. The produced DEPDC is stored in hexane with molecular sieves at -18°C. The concentration of DEPDC in hexane is measured to 0.15 M by titration with iodine.[14] The initiator mixture is regularly examined by semi-quantitative peroxide test stick Quantofix supplied by Macherey-Nagel

(Germany). Iodine titrations showed that DEPDC is stable at  $-18^{\circ}\text{C}$  for several months.

### 2.3 Polymerizations

The experimental setup is illustrated in figure 1. The free radical polymerization of HEMA in  $\text{scCO}_2$  with ethylene glycol as co-solvent is carried out in a high pressure, window-equipped, stainless steel reactor (3) ( $V = 73.4$  mL) (Max Planck, Germany) coupled to a high pressure online ATR-FTIR element (1,2) (ReactIR 1000, Mettler Toledo). Vigorous mechanical stirring (2000 rpm) ensured a homogenous mixture (6). In addition, a small dosing unit for HEMA (5) is connected to the reactor via a needle valve. The reactor (3) is loaded with ethylene glycol (14.7 ml) and  $\text{CO}_2$  (44.4 g) in the given order and heated (4) to the desired reaction temperature ( $75^{\circ}\text{C}$ ) (7) ensuring a pressure of approx. 300 bar (8). When the experimental conditions is stable a FT-IR background is taken (1,2), i.e. the background is on the 20%Vol ethylene glycol and  $\text{CO}_2$  mixture at the reaction conditions. Simultaneous with the addition of HEMA (2.9 mL) by diffusion from the filled dosing unit (5), IR monitoring (1) is started. No temperature change (7) is detected inside the reactor (3) under these conditions.

After approx. one hour the absorption at  $814\text{ cm}^{-1}$  (including carbon-carbon double bond (C=C) stretching frequency) achieved a constant value meaning that all HEMA is transferred to the reactor and a homogenous mixture is obtained. Then DEPDC (1.5 mL 0.15 M) is added by the HPLC pump (9) during one minute. An exotherm of approx.  $5^{\circ}\text{C}$  is immediately registered due to the heat produced from the free radical polymerization of HEMA.

During the experiment the reactions shown in figure 2 are expected to occur.

## 3 Results

Figure 3 shows the FT-IT spectra of the reaction mixture at different times. Furthermore figure 3 include the interpretation of the peaks. The polymerization progress of HEMA is clearly seen. As the characteristic peaks for C=C in HEMA are diminished, new peaks for methylene ( $-\text{CH}_2-$ ) in PHEMA are produced.

Figure 4 shows two spectra of the in-situ FT-IR monitoring of the free radical polymerization of HEMA. It is seen from figure 4 that high monomer conversion is reached within four hours. It is in accordance with literature that high

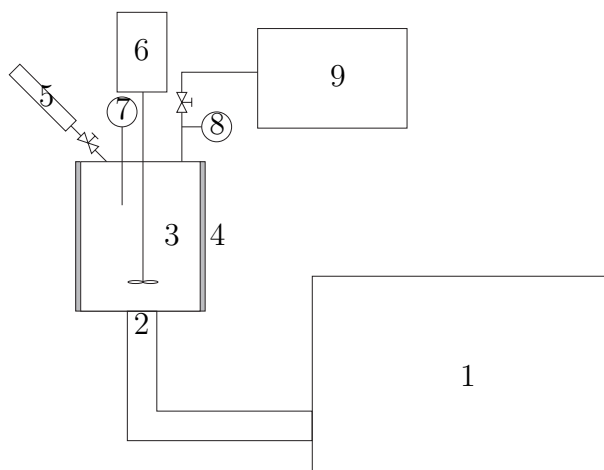
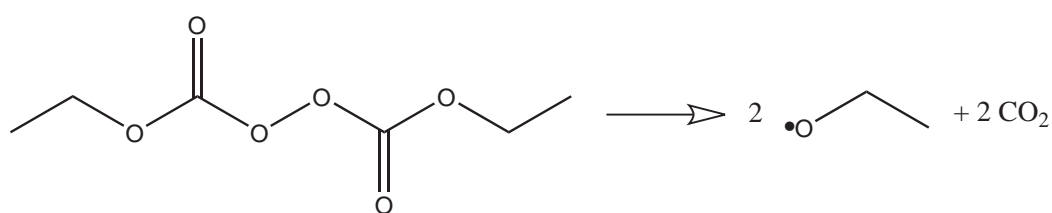
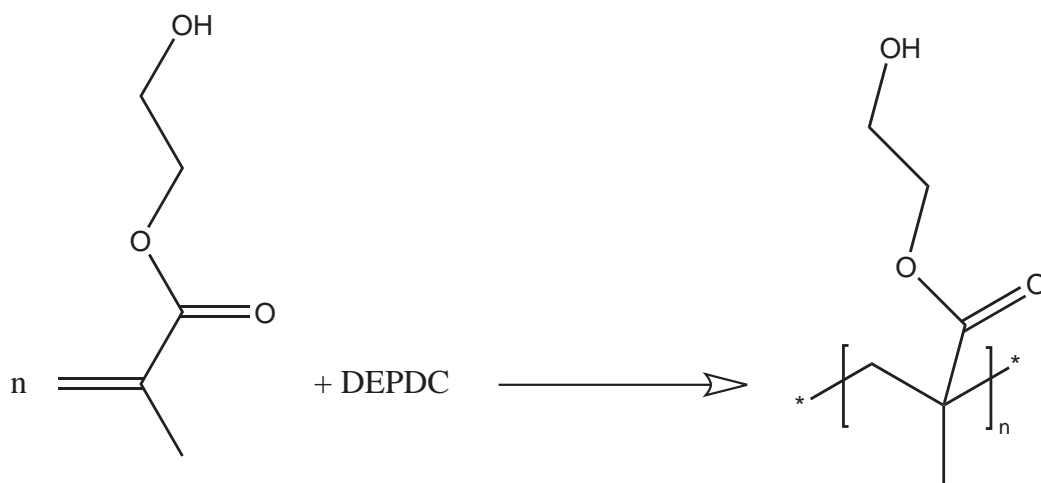


Fig. 1. Illustration of the experimental setup. 1 is the FT-IR equipment, 2 is the ATR-FTIR mirror which is special designed to scCO<sub>2</sub>, 3 is the reactor, 4 is the electrical heating jacket, 5 is the dosing unit, 6 is the mixing unit, 7 is the electric thermocouple, 8 is the electrical pressure transmitter and 9 is the HPLC pump.



(a)



(b)

Fig. 2. Reaction scheme for (a) the decomposition of DEPDC and (b) the polymerization of HEMA.

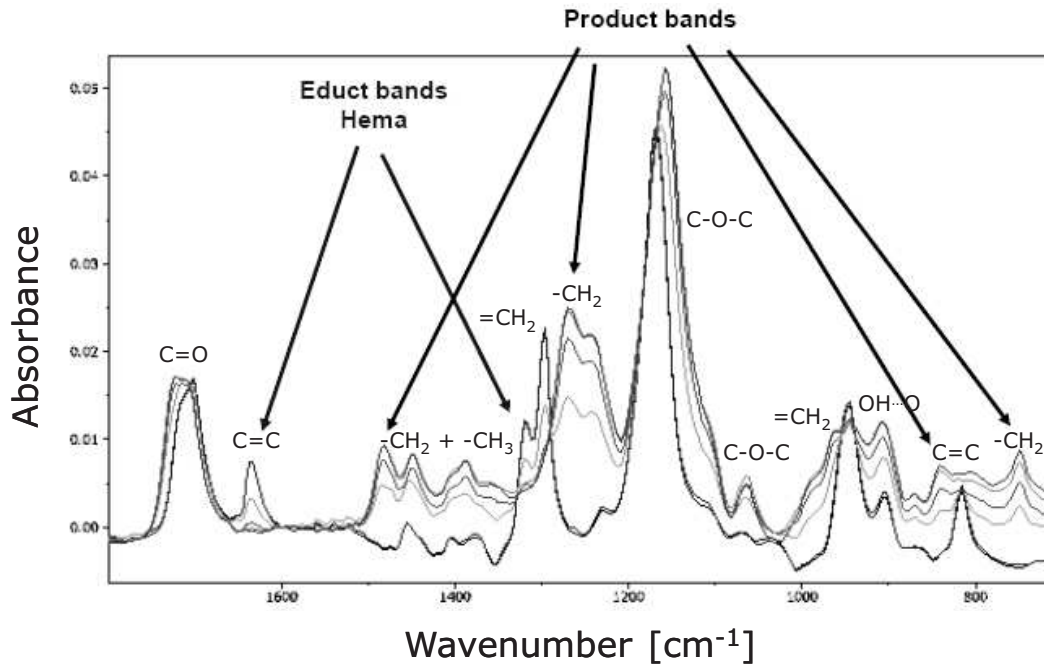


Fig. 3. FI-IT spectra of the free radical polymerization of HEMA at different times.

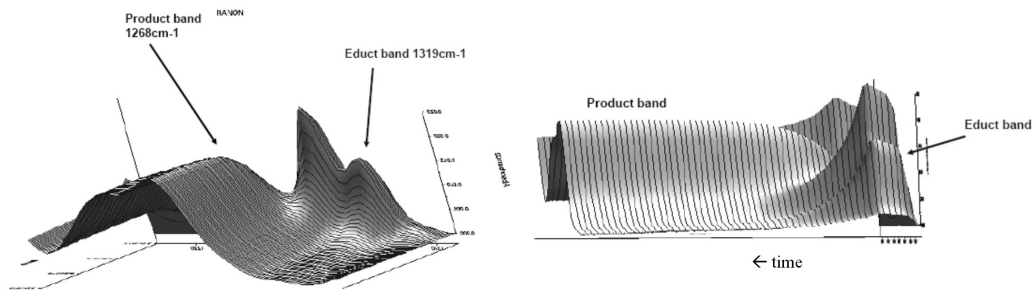


Fig. 4. Spectra of the FT-IR online-reaction-monitoring of the free radical polymerization of HEMA in a mixture of ethylene glycol and  $s\text{CO}_2$  as function of time. Product and educt peaks are clearly seen.

monomer conversions may be reached in homogeneous phase in the presence of significant amounts of  $\text{CO}_2$ .<sup>[5]</sup>

#### 4 Discussion

From analysis of the obtained data it is possible to determine the rate of polymerization ( $R_p$ ). If steady-state free radical polymerization kinetics is assumed, i.e. the concentration of free radicals is constant over time,  $R_p$  is given by equation (3):<sup>[15]</sup>

$$R_p = -\frac{d[M]}{dt} = k_p[M]\sqrt{\frac{fk_d[I]}{k_t}} \quad (3)$$

where  $[M]$  and  $[I]$  are the concentration of monomer and initiator respectively,  $f$  is the initiator efficiency and  $k_d$ ,  $k_p$  and  $k_t$  are the rate constants for decomposition of initiator, propagation and termination respectively.

By applying the Euler-Cauchy numerical method for solving first order differential equations to equation (3) it is possible to model the kinetics of the free radical polymerization of HEMA in ethylene glycol and scCO<sub>2</sub> at 300 bar and 75°C. This is given in equation (4):

$$[M]_{t+1} = [M]_t \left( 1 - \Delta t k_p \sqrt{\frac{fk_d[I]}{k_t}} \right) \quad (4)$$

where the subscript  $t$  on  $[M]$  is a time index. By applying equation (4) the concentration of monomer can be modeled as function of time by knowing the different rate constants and start concentrations. Values for  $f$  and  $k_d$  for DEPDC are found in literature and are listed in table 1.[11] It is found that the decomposition parameters for DEPDC are independent of the pressure in the range from 240 to 310 bar.

The ratio  $\frac{k_p}{\sqrt{k_t}}$  can be estimated by modeling the molar concentration of HEMA as function of time by applying equation (4). By minimizing the root mean square error about the regression curve (RMSE), the best estimate for  $\frac{k_p}{\sqrt{k_t}}$  is found to  $0.23 \frac{1}{\sqrt{M s}}$  with a RMSE of  $2.1 \cdot 10^{-4}$ . Figure 5 shows the measured data of the descending peak at  $814 \text{ cm}^{-1}$  (points) and the modeled best fit (solid line).

Figure 5 and the low RMSE indicate that FT-IR online reaction monitoring is a feasible method for analyzing the kinetics of the free radical polymerization of HEMA in a 20%Vol ethylene glycol and scCO<sub>2</sub> mixture at 300 bar and 75°C. Furthermore the good fit suggests, that steady state is obtained and that the kinetics follow first order as previously assumed.

Unfortunately  $k_p$  and  $k_t$  cannot be determined directly by this method. However, an estimate for  $k_p$  for the free radical polymerization of HEMA in bulk at 75°C and 300 bar can be calculated by applying equation (1) and (2). From equation (1)  $k_p$  at 75°C and 1 bar can be calculated to  $4713 \frac{1}{M s}$  ( $\ln k_p = 8.46$ ). The pre-exponential factor ( $C$ ) in equation (2) can now be estimated at 75°C from equation (5):

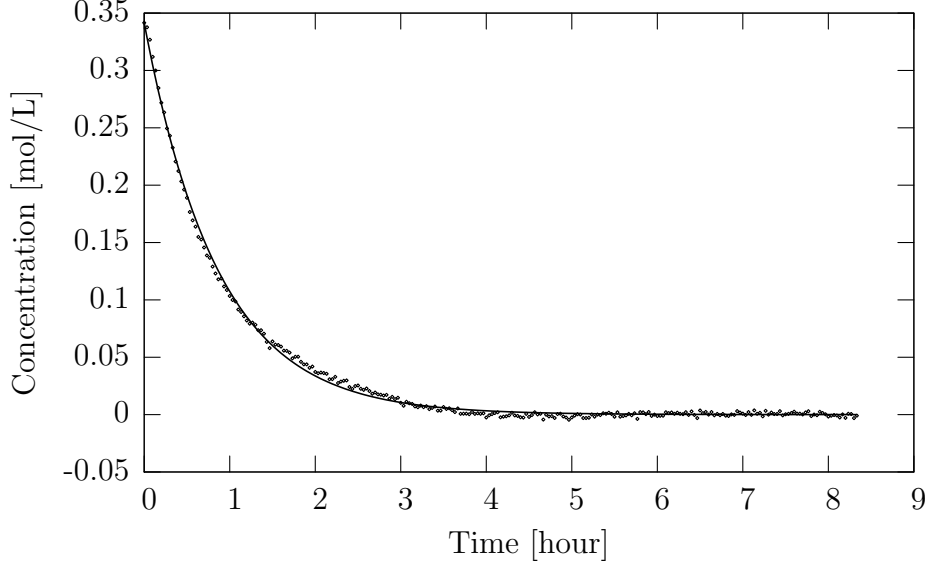


Fig. 5. The concentration of HEMA as function of time based on the descending peak at  $814 \text{ cm}^{-1}$ . The points are measured data, and the solid line is the model. A value of  $0.23 \frac{1}{\sqrt{\text{M s}}}$  is obtained for  $\frac{k_p}{\sqrt{k_t}}$  with a RMSE of  $2.1 \cdot 10^{-4}$ .

$$\begin{aligned}
 \ln k_p &= C + \frac{\Delta V^\ddagger \cdot P}{RT} \\
 \Downarrow \\
 C &= \ln k_p - \frac{\Delta V^\ddagger \cdot P}{RT} \\
 \Downarrow \\
 C &= 8.46 - \frac{0.0152 \frac{\text{L}}{\text{mol}} \cdot 1\text{bar}}{0.08314472 \frac{\text{L bar}}{\text{mol K}} \cdot 348\text{K}} = 8.46 \quad (5)
 \end{aligned}$$

From equation (2)  $k_p$  at 300 bar and  $75^\circ\text{C}$  can be calculated to  $5514 \frac{1}{\text{M s}}$ .  $k_p$  may be up to 40% reduced when  $\text{scCO}_2$  is applied as polymerization solvent compared to bulk polymerization.[5] From the relationship  $\frac{k_p}{\sqrt{k_t}} = 0.23 \frac{1}{\sqrt{\text{M s}}}$ ,  $k_t$  may be estimated to be in the range of  $2.07\text{--}5.74 \cdot 10^8 \frac{1}{\text{M s}}$ .  $k_t$  values of methacrylates are known to be enhanced by a factor of 4 when  $\text{scCO}_2$  is applied as solvent compared to bulk polymerization.[5] By applying this, the obtained  $k_t$  values in  $\text{scCO}_2$ , correspond to  $k_t$  values, in bulk polymerization at  $75^\circ\text{C}$  and 300 bar, in the range of  $0.516\text{--}1.43 \cdot 10^8 \frac{1}{\text{M s}}$ , this is in agreement with reported values for PMMA and PDMA.[5] Table 2 summarize the kinetic parameters.

Table 2

Kinetic values for the polymerization of HEMA, based on a  $k_p$  value in the range of 3309–5515  $\frac{1}{\text{M s}}$  and  $\frac{k_p}{\sqrt{k_t}}$  value of 0.23  $\frac{1}{\sqrt{\text{M s}}}$ .

Polymer	method	Temperature	Pressure	$k_t$
		[°C]	[bar]	$[\frac{1}{\text{M s}}]$
HEMA	scCO <sub>2</sub>	75	300	2.07–5.74·10 <sup>8</sup>
	Bulk	75	300	0.516–1.43·10 <sup>8</sup>
MMA[5]	scCO <sub>2</sub>	80	300	1.26 · 10 <sup>8</sup>
	Bulk	80	300	0.316 · 10 <sup>8</sup>
DMA[5]	scCO <sub>2</sub>	80	300	0.501 · 10 <sup>8</sup>
	Bulk	80	300	0.0794 · 10 <sup>8</sup>

## 5 Conclusion

From FT-IR online reaction monitoring of the free radical polymerization of HEMA in a mixture of 20%Vol ethylene glycol and scCO<sub>2</sub> at 300 bar and 75°C it is possible to model the rate of polymerization ( $R_p$ ) and determine the ratio between the rate constant of propagation and the square root of the rate constant of termination ( $\frac{k_p}{\sqrt{k_t}}$ ) for HEMA to 0.23  $\frac{1}{\sqrt{\text{M s}}}$  with a RMSE of  $2.1 \cdot 10^{-4}$ . It is shown that *in-situ* FT-IR online reaction monitoring is a suitable method for determining the kinetics of the free radical polymerization of HEMA in 20%Vol ethylene glycol and CO<sub>2</sub> at 75°C and 300 bar, and that the polymerization can be described by first order kinetics and proceeds at steady state. From previous studies[9] of the dependence of temperature and pressure on  $k_p$  for HEMA in free radical bulk polymerization, and general considerations on how the kinetic parameters change when scCO<sub>2</sub> is applied as solvent,  $k_p$  and  $k_t$  are estimated to be in the range from 3309–5515  $\frac{1}{\text{M s}}$  and 2.07–5.74·10<sup>8</sup>  $\frac{1}{\text{M s}}$  respectively.

## Acknowledgements

The authors would like to thank: Dr. Nils Theyssen (Max Planck: Institut für Kohlenforschung). Dr. Harald Behl (Mettler Toledo: AutoChem). Per Torenstam (Mettler Toledo: Product Manager Nordic).

## References

- [1] C. K. Mathews, K. E. Van Holde, Biochemistry, The Benjamin/Cummings publishing company, Inc., 2725 Sand Hill Road, Menlo Park, CA, USA, 1996.
- [2] N. A. Peppas, Hydrogels in medicine and pharmacy, Vol. 2: Polymers, CRC Press, 1987.
- [3] A. M. Mathur, S. K. Moorjani, A. B. Scranton, Methods for synthesis of hydrogel networks: A review, Journal of Macromolecular Science - Reviews in Macromolecular Chemistry and Physics C36 (2) (1996) 405–430.
- [4] P. C. Nicolson, J. Vogt, Soft contact lens polymers: an evolution, Biomaterials 22 (2001) 3273–3283.
- [5] S. Beuermann, M. Buback, Supercritical carbon dioxide: in polymer reaction engineering, Wiley-VCH Verlag GmbH & Co. KgaA, Weinheim, Germany, 2005, Ch. Kinetics of free-radical polymerization in homogeneous phase of supercritical carbon dioxide, pp. 55–80.
- [6] J. L. Kendall, D. A. Canelas, J. L. Young, J. M. DeSimone, Polymerizations in supercritical carbon dioxide, Chemical Review 99 (2) (1999) 543–564.
- [7] M. Alm, A. M. Jensen, M. Benter, K. Schamburg, Free radical polymerization of 2-hydroxyethyl methacrylate in supercritical carbon dioxide, Submitted to Macromolecules, Not Published xx (xx) (2007) xx.
- [8] M. D. Goodner, H. R. Lee, C. h. N. Bowman, Method for determining the kinetic parameters in diffusion-controlled free-radical homopolymerizations, Industrial and Engineering Chemistry Research 36 (1997) 1247–1252.
- [9] M. Buback, C. H. Kurz, Free-radical propagation rate coefficients for cyclohexyl methacrylate, glycidyl methacrylate and 2-hydroethyl methacrylate homopolymerizations, Macromolecular Chemistry and Physics 199 (10) (1998) 2301–2310.
- [10] C. Kowollik, C. H. Kurz, Unpublished results (1998).
- [11] P. A. Charpentier, J. M. DeSimone, G. W. Roberts, Decomposition of polymerisation initiators in supercritical co<sub>2</sub>: a novel approach to reaction kinetics using a cstr, Chemical Engineering Science 55 (2000) 5341–5349.
- [12] W. Z. Xu, X. Li, P. A. Charpentier, *insitu* atr-ft-ir study of the thermal decomposition of diethyl peroxydicarbonate in supercritical carbon dioxide, Polymer 48 (2007) 1219–1228.
- [13] P. Charpentier, Preparation of depdc, recipe (2004).
- [14] A. S. Methods, Standard test methods for assay of organic peroxides: E298-01, ASTM, 100 Barr Harbor Drive, West Conshohocken, PA USA, 2001.
- [15] M. C. Stevens, Polymer chemistry, an introduction, Oxford university press, 198 Madison Avenue, New York 10016, 1999.



## Chapter 5

# Hydrophilicity

As described in chapter 4 HEMA can be polymerized in scCO<sub>2</sub> by applying DEPDC as initiator. It is therefore convenient to investigate the production of interpenetrating polymer networks (IPNs) of silicone elastomer and HEMA in scCO<sub>2</sub>. Generally when making IPNs the amount of guest polymer is measured by weight. This however is not an option when making IPNs in scCO<sub>2</sub> where silicone is applied as substrate material due to extraction of silicone oils as described in section 3.2. This means, that even when there is pronounced effect from the impregnated polymer the weight of the IPN may be lower than that of the initial silicone elastomer. In chapter 1 it was described that contact lenses have to be hydrophilic. In this chapter it is examined if the hydrophilicity of silicone elastomers can be increased by producing IPNs with HEMA as guest monomer.

### 5.1 Experimental

98% 2-hydroxyethyl methacrylate (HEMA) with 200 ppm monomethyl ether hydroquinone (MEHQ) as inhibitor supplied by Acros Organics (Belgium) is passed through an inhibitor remover disposable column (Cat no. 306312) supplied by Aldrich (USA) for removal of inhibitor. HEMA is then purified by distillation at reduced pressure, and the fraction at 67°C and 3.5 mbar is collected and stored at 5°C under a N<sub>2</sub> atmosphere. A 0.2 M DEPDC in hexane solution is prepared as previously described and applied as initiator.[7] Silicone elastomer contact lenses supplied by Nanon's cooperating partner, 99.9% ethanol supplied by Merck (Germany) and CO<sub>2</sub> N48 supplied by Air Liquide Denmark A/S (Denmark) are all used as received. A Thar P-50 electrical driven high pressure pump from Thar Designs Inc. USA is applied for assuring the operation pressure. The pump is equipped with a heat exchanger and is supplied with cooling water at 5°C. A stainless steel high-pressure reactor equipped with pressure transmitter, magnet and grid is applied. The total volume of the system is experimentally determined to 4.75 mL.

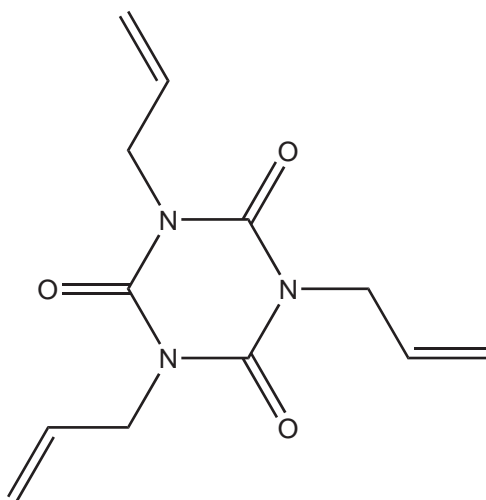
In a typical experiment the reactor is loaded with 500 μL ethanol, 50 μL HEMA and 50 μL DEPDC solution and a contact lens (approx 50 mg) is placed on the grid in the given order. Then the reactor is pressurized with CO<sub>2</sub> to 100 bar at room temperature and heated to 75°C. All polymerizations are carried out over night in order to get high conversions. After a polymerization time ( $t_{\text{poly}}$ ) the reactor is removed from the water bath and allowed to return to ambient temperature before the pressure is slowly decreased. The contact lens is placed in approx. 3 mL saline solution (0.9% NaCl in water) for storage.

## 5.2 Results and discussion

All of the produced IPNs are opaque or white. Explanations and possible solutions of this issue are described in chapter 6. The produced IPNs show a different behavior in saline solution than untreated contact lenses, which move extremely fast toward the surface of saline solution when the vial is shaken, the IPNs move slower or stay on the bottom of the vial. Furthermore untreated contact lenses stays on top of the saline solution with air-bubbles at the water-side of the untreated contact lens, the IPNs on the other hand are not repelled by the saline solution and stays completely wetted on both sides. In this work contact angles with water in ambient air (WCA) are used as a relative measure for the the hydrophilicity. WCA measurements are carried out on a Dataphysics CAI5 at standard conditions, the baseline is placed so it follows the shape of the contact lens. The contact lens is removed from saline solution and gently wiped with paper to remove the water film on the surface. Then a 1.00  $\mu\text{L}$  drop of water is placed on the surface of the contact lens, and when the drop has taken its equilibrium form a picture is taken and used for the analysis. The contact angles ( $\theta$ ) for the obtained IPNs are in the range of 65–85°.  $\theta$  for untreated silicone contact lenses and dry PHEMA are 118° and 58° respectively.  $\theta$  can be decreased by making IPNs with PHEMA in  $\text{scCO}_2$ , i.e. the hydrophilicity is increased. Some of the measured contact angles are lower than that of dry PHEMA, this might be because the surface of the IPN contains a thin physisorbed film of water and the water droplet therefore rests on a surface of its own kind. If the water film had been thick complete wetting instead of a lowered contact angle would have been the result. All the produced IPNs must have some extent of PHEMA on the surface, due to the lowered contact angle compared to the untreated silicone contact lens. However, no direct correlation between the measured contact angles and the experimental settings is found.

In theory two very distinct contact angles should be measured on the IPNs, that of silicone (118°) and that of PHEMA (58.6°) depending on the location of the water drop. If the drop is placed on an interphase between silicone and PHEMA, it would *jump* from the PDMS ocean to the PHEMA isle. The contact angle is independent of the surface geometry. The contact angle is a derivative measurement of the contribution of silicone and PHEMA on the surface, however  $\theta$  is a thermodynamic, and hence a purely macroscopic, quantity—independent of the nature of the forces between the molecules so long as these are of shorter range than the dimensions of the drop. Thus  $\theta$  tells nothing about the microscopic contact angle or the shape of the liquid at the point where it meets the surface, i.e.  $\theta$  does not give this contribution since it is a macroscopic test and does not give information on the morphology and chemical composition on the microscopic and molecular scale. Since the drop does not jump when it is placed on the contact lenses, the areas of the isles of PHEMA and the intermediate silicone ocean must be smaller than the contact area between the water drop and the IPN surface, and the PHEMA isles must be homogeneous distributed on the surface. The obtained contact areas are between 1.1 and 3.2  $\text{mm}^2$  and hence the individual area of a PHEMA isle and the intermediate silicone ocean must be much less than that. Due to the low concentration of HEMA in the reactor it must be expected that a sea-island morphology is produced, c.f. section 1.2. Furthermore no impregnation time was used in the produced IPNs. In the following experiments an impregnation time is used to impregnate the guest monomer before the polymerization starts. When some of the produced IPNs are placed in saline solution it is observed that some polymer material is extracted. To avoid this, a cross-linker [1,3,5-triallyl-1,3,5-triazine-2,4,6-(1H,3H,5H)-trione (TTT)] is applied to the system

in the following experiments. Its chemical structure is shown in scheme II. 98% TTT is supplied by Sigma Aldrich (USA) and used as received. Addition of TTT solved the issue of extracting polymer material, and the surface of the IPNs with TTT appears to be more smooth than without. When TTT is applied as cross-linker no polymer material is extracted from the IPNs when placed in saline solution.



(II)

### 5.3 Surface characterization

Different types of surface structures are possible for the produced IPNs, figure 5.1 shows six different compositions. In this section water uptake, x-ray photoelectron spectroscopy (XPS), fourier transformation infrared spectroscopy (FT-IR) and focused ion beam / scanning electron microscope (FIB-SEM) are applied to characterize the morphology the produced IPNs.

#### 5.3.1 Experimental

For the surface characterization analyzes discs of Elastosil LR 3003/10 shore A (diameter 10 mm, thickness 1 mm) are used instead of contact lenses as substrate material. The discs are extracted in liquid CO<sub>2</sub> prior to use to remove silicone oil.

A 4.75 mL reactor is loaded with 1.00 mL 99.9% ethanol, 100  $\mu$ L HEMA and 0%–40%mol TTT with respect to HEMA and an Elastosil silicone disc (approx 75 mg) is placed on the grid in the given order, then pressurized with CO<sub>2</sub> to approx. 60 bar at room temperature and heated to 75°C. When the temperature reaches 75°C the pressure is increased to 200 bar. After six hours of impregnation, 50  $\mu$ L 0.2 M DEPDC solution is added to the reactor by applying an HPLC-injection valve and increasing the pressure to 300 bar. Polymerization is carried out over 16 hours and 20 min. After the polymerization the reactor is removed from the water bath and the temperature is allowed to return to ambient temperature before the pressure is slowly decreased. The resulting IPNs are washed in EtOH and dried on filter paper to remove excess polymer material.

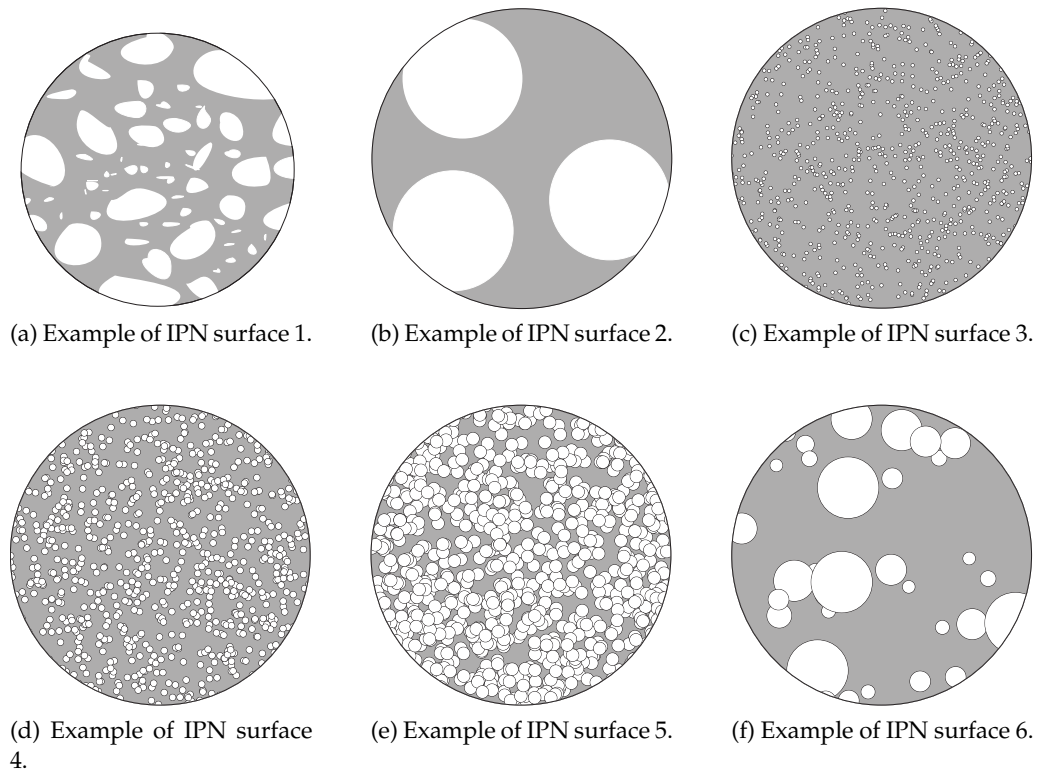


Figure 5.1: Different examples of IPN surfaces on the microscopic scale. The grey areas are silicone and the white areas are PHEMA.

### 5.3.2 Result and discussion

#### 5.3.2.1 Wettability

The obtained contact angles with water in ambient air for the produced IPNs are comparable with those on contact lenses currently on the market, which are about  $72^\circ$ . [31] However, the produced IPNs' ability to make a water film on the surface is an issue. Initially, it was believed that obtaining a high surface energy in itself was the goal (i.e. low contact angle with water in ambient air), the surface energy has to be above  $73 \text{ mN/m}$ , but even the IPN with the highest surface tension dried out too fast, i.e. the obtained surface energies are too low. Therefore another test method is required. The contact lenses are placed in saline solution to be wetted and swelled to absorb water. Then a contact lens is removed and the behavior of the water film on the surface is observed. The water film must remain unchanged in at least 10 seconds after removal from the saline solution in order to be suitable as a contact lens material. [31] This method is denoted as wettability test throughout the text. None of the produced IPNs are wettable according to the wettability test. A small reduction of the contact angle with water in ambient air is found, but not sufficient to make the surface wettable. IPNs placed in saline solution for a month to half a year show a momentarily wettability, which however disappears relative fast. This indicates that the potential to make a hydrogel (the ability to bind water) is relatively small. Different reasons for having semi-hydrophilic surfaces that are not wettable are discussed in the following.

- Approx. 60% of the matrix must consist of PHEMA in order to make a hydrogel

suitable as contact lens material.[31]

- PHEMA is a too weak hydrogel material and does not swell enough in water to make a long lasting reservoir.
- The volumes of PHEMA isles are too small to absorb water
- The swell of PHEMA is restricted by the elastic forces from the silicone network.

When the contact lens is removed from the saline solution, the water film on the surface immediately begins to evaporate and dry out. The speed of drying is controlled by the intermolecular forces between 1) the surface of the IPN and water, 2) water and the ambient air and 3) the ambient air and the surface. The presence of a water film on the surface might be prolonged if water is absorbed in the matrix, because it will act as a reservoir, adding water molecules to the water film as it evaporates. In order to obtain stable water films for more than 10 seconds in ambient air the obtained hydrophilicity of the produced IPNs, giving contact angles of 60–90°, is not enough, and hence some swelling and hydrogel formation are necessary.

In order to determine the produced IPNs' ability to make hydrogels the water uptake is measured on IPNs with varied amounts of cross-linker. The IPNs are cleaned in EtOH and gently wiped in filter paper in order to remove excess polymer material. After three days the IPNs are weighed and placed in approx. 3 mL saline solution and weighed regularly. Before each weighing, the IPNs are removed from the saline solution, placed on filter paper and turned upside down until no marks are left on the filter paper. The water absorbed by a hydrogel network is quantitatively represented by the equilibrium water content (*EWC*) given by equation (5.1):

$$EWC = \frac{\text{Weight of water in the gel}}{\text{Total weight of hydrated gel}} \cdot 100\% \quad (5.1)$$

The obtained *EWC* of IPNs with varying amounts of cross-linker as function of time are shown in figure 5.2. From figure 5.2 the amount of swell after approx. 11 weeks is below 5%wt which is too low for contact lenses. The contact lenses on the market today have water uptakes between 24–79%.[32] The IPNs loses weight during the first 24 hours when placed in water. The loss of weight during the first 24 hours might be due to extraction of polymer material. Surprisingly, the IPN without cross-linker has the highest water uptake. This is inconsistent with the explanation that the weight loss is due to extraction of polymer material. It is expected that uncross-linked PHEMA would be easier to extract than cross-linked, as the cross-linked should be more mechanical interlocked in the silicone elastomer. This suggest that the weight loss during the first 24 hours is not due to extraction of polymer material. Another explanation is the experimental uncertainty of removing the excess water from the surface and weighing the samples, since the changes in weight are within the uncertainty of the scale/balance. This can be overcome by making larger samples, however it is not an option with the current available laboratory equipment. However, the produced IPNs have an extremely low water uptake, in spite of the IPNs being white and hence must contain PHEMA in the matrix. This might be due to the obtained morphology, and it suggest that a sea-island morphology is formed.[16]

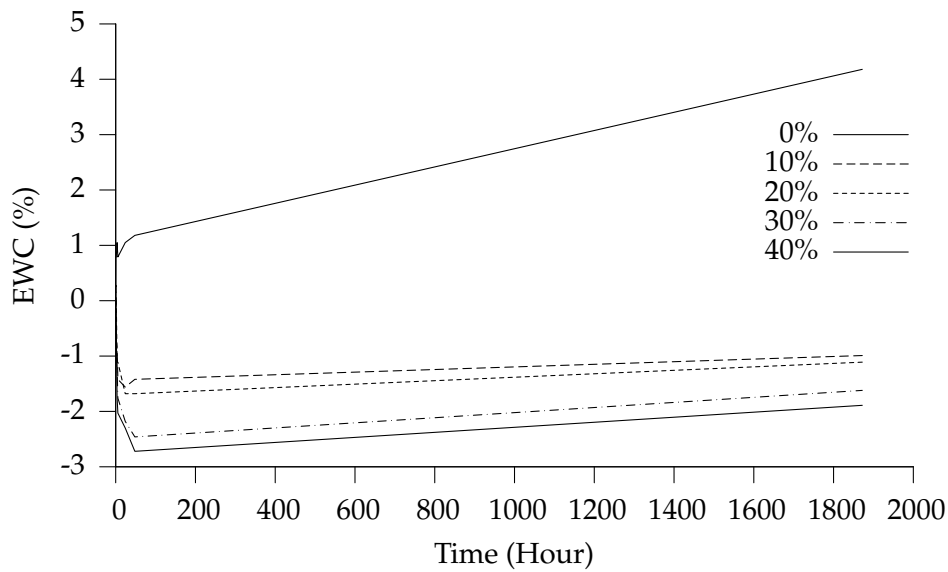


Figure 5.2: Equilibrium water content of IPNs with varying amounts of cross-linker as function of time. Note the relationship between the concentration of cross-linker and the obtained EWC. EWC decreases with an increase in cross-linker concentration. Both the EWC for the IPN with 0%mol and 40%mol are represented with a solid line.

### 5.3.2.2 X-ray photoelectron spectroscopy

XPS reveals the distribution of atoms in the upper 2–10 nm in a cross-section area of  $20 \times 20 \mu\text{m}$  of the sample, but not whether the PHEMA is present in one big isle or in many small. The chemical composition of silicone and PHEMA are 2C:1O:1Si and 2C:1O respectively. Since there are no Si-atoms in PHEMA, the amount of Si can be used to estimate the amount of PHEMA on the surface by subtracting the amount of silicone. The amount of C-atoms and O-atoms that are not attributed silicone are given by equation (5.2) and (5.3) respectively:

$$C_{\text{remain}} = C_{\text{measured}} - 2Si_{\text{measured}} \quad (5.2)$$

$$O_{\text{remain}} = O_{\text{measured}} - Si_{\text{measured}} \quad (5.3)$$

The measured chemical compositions by XPS are listed in table 5.1. As can be seen from table 5.1 PHEMA is found on the surface when the concentration of cross-linker is 20%mol and above, with approx. 10% of the surface area covered by PHEMA.  $\frac{C_{\text{remain}}}{O_{\text{remain}}}$  is close to two which supports that PHEMA is present.

If a strictly entropic approach is taken some of the produced hydrophilic polymers should be present on the surface of the IPN. In the beginning of an experiment there are only monomers present in the bulk (outside the silicone), but as time goes by the hydrophilic monomers will diffuse into the silicone due to the difference in concentration. During the polymerization, polymers will therefore be formed both outside and inside the substrate material, and hence also across the surface. The obtained IPNs are opaque in appearance, which suggest that some PHEMA is present inside the IPN due to differences in refractive indices between silicone and PHEMA. It further suggests that the individual PHEMA isle and intermediate silicone sea are larger than the wavelength of

Table 5.1: Chemical composition of IPNs with HEMA and silicone with varying amount of cross-linker measured by XPS. The amount of cross-linker TTT is varied between 0–40%mol with respect to HEMA.

TTT (%)	Measured			$C_{\text{remain}}$	$O_{\text{remain}}$	PDMS	PHEMA
	C (%)	O (%)	Si (%)	C–2Si (%)	O–Si (%)	4 Si (%)	100–4 Si (%)
0%	49.2	26.3	24.5	0.2	1.8	98	2
10%	49.1	26.2	24.8	-0.5	1.4	99	1
20%	52.1	26.0	21.9	8.3	4.1	88	12
40%	51.8	25.7	22.5	6.8	3.2	90	10

visual light (380 to 780 nm), cf. chapter 6. It is possible to collect polymer material from the reactor outside the IPN. Since PHEMA is present both outside and inside the IPN, some polymers must be present at the surface with a part of the polymer-chain inside the silicone and a part of it sticking out, but only the IPNs with 20% and 40% cross-linker were found to have PHEMA on the surface.

The fact that the IPN are opaque, but PHEMA is not present on the surface of all the IPNs analyzed by XPS, suggests that PHEMA is present inside the produced IPNs, but not on the surface. An explanation can be found by considering the rotational energy around the covalent bonds in silicone, which is very small, cf. section 1.1, resulting in almost free rotation around the bonds. This makes silicone hydrophobic because the methyl-groups, which have affinity to the ambient air, are exposed on the surface. At the same time silicone's polar (hydrophilic) backbone has to be exposed inside the silicone matrix. As is the case with water; Water does not wet silicone, but silicone has a remarkable moisture uptake (3–5%), due to this phenomenon. Similar effects might be involved for hydrophilic polymers; the hydrophilic groups on PHEMA will diffuse inside the silicone matrix, and not be exposed to the surface. To test this self-assembly hypothesis, a non-polar monomer, butyl methacrylate (BMA), is applied as guest monomer instead of HEMA.

Experiments with BMA as guest monomer are carried out with the same procedure as for the IPNs with HEMA for the XPS analysis. Table 5.2 lists the results obtained from XPS. It is found that larger fractions of the surfaces are covered with the guest polymer (PBMA) than for the IPNs with PHEMA, however the ratios between  $C_{\text{remain}}$  and  $O_{\text{remain}}$  do not match with the chemical composition of PBMA, this however might be due to interference from the cross-linker (TTT). From table 5.2 it is seen that most PBMA (> 10%) is found on the surface of the IPNs with the lowest cross-linker concentrations (up to 20%). If too much cross-linker is added (+30%) less PBMA is found on the surface (< 10%). Especially, the IPN with 10% cross-linker is found to have a lot of PBMA on the surface. The tendency observed for IPNs with PBMA is not consistent with that obtained with PHEMA where the IPNs with 20% and 40% cross-linker are found to have the most guest polymer on the surface. It is therefore not known if the obtained results can be attributed to the differences in cross-linker concentration or if it is a measure of local concentration differences on the surface of the IPNs, i.e. there is no difference in the amount of guest polymer on the surface of the different IPNs. However, the fact that more guest polymer is found on the surface of the IPNs with PBMA than PHEMA supports the self-assembly hypothesis that the hydrophilic PHEMA is encapsulated in

Table 5.2: Chemical composition on the surface of IPNs with BMA and silicone with varying amount of cross-linker measured by XPS.

TTT (%)	Measured			$C_{\text{remain}}$	$O_{\text{remain}}$	PDMS	PHEMA
	C (%)	O (%)	Si (%)	C-2 Si (%)	O-Si (%)	4 Si (%)	100-4 Si (%)
0%	49.6	28.2	22.3	5.0	5.9	89	11
10%	55.6	27.8	16.6	22.4	11.2	66	34
20%	51.9	26.8	21.3	9.3	5.5	85	15
40%	51.0	26.1	22.9	5.2	3.2	92	8

the silicone matrix when placed in ambient air.

### 5.3.2.3 Fourier transformation Infrared spectroscopy

Another support for the self-assembly hypothesis is that when an IPN of PHEMA and silicone elastomer is placed in saline solution for some time, more PHEMA is present on the surface than before it was added to the saline solution. However, it loses this effect quite fast. Figure 5.3 shows the FT-IR spectra of an IPN with 40% cross-linker, which has been placed in saline solution for three days and afterwards placed in ambient air over night. The IPN is dried by placing it on filter paper and turning it upside down until no marks are left before the FT-IR measurement is run on a Thermo Nicolet Nexus 470 FT-IR e.s.p. using the attenuated total reflectance method. FT-IR spectra for other cross-linker concentrations are similar. The peak around  $1723\text{ cm}^{-1}$  corresponds to the ester group on PHEMA and is a strong indicator that PHEMA is present on the surface. It is seen from figure 5.3 that the peak around  $1723\text{ cm}^{-1}$  decreases when the IPN is placed in ambient air over night. Table 5.3 lists the ratio between the integrals of the peak around  $1723\text{ cm}^{-1}$  for normalized and baseline corrected FT-IR spectra measured just after removal from saline solution and after the IPNs have been placed in ambient air over night for different cross-linker concentrations. Table 5.4 lists the ratios between the integral of the peak around  $1723\text{ cm}^{-1}$  for different cross-linker concentrations relative to the IPN with 40% cross-linker, just after removal from saline solution and after the IPNs have been placed in ambient air over night.

From table 5.3 and 5.4 it is obvious that when TTT is added as cross-linker, more PHEMA can be detected on the surface. For the FT-IR analyzes the IPNs were removed from the saline solution and dried with lens paper (physical rubbing), then a FT-IR measurement was performed. Then they were placed in ambient air over night and a new FT-IR measurement was performed. There is a notable decrease in measured PHEMA on the surface between the two measurements ( $\frac{A_{\text{Over night}}}{A_{\text{After water}}}$ ). This supports the self-assembly hypothesis and suggests a significant polymer diffusion over night. However, the effect is less dramatic in IPNs where TTT is added. This indicates that some PHEMA chains are interlocked on the surface.

### 5.3.2.4 Focused ion beam scanning electron microscope

An IPN with PHEMA and 40% TTT is examined by focused ion beam / scanning electron microscope (FIB-SEM). FIB-SEM gives images of the concentration of the different chemical atoms in a cross-section area of  $135 \times 110\ \mu\text{m}^2$ . The IPN is cut perpendicular to

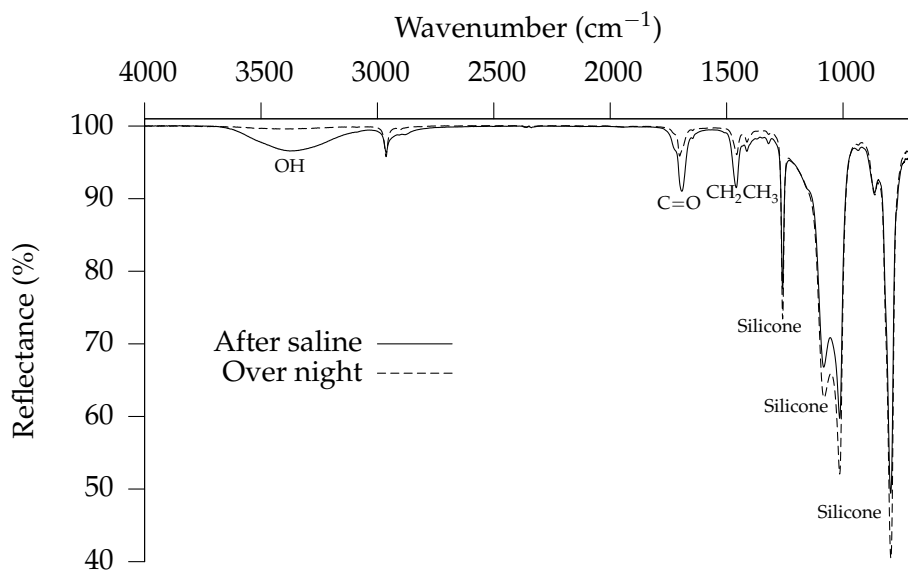


Figure 5.3: FT-IR spectra of IPN with 40% cross-linker which has been placed in saline solution for three days (solid line) and afterwards placed in ambient air over night (dashed line).

Table 5.3: Ratio between the integrals of the peak around  $1723\text{ cm}^{-1}$  for the IPNs just after they are removed from saline solution (and dried) and after they have been placed in ambient air over night.

Cross-linker (%mol)	$\frac{A_{\text{Over night}}}{A_{\text{After water}}}$ (%)
0	38.9
10	65.0
20	54.4
30	51.7
40	38.4

Table 5.4: Relative amount of PHEMA on the surface of the IPNs compared to the IPNs with 40%mol cross-linker just after removal from saline solution and drying and after the IPNs are placed in ambient air over night.

Cross-linker (%mol)	After Saline (%)	Over night (%)
0	26.8	27.2
10	36.4	61.7
20	44.2	62.6
30	47.3	63.7
40	—	—

the surface in a cryo-microtome, in order to measure the concentration of the different atoms as function of impregnation depth in the IPN. The FIB-SEM measurements are run within 20 min from the slicing to delimit the self-assembly of silicone to the surface. Figure 5.4 shows the obtained images from the FIB-SEM analysis. It is expected that the intensity of C- and O-atoms increases as the intensity of Si-atoms decreases and vice versa. As can be seen on figure 5.4 no change in concentration of carbon, oxygen and silicon as function of impregnation depth can be detected by FIB-SEM, i.e. no PHEMA isles can be detected by FIB-SEM. Even though the images show a cross-section area of approx.  $135 \times 110 \mu\text{m}^2$ , each measurement only analyze a few  $\text{nm}^2$ . Therefore it should be possible to detect differences in concentration even in a small area ( $10 \text{nm}^2$ ). However no differences are found on the images. This suggest that the PHEMA isles are relatively small and homogeneously distributed throughout the matrix, but since the IPN is white, the PHEMA isles must be larger than the wavelength of visual light. It is therefore surprising that no intensity differences are found. One possibility is that even though the individual PHEMA isle is smaller than the wavelength of visual light, they are distributed so close to one another and homogeneously that they are perceived as one large isle visually. Another possibility is that the self-assembly of silicone to the surface and PHEMA inside the IPN is so fast that it happens within 20 min.

Silicone elastomer and PHEMA have contact angles with water in ambient air of  $118^\circ$  and  $58^\circ$  respectively. The produced IPNs have a contact angle with water in ambient air of  $60\text{--}90^\circ$ . Therefore PHEMA must be present on the surface of the produced IPNs, however, there is not enough material to make a hydrogel and hence a wettable surface. It is not possible to measure the actual amount of PHEMA in the produced IPNs, as it is discussed in section 5.3. However, it seems unrealistic that the IPN matrix should contain at least 60% PHEMA, considering the theoretical degree of swell of silicone in  $\text{scCO}_2$  at 300 bar and  $75^\circ\text{C}$  of approx 35% described in section 3.1. The probability of success by applying HEMA as the hydrophilic monomer may be questioned, since the water uptake of PHEMA is relatively low.[31] Applying other hydrophilic monomers, which have a higher water uptake like e.g. NVP, amides, glycols, betain, and dimethylacrylamide might increase the probability of success. Soft contact lenses only contain enough PHEMA that it is just possible to make a suitable hydrogel.[31] It might therefore be an idea to examine other more water swell-able polymers, however it is outside the scope of this dissertation.

Literature describes IPNs of silicone elastomers and poly(methacrylic acid) (PMAA) that contain up to 50% of monomer before the polymerization and 30% after the polymerization, with an EWC of 84%.[16] It suggests that not enough hydrophilic monomer is impregnated into the silicone matrix before polymerization in the IPNs produced in this study. The silicone elastomer in literature is soaked in the monomer for 18 hours before polymerization, compared to the approx. six hours in the experiments in this study. Furthermore the concentration of monomer in which the silicone elastomer is soaked in this study is relative low ( $0.174 \frac{\text{mol}}{\text{L}}$ ) compared to swelling in pure monomer ( $8.245 \frac{\text{mol}}{\text{L}}$ ). However, in this study the substrate material is placed in  $\text{scCO}_2$  (200 bar at  $75^\circ\text{C}$ ) which assist the swelling, c.f. section 3.1. For future experiments the concentration of HEMA, pressure of  $\text{CO}_2$  and impregnation time should all be increased. Another possibility would be to apply liquid  $\text{CO}_2$  instead of  $\text{scCO}_2$  because of the higher degree of swell of silicone. The IPNs obtained in literature are white and brittle, those in this study are opaque and flexible. This supports that less guest polymer is present in the IPN in this study than that in literature. However, producing white and brittle IPNs are

Focused ion beam scanning electron microscope

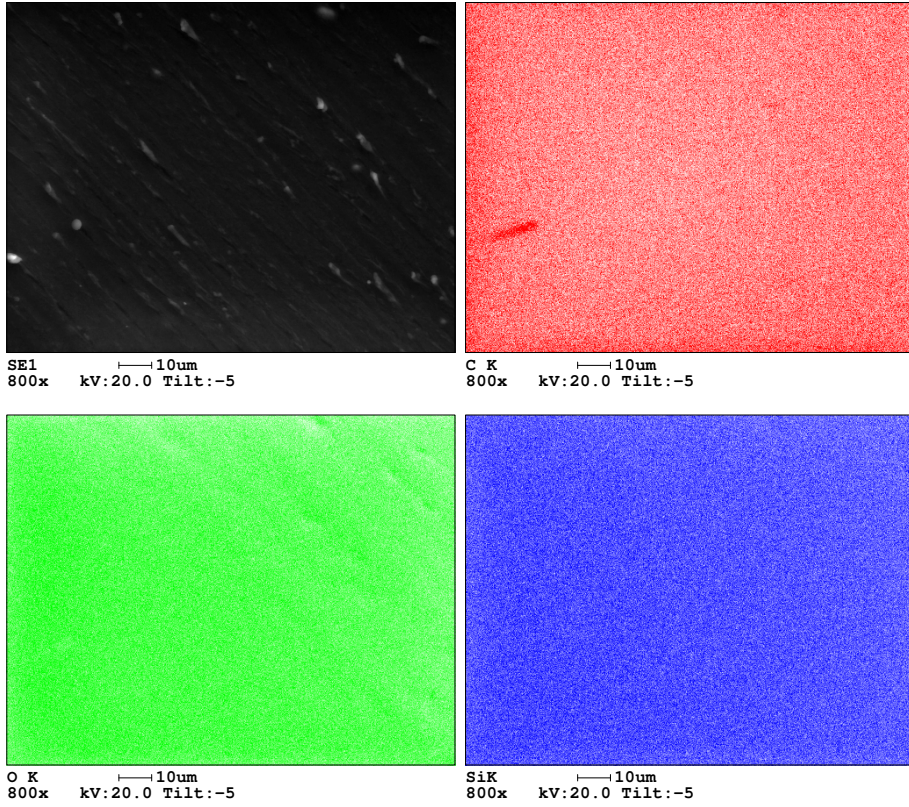


Figure 5.4: FIB-SEM images. Upper left picture is a scanning electron image. Upper right is a map of the carbon atom distribution. Lower left and right are maps of the oxygen and silicon atom distributions, respectively.

not suitable for contact lenses. Literature states that in order to obtain an IPN that has a pronounced water uptake, a nodular morphology is necessary. In this study it must be expected that an island-sea morphology with small phase dimensions is created, c.f. figure 5.1c and 5.1d. Therefore in future work the concentration of monomer during impregnation should be increased.

## Chapter 6

# Transparency

As described in section 1.2 one of the requirements of contact lenses is that they are transparent. In chapter 5 it is described that the surface tension of silicone can be increased (lower contact angle) by making IPNs with PHEMA, however many of the produced IPNs are opaque or white. This chapter concerns the transparency of IPN. This includes a description of the different reasons why the produced IPNs are not transparent. A beam of light can be restricted in its travel through a media in at least three ways.[33] It can either be absorbed by the media. This happens when electromagnetic energy is transferred to the atoms, ions or molecules composing the media, making them jump from their ground state to one or more higher-energy excited states. Another possibility is that the beam of light is scattered by the media due to molecules, aggregates of molecules, colloids, particles, etc.. Scattering is dependent on the wavelength of the beam of light, the domain size and polarizability of the media. The third possibility is reflection of the beam of light, which always occurs when a beam of light crosses an interface between two media with different refractive indices.

Only the two latter reasons are relevant for IPNs and considered further in this study: Particle formation, which gives scattering, and differences in refractive indices, which gives reflection and refraction. It is described how to choose a suitable comonomer for changing the refractive index by considering i.a. the kinetics of copolymerization in terms of the  $Qe$ -scheme and composition vs. conversion curves. Finally the theory is applied and experiments are run resulting in transparent IPNs.

### 6.1 Scattering

Transmission of radiation in a matter can be understood as a momentary retention of the radiant energy by particles followed by re-emission of the radiation in all directions as the particles return to their original state.[33] For small particle sizes relative to the wavelength of the radiation, destructive interference removes most, but not all of the re-emitted radiation, leaving only the radiation that travels in the original direction of the beam. The path of the beam therefore appears to be unaltered as a consequence of the interaction. The fraction of the radiation that is transmitted in all directions from the original path increases with particle size. Hence, if the particle sizes of the PHEMA isles are lower than the wavelength of the radiation that travels in the IPN (visual light,  $\lambda = 380\text{--}740\text{ nm}$ ), scattering does not influence the transparency. Whereas if the particle sizes are larger than the wavelength of the radiation that travels in the IPN scattering affects the transparency.

In the article "Free radical polymerization of 2-hydroxyethyl methacrylate in supercritical carbon dioxide" in chapter 4 it is described how HEMA is polymerized in  $\text{scCO}_2$  as insoluble particles due to the Trommsdorff effect and a chain-transfer to monomer side-reaction. Furthermore it is described how to avoid particle formation by addition of a cosolvent. In chapter 5 it is described that similar effects are observed when producing IPNs, which results in scattering and hence white IPNs. Furthermore it is described that particle formation can be avoided by adding a cosolvent. However, the produced IPNs remain opaque. That might be due to reflection.

## 6.2 Reflection

Reflection always occurs when a beam of light crosses an interface between two media with different refractive indices (RI).[33] The fraction of the beam of light which is reflected increases with increasing difference in refractive index, and is given by equation (6.1):

$$\frac{I_r}{I_0} = \frac{(n_2 - n_1)^2}{(n_2 + n_1)^2} \quad (6.1)$$

where  $I_0$  is the intensity of the incident beam of light,  $I_r$  is the reflected intensity, and  $n_1$  and  $n_2$  are the refractive indices of the two media. The total reflective loss when a beam of light passes through an IPN is given by the sum of losses occurring at each of the interfaces taking into account that the beam intensity decreases for each reflection. This is given by equation (6.2):

$$\sum_{i=1}^{\max} \frac{I_{ri}}{I_{0i}} = \sum_{i=1}^{\max} \frac{(n_{2i} - n_{1i})^2}{(n_{2i} + n_{1i})^2}$$

$$\Downarrow \quad I_{0i} = I_{0i-1} - I_{ri-1}$$

$$\sum_{i=1}^{\max} \frac{I_{ri}}{I_{0i-1} - I_{ri-1}} = \sum_{i=1}^{\max} \frac{(n_{2i} - n_{1i})^2}{(n_{2i} + n_{1i})^2} \quad (6.2)$$

Equation (6.2) shows that the total reflective loss increases with the number of interfaces between the two media. For an IPN the number of interfaces between the two media must be assumed to be relatively high. If it is requested that the IPN is transparent the refractive indices for two media may therefore not differ too much. The refractive indices of silicone and PHEMA are 1.43 and 1.51 respectively. Since the produced IPNs are opaque the difference between the refractive indices is too large. One approach to change the refractive index is to produce copolymers.

## 6.3 Free radical copolymerization

The purpose for adding a comonomer is to verify that the IPNs become opaque due to too large differences in RI between silicone and PHEMA. This hypothesis is tested by making copolymers with a RI in the vicinity of that of silicone elastomer. Different aspects influence the choice of the comonomer. One requirement to the applied

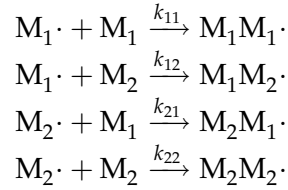


Figure 6.1: Possible propagation sequences in free radical copolymerization

comonomer is that its polymer must have a lower RI than silicone elastomer, since RI for PHEMA is larger. Another requirement is that the resulting copolymers should have an alternating or random structure, in order to avoid phase separation from block-copolymers and assure that the domain sizes are below the wavelength of visual light. The composition of a copolymer can be modeled by considering the relative reactivities. For a system with two different types of monomers ( $M_1$  and  $M_2$ ), the four different propagating reactions shown in figure 6.1 may take place.  $k_{11}$ ,  $k_{12}$ ,  $k_{21}$  and  $k_{22}$  are the rate constants for the four propagating reactions respectively, and the dot ( $\cdot$ ) denotes a free radical.[15, 34, 35]

The ratio between  $k_{11}$  and  $k_{12}$  is called the reactivity ratio ( $r_1 = \frac{k_{11}}{k_{12}}$ ;  $r_2 = \frac{k_{22}}{k_{21}}$ ). The reactivity ratio is a measure of a chain-end radical's tendency to self-propagate (react with a monomer of its own type) or to cross-propagate (react with a monomer of a different type). By comparing sets of values of  $r_1$  and  $r_2$  different scenarios arise. If  $r_1 = r_2 = 0$  both types of chain-end radicals will much rather cross-propagate than self-propagate and hence a true alternating copolymer is produced. If  $r_1 = r_2 = 1$  the probabilities of self-propagation and cross-propagation are the same and hence a random copolymer is formed. If  $r_1$  is much larger than  $r_2$ , radicals of type  $M_1$  will rather self-propagate than cross-propagate whereas the radicals of type  $M_2$  will rather cross-propagate than self-propagate, this means that at low conversions a homopolymer of  $M_1$  is formed, and at high conversions a homopolymer of  $M_2$  is formed and hence a block-copolymer is produced, and visa versa if  $r_2$  is much larger than  $r_1$ .

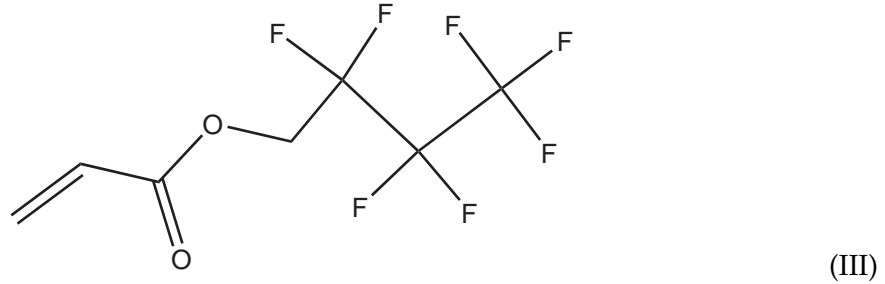
For identifying a comonomer which fulfills the criteria of a RI that is lower than that of silicone and yields an alternating or random copolymer with HEMA, values of the reactivity ratios are needed. Information on the reactivity ratios can be obtained by applying the semi-quantitative  $Qe$ -scheme. Each monomer is given an universal  $Q$  and  $e$ -value, describing its intrinsic reactivity (e.g. steric hinderance) and polar effects respectively. According to the  $Qe$ -scheme, the reactive ratios  $r_1$  and  $r_2$  are given by equation (6.3) and (6.4) respectively:[15, 35]

$$r_1 = \frac{k_{11}}{k_{12}} = \left( \frac{Q_1}{Q_2} \right) \exp [-e_1 (e_1 - e_2)] \quad (6.3)$$

$$r_2 = \frac{k_{22}}{k_{21}} = \left( \frac{Q_2}{Q_1} \right) \exp [-e_2 (e_2 - e_1)] \quad (6.4)$$

$Q$  and  $e$  values for free radical polymerization in bulk for different monomers can be found in literature.[36] In the article "Kinetics of the free radical polymerization of 2-hydroxyethyl methacrylate in supercritical carbon dioxide" in chapter 4 it was described how the kinetics of free radical polymerization are changed when  $scCO_2$  is applied as reaction media instead of bulk and organic solvents. However, even though the kinetics of each homo-polymerization are changed, the reactive ratios ( $r_1$  and  $r_2$ ) are not affected

by  $\text{scCO}_2$ .<sup>[37]</sup> Therefore  $Qe$ -values found in literature for bulk polymerization may be unconditionally applied to the free radical copolymerization in  $\text{scCO}_2$ . By evaluating values of  $Q$  and  $e$  for different monomers listed in literature one comonomer that has a lower RI than silicone and gives semi-alternating copolymers with HEMA is found; heptafluorobutyl acrylate (HFBA). The chemical structure of HFBA is shown in scheme III.



For copolymeric systems whose phase dimensions are below the wavelength of the radiation that travels in it (visual light), hence alternating and random copolymers, the Maxwell relation is valid and the refractive index of the copolymer may be expressed in terms of the dielectric constants of the constituent phases.<sup>[38]</sup> The dielectric constant ( $\epsilon$ ) is equivalent to the square of the refractive index ( $\epsilon = n^2$ ). The upper bound of the refractive index of the copolymer can be obtained as the sum of dielectric constants of the constituent phases, this is given by equation (6.5):<sup>[38]</sup>

$$n^2 = \sum_i \phi_i \cdot n_i^2 \quad (6.5)$$

where  $n_i$  and  $\phi_i$  are the refractive indices and volume fractions of the constituent phases of components that make up the copolymer. Similar, the lower bound of a copolymer's refractive index is given by the sum of the inverse dielectric constants of the constituent phases, this is given by equation (6.6):<sup>[38]</sup>

$$\frac{1}{n^2} = \sum_i \frac{\phi_i}{n_i^2} \quad (6.6)$$

For copolymers where RI of the constituent phases differ by less than 0.2, i.e. ( $n_i - n_j < 0.2$ ), the refractive index of the copolymer is given by the Gladstone-Dale relation assuming additivity of the refractive indices of the constituent phases. This is given by equation (6.7):

$$n = \sum_i \phi_i \cdot n_i \quad (6.7)$$

The refractive index of PHFBA is 1.37. Since the difference between the RI of PHEMA and PHFBA is less than 0.2 the Gladstone-Dale relation can be applied to determining the composition in the copolymer giving a RI equal to that of silicone. From the Gladstone-Dale relation given in equation (6.7) the volume fraction of PHEMA in the copolymer ( $\phi_{\text{HEMA}}$ ) can be determined from equation (6.8):

Table 6.1: Applied system parameters.  $\phi$  is the needed volume fraction of the monomer in the copolymer to obtain a RI of 1.43.

Parameter	PHEMA	PHFBA
RI	1.51	1.37
$Q$	1.78	0.96
$e$	-0.39	1.34
$r$	0.944	0.053
$\phi$	0.42	0.58

$$\begin{aligned}
 n_{\text{PDMS}} &= \phi_{\text{HEMA}} \cdot n_{\text{PHEMA}} + \phi_{\text{HFBA}} \cdot n_{\text{PHFBA}} \\
 \Downarrow \quad \phi_{\text{HEMA}} + \phi_{\text{HFBA}} &= 1 \\
 n_{\text{PDMS}} &= \phi_{\text{HEMA}} \cdot n_{\text{PHEMA}} + (1 - \phi_{\text{HEMA}}) \cdot n_{\text{PHFBA}} \\
 \Downarrow \\
 n_{\text{PDMS}} &= \phi_{\text{HEMA}} \cdot n_{\text{PHEMA}} + n_{\text{PHFBA}} - \phi_{\text{HEMA}} \cdot n_{\text{PHFBA}} \\
 \Downarrow \\
 n_{\text{PDMS}} - n_{\text{PHFBA}} &= \phi_{\text{HEMA}} (n_{\text{PHEMA}} - n_{\text{PHFBA}}) \\
 \Downarrow \\
 \phi_{\text{HEMA}} &= \frac{n_{\text{PDMS}} - n_{\text{PHFBA}}}{n_{\text{PHEMA}} - n_{\text{PHFBA}}} \tag{6.8}
 \end{aligned}$$

By inserting the RI for silicone, PHEMA and PHFBA,  $\phi_{\text{HEMA}}$  is determined to 0.42 from equation (6.8). Table 6.1 lists different system parameters.

As can be seen from table 6.1,  $r_{\text{HEMA}}$  has a value of approx. 1 and is about 17 times larger than  $r_{\text{HFBA}}$ . That means that a HEMA chain-end radical shows no preference between self- or cross-propagation, while a HFBA chain-end radical has a tendency to cross-propagate. The composition in the copolymer can be modeled by applying the copolymer equation, which is given by equation (6.9):[34]

$$\frac{\partial[\text{HEMA}]}{\partial[\text{HFBA}]} = \frac{[\text{HEMA}]}{[\text{HFBA}]} \left( \frac{r_{\text{HEMA}} \cdot [\text{HEMA}] + [\text{HFBA}]}{[\text{HEMA}] + r_{\text{HFBA}} \cdot [\text{HFBA}]} \right) \tag{6.9}$$

where  $[\text{HEMA}]$  and  $[\text{HFBA}]$  are the concentrations of HEMA and HFBA, respectively. The left hand side gives the momentary composition in the produced copolymer, based on the actual monomer feed concentrations given by the right hand side. By numerical integration of equation (6.9) the composition as function of conversion can be modeled. Figure 6.2 and 6.3 show how the composition in the copolymer and feed changes as function of conversion for two different start compositions. In figure 6.4 the momentary RI of the copolymer as function of conversion is modeled by applying equation (6.7) and (6.9) for different start concentrations of HEMA ( $\phi_{0,\text{HEMA}}$ ). Two different scenarios are seen: If  $\phi_{0,\text{HEMA}}$  is 0.60, the composition in the copolymer, and hence RI, does not change so much with conversion, however the resulting RI (1.47–1.48) is slightly above that of silicone elastomer (1.43). If  $\phi_{0,\text{HEMA}}$  is 0.27 the initial refractive index is closer to that of silicone, but changes much with conversion. Furthermore, the total conversion has to be lower than approx 55% in order not to produce homo-polymers of HFBA. In the following these two scenarios are examined experimentally.

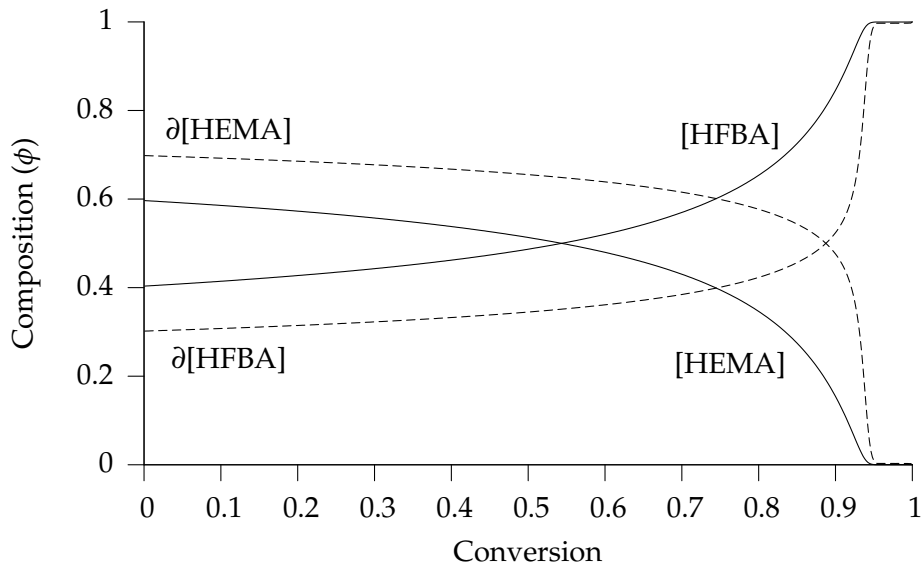


Figure 6.2: Composition-conversion curve for the copolymerization of HEMA and HFBA with initial conditions of  $\phi_{0,\text{HEMA}} = 0.60$  and  $\phi_{0,\text{HFBA}} = 0.40$ . The solid lines represent the momentary composition in the feed and the dashed lines the composition in the produced copolymer.

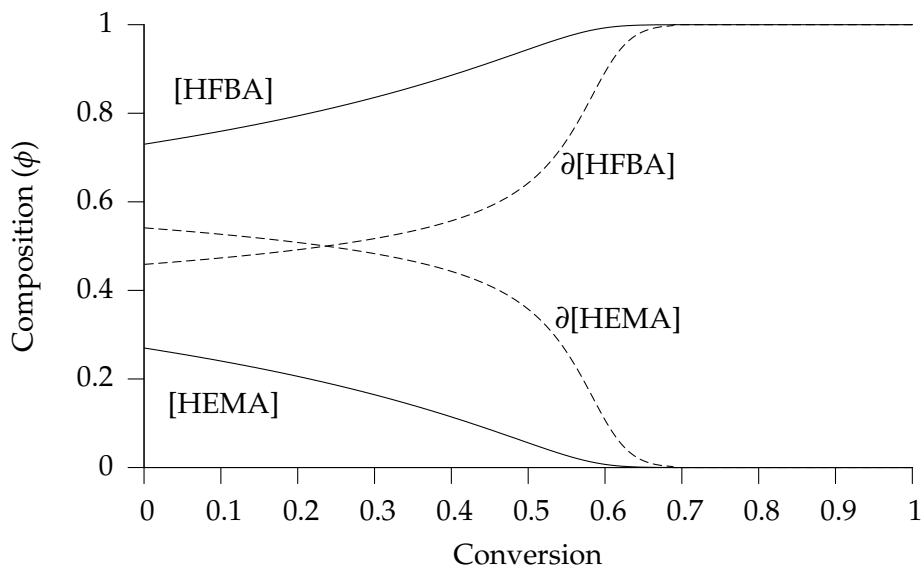


Figure 6.3: Composition-conversion curve for the copolymerization of HEMA and HFBA with initial conditions of  $\phi_{0,\text{HEMA}} = 0.27$  and  $\phi_{0,\text{HFBA}} = 0.73$ . The solid lines represent the momentary composition in the feed and the dashed lines the composition in the produced copolymer.

## Experimental

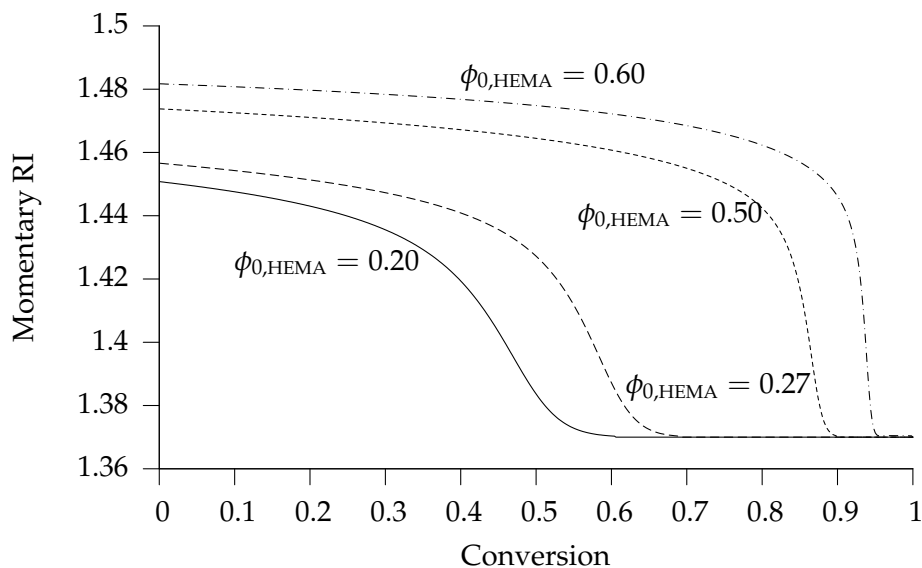


Figure 6.4: Momentary RI as function of conversion for different initial composition in the feed.

## 6.4 Experimental

97% HFBA supplied by Sigma (Germany) is used as received and stored at 5° under a N<sub>2</sub> atmosphere. A 4.75 mL reactor is loaded with 500 μL ethanol, 50 μL HEMA, 50 μL ( $\phi_{0,\text{HEMA}} = 0.60$ ) or 200 μL ( $\phi_{0,\text{HEMA}} = 0.27$ ) HFBA and 50–150 μL DEPDC solution and a contact lens is placed on the grid in the given order. Then the reactor is pressurized with CO<sub>2</sub> to 100 bar at room temperature and heated to 75°C. All experiments are carried out overnight in order to get high conversions. After a polymerization time ( $t_{\text{poly}}$ ) the reactor is removed from the water bath and the temperature is allowed to return to ambient temperature before the pressure is slowly decreased. The contact lens is placed in approx. 3 mL saline solution for storage.

## 6.5 Results and discussion

Table 6.2 shows that transparent IPNs can be produced. The production of transparent IPNs are most successful when  $\phi_{\text{HEMA}} = 0.6$ , as  $\phi_{\text{HEMA}}$  is decreased the IPNs shows a tendency to be opaque. This might be due to production of PHFBA with a RI of 1.37 at conversions above approx. 55%, c.f. figure 6.4. The produced IPNs with copolymers of HEMA and HFBA have slightly higher contact angles with water in ambient air than those made with homo-polymers of HEMA. This might be due to the presence of HFBA, which is hydrophobic. However, a reduced contact angle compared to untreated silicone elastomer is observed. The main purpose of producing IPNs with copolymers of HEMA and HFBA is not to produce hydrophilic IPNs, but to verify that the IPNs with PHEMA become opaque due to too large difference in RI between the substrate material and the guest polymer. The fact that transparent IPNs can be reproduced verifies the hypothesis. Furthermore, it shows that the refractive index of the guest (co)polymer does not have to be equal to that of the substrate material, but having a similar value is enough. According to figure 6.4 the produced copolymers when  $\phi_{0,\text{HEMA}} = 0.6$  have RI in the

Table 6.2: Typical WCAs ( $\theta$ ) and transparencies of IPNs with silicone contact lenses as substrate material and copolymers of HEMA and HFBA. The listed WCAs are average of five measurements.

$\phi_{0,\text{HEMA}}$	$V_{\text{DEPDC}}$ ( $\mu\text{L}$ )	$t_{\text{poly}}$ (h:min)	$\theta$ ( $^\circ$ )	Transparency
PDMS			118.0	
PHEMA			58.6	
0.60	150	18:00	66.9	Transparent
0.27	100	20:25	84.4	Greenish opaque

range of 1.44–1.47, which apparently is close enough to that of silicone elastomer for the produced IPNs to be transparent. It furthermore supports the assumption that the reactive ratios are not effected when  $\text{scCO}_2$  is applied as polymerization media compared to free radical polymerization in bulk. And it suggests that the kinetics of impregnation of HEMA and HFBA are similar in magnitude, if the kinetics of impregnation of one of the monomers were faster than the other, homo-polymers would be produced resulting in opaque IPNs.

From table 6.2 it is seen that when  $\phi_{\text{HEMA}}$  is decreased the produced IPNs became greenish. This might be due to a decomposition of HFBA. HFBA is not a very stable product and can undergo hydrofluoric acid (HF) elimination in the presence of base, forming colored species from the produced carbon-carbon double bond. Another possible side-reaction is hydrolysis of the ester in the presence of water, forming  $\text{C}_3\text{F}_7\text{CH}_2\text{OH}$  alcohol which is rather acidic. It is not possible to make a completely fluoro-substituted compound, such as nonafluorobutyl methacrylate, since the starting alcohol nonafluorobutanol is unstable and immediately splits of HF. The reason for making IPNs with copolymers of HEMA and HFBA is to test the hypothesis that the IPNs becomes opaque due to the differences in refractive indices between the guest polymer and the substrate material. As can be seen from table 6.2 most of the produced IPNs with copolymers of HEMA and HFBA are transparent, which supports the hypothesis. However the produced IPNs are not suitable as a contact lens material, due to the risk of elimination of HF which is not compatible with the eye. Another issue is that HFBA is hydrophobic, that means that the produced IPNs with copolymers are not as hydrophilic as those made with PHEMA, cf. section 5.2 and table and 6.2. Other comonomers than HFBA might have suitable reaction ratios and RI, however most such monomers contain fluor and hence will have a hydrophobic nature. Another solution could be to increase the refractive index of the silicone elastomer substrate. The refractive index of silicone can be increased by adding phenyl groups on the side-chains.[10] Any increase in refractive index of the substrate material will be an improvement, and require less amount of fluor incorporated in the copolymer. Another possibility is to identify other hydrophilic polymers with lower RI and higher water uptake than HEMA.

## Chapter 7

# Conclusion

The purpose of this work has been to examine the possibility to make a contact lens material consisting of interpenetrating polymer networks (IPNs) of silicone elastomers and poly(2-hydroxyethyl methacrylate) (PHEMA) where supercritical carbon dioxide (scCO<sub>2</sub>) is applied as an auxiliary solvent. Focus was given to two of the major requirements for contact lenses; hydrophilicity and transparency.

The compatibility between CO<sub>2</sub> and silicone elastomer was quantified in terms of the free energy of mixing ( $F_m$ ) as function of pressure ( $P$ ) and temperature ( $T$ ). The Flory-Huggins lattice model for the free energy of mixing is applied to model the compatibility, and Hansen's solubility parameters (HSP) are applied to estimate the Flory-Huggins interaction parameter ( $\chi$ ). In order to model how the compatibility between CO<sub>2</sub> and silicone elastomer depends on pressure and temperature it is necessary to model HSP as function of pressure and temperature, therefore mathematical models are derived. Furthermore HSP for silicone elastomer is determined experimentally to  $\delta_d = 17.0\sqrt{\text{MPa}}$ ,  $\delta_p = 2.9\sqrt{\text{MPa}}$  and  $\delta_h = 2.6\sqrt{\text{MPa}}$ . It was found that in the liquid phase, CO<sub>2</sub> and silicone elastomer are compatible, whereas the scCO<sub>2</sub> phase is split into a compatible and a non compatible part. If the pressure is higher than the pressure where  $F_m$  is zero ( $P > P|_{F_m=0}$ ) spontaneous mixing occurs.  $P|_{F_m=0}$  is found to depend strongly on the temperature of the system and is exclusively given by equation 7.1 in the supercritical phase:

$$P|_{F_m=0} = -6.21 \cdot 10^{-3}T^2 + 4.03T - 30.92 \quad (7.1)$$

The obtained thermodynamic results were applied to model the degree of swell of silicone elastomer in CO<sub>2</sub> as function of pressure and temperature. It was found that silicone elastomer swells more in liquid CO<sub>2</sub> than in scCO<sub>2</sub>, which is attributed to the lower free energy of mixing, which mainly results from the higher density in the liquid phase. Therefore, for many applications, such as extraction of un-cross-linked silicone oligomers (silicone oil) from silicone elastomers, a liquid CO<sub>2</sub> approach would be more feasible than a scCO<sub>2</sub> approach. The diffusion of silicone oil out of silicone elastomers is modeled by applying Fick's second law of diffusion for extraction in liquid CO<sub>2</sub> and traditional heat treatment in an oven at 200°C. It was found that the diffusion constant is approx. 85 times larger in liquid CO<sub>2</sub> compared to heat treatment.

The compatibility between CO<sub>2</sub> and silicone elastomers, and especially the degree of swell, suggests that CO<sub>2</sub> would be a suitable auxiliary solvent for opening the silicone elastomer and assist the impregnation of a non-silicone-compatible guest monomers, and hence for producing IPNs. The free radical polymerization of 2-hydroxyethyl meth-

acrylate (HEMA) in  $\text{scCO}_2$  has been studied. It was found that PHEMA precipitates during the polymerization, resulting in propagating particles which initiate the Trommsdorff effect: an auto-acceleration due to the dramatic decrease in the rate of termination. Due to the excess energy produced during this auto-acceleration a chain-transfer to monomer side-reaction occurs which in turn causes cross-linking and produces insoluble particles. The first step that leads to the production of insoluble particles is the precipitation during polymerization. It is found that if ethanol is applied as co-solvent insoluble particles are no longer produced.

The tacticity of the produced PHEMA in terms of triads and pentads are analyzed by  $^1\text{H-NMR}$  and  $^{13}\text{C-NMR}$ . From analysis of the  $\alpha\text{-CH}_3$  resonance signals from  $^1\text{H-NMR}$  it is found that the produced polymers have approx. 6% isotactic, 37% heterotactic and 57% syndiotactic triads. The carbonyl carbon group gives resonance signals with different chemical shifts sensitive to sequences of tactic pentads. The experimental results are in fairly good agreement with those calculated statistically from Bernoullian and Markov first order statistics. Furthermore, the kinetics of the free radical polymerization of HEMA in  $\text{scCO}_2$ , where ethylene glycol is applied as co-solvent, are modeled by applying *in-situ* FT-IR online reaction monitoring. It is found that the free radical polymerization follows first order kinetics and occurs at steady state, i.e. the concentration of free radicals is constant over time. The ratio between the rate of propagation and the square root of the rate of termination ( $\frac{k_p}{\sqrt{k_t}}$ ) has been estimated to  $0.23 \frac{1}{\sqrt{\text{M s}}}$ .

It is found that the hydrophilicity of silicone elastomers can be increased by producing IPNs with PHEMA as guest polymer. The measured contact angles with water in ambient air of  $65\text{--}85^\circ$  for the produced IPNs are comparable with that of a existing contact lens on the market of  $72^\circ$ . However, the IPNs' ability to make a water film on the surface is not good enough, and the obtained effects are not sufficient for the produced IPNs to be used as contact lens material. This might be due to too little impregnation of the hydrophilic monomer and hence formation of a sea-island morphology. This is supported by the low or non-existing water uptake of the produced IPNs. The fact that PHEMA is present inside the IPNs is known because they are opaque. It is the outlook to increase the amount of impregnated guest monomer to get a nodular morphology and hence a higher water uptake. The amount of impregnated guest monomer may be increased by increasing the concentration of HEMA in the system and impregnation time, however, some effect may also be obtained by applying experimental parameters where the degree of swell in silicone elastomer in  $\text{CO}_2$  is larger, i.e. liquid  $\text{CO}_2$ .

The combined results obtained by repeated FT-IR analyzes over night, XPS of IPNs with PHEMA and poly(butyl acrylate) (PBMA) as guest polymers and FIB-SEM of an IPN with PHEMA containing 40% cross-linker suggest a self-assembly of the molecules in the IPNs, exposing the hydrophobic silicone to the surface and the hydrophilic PHEMA inside the IPN, even when high amounts of cross-linker are applied. FT-IR analyzes suggest that this self-assembly is to some extent reversible. PHEMA can be exposed to the surface by placing the IPNs in saline solution. However since PHEMA is cross-linked inside the silicone elastomer the amount of PHEMA that can diffuse to the surface is relative low. The amount of PHEMA on the surface may therefore be increased by making the IPNs in a solvent that is more compatible with PHEMA than  $\text{scCO}_2$ , i.e. in a polar solvent. This is supported by the obtained results from XPS. When BMA is applied as guest monomer, more PBMA is present on the surface of the produced IPNs.

The produced IPNs with PHEMA are opaque, because the difference between the refractive index (RI) of the silicone elastomer and PHEMA is too large. The RI of the

guest polymer can be altered by making copolymers. A suitable comonomer that fulfills the requirements to RI and reactivity with HEMA has been identified: heptafluorobutyl acrylate (HFBA). Experiments have shown that it is possible to make copolymers with a RI similar to that of silicone elastomer and produce transparent IPNs. It is found that the RI of the produced guest polymer does not have to equal that of the substrate material, but being in the vicinity is enough. Therefore, the possibility of increasing the RI of silicone elastomer by incorporating phenyl group on the side chains should be examined.



# Appendices



## Appendix A

# Phase diagram for carbon dioxide

This appendix describes the thermodynamics to describe the phase behavior of carbon dioxide and the how to make the phase diagram. When a system at constant pressure ( $P$ ) and temperature ( $T$ ) has reached equilibrium, the molar Gibbs free energy ( $G$ ) for the two phases, say  $\alpha$  and  $\beta$ , are equal. This is mathematically given by equation (A.1) and (A.2):[39]

$$G_\alpha = G_\beta \quad (\text{A.1})$$

$$\partial G_\alpha = \partial G_\beta \quad (\text{A.2})$$

The dependence of  $P$  and  $T$  on  $\partial G$  can be described on the basis of the definition of  $G$ , which is given by equation (A.3) and (A.4):

$$G = H - TS \quad (\text{A.3})$$

$$\Downarrow$$
$$\partial G = \partial H - T\partial S - S\partial T \quad (\text{A.4})$$

where  $S$  is the entropy, and  $H$  is the enthalpy given by equation (A.5):

$$H = U - PV_m \quad (\text{A.5})$$

$$\Downarrow$$
$$\partial H = \partial U - P\partial V_m - V_m\partial P \quad (\text{A.6})$$

where,  $V_m$  is the molar volume, and  $U$  is the internal energy.  $dU$  is according to the first rule of thermodynamics given by equation (A.7):

$$\partial U = \partial q + \partial w \quad (\text{A.7})$$

$$\Downarrow$$
$$\partial U = \partial q - P\partial V_m \quad (\text{A.8})$$

where  $\partial q$  is the heat exchange between the system and the surroundings, and  $\partial w$  is the work done by the system on the surroundings. For a reversible process  $\partial q$  equals  $T\partial S$ . Substituting this into equation (A.6) gives equation (A.9):

$$\begin{aligned}\partial H &= T\partial S - P\partial V_m + P\partial V_m + V_m\partial P \\ &= T\partial S + V_m\partial P\end{aligned}\quad (\text{A.9})$$

Substituting equation (A.9) into equation (A.4) gives equation (A.10):

$$\partial G = V_m\partial P - S\partial T \quad (\text{A.10})$$

If equation (A.10) is applied to the equilibrium condition described in equation (A.2) the system may be described by equation (A.11):

$$\begin{aligned}\partial \bar{G}_\alpha &= \bar{V}_{m\alpha}\partial \bar{P} - \bar{S}_\alpha\partial T = \partial \bar{G}_\beta = \bar{V}_{m\beta}\partial \bar{P} - \bar{S}_\beta\partial T \\ \Downarrow \\ \frac{\partial P}{\partial T} &= \frac{\Delta \bar{S}}{\Delta \bar{V}_m}\end{aligned}\quad (\text{A.11})$$

where  $\Delta \bar{S}$  and  $\Delta \bar{V}_m$  are the change in molar entropy and molar volume respectively for the  $\alpha\beta$ -phase transition. At equilibrium  $\Delta G = 0 \Rightarrow \Delta \bar{S} = \frac{\Delta \bar{H}}{T}$ , inserting this in equation (A.11) gives equation (A.12):

$$\frac{\partial P}{\partial T} = \frac{\Delta \bar{H}}{T\Delta \bar{V}_m} \quad (\text{A.12})$$

where  $T$  is the phase transition temperature. Equation (A.12) is known as the Clapeyron equation and applies to fusion, vaporizing, and sublimation. To produce the phase diagram the change in molar enthalpy and molar volume for the process ( $\Delta \bar{H}$  and  $\Delta \bar{V}_m$ ) are needed as functions of temperature.

For the **vaporization and sublimation** processes the molar volume of the vaporized phase is much larger than that of the condensed phase ( $\bar{V}_{m\text{vap}} \gg \bar{V}_{m\text{con}}$ ), hence  $\Delta \bar{V}_m \approx \bar{V}_{m\text{vap}}$ . Furthermore if ideal gas behavior is assumed, equation (A.12) is given by equation (A.13), the Clausius-Clapeyron equation:

$$\begin{aligned}\frac{\partial P}{\partial T} &= \frac{P\Delta \bar{H}}{RT^2} \\ \Downarrow \\ \partial \ln P &= \frac{\Delta \bar{H}\partial T}{RT^2}\end{aligned}\quad (\text{A.13})$$

where  $R$  is the gas constant. Integrating between the limits ( $P_1, P_2$  and  $T_1, T_2$ ) gives equation (A.15):

$$\begin{aligned}\ln \frac{P_2}{P_1} &= \frac{\Delta \bar{H}}{R} \frac{T_2 - T_1}{T_1 \cdot T_2} \\ \Downarrow \\ P_2 &= P_1 \cdot \exp \left[ -\frac{\Delta H_{\text{vap}}}{R} \cdot \left( \frac{1}{T_2} - \frac{1}{T_1} \right) \right]\end{aligned}\quad (\text{A.15})$$

Table A.1: Known physical data for CO<sub>2</sub>.

Condition	$P$ [bar]	$T$ [°C]
Critical point	73.8	31.1
Triple point	5.2	-56.6
Standard	1.0	-78

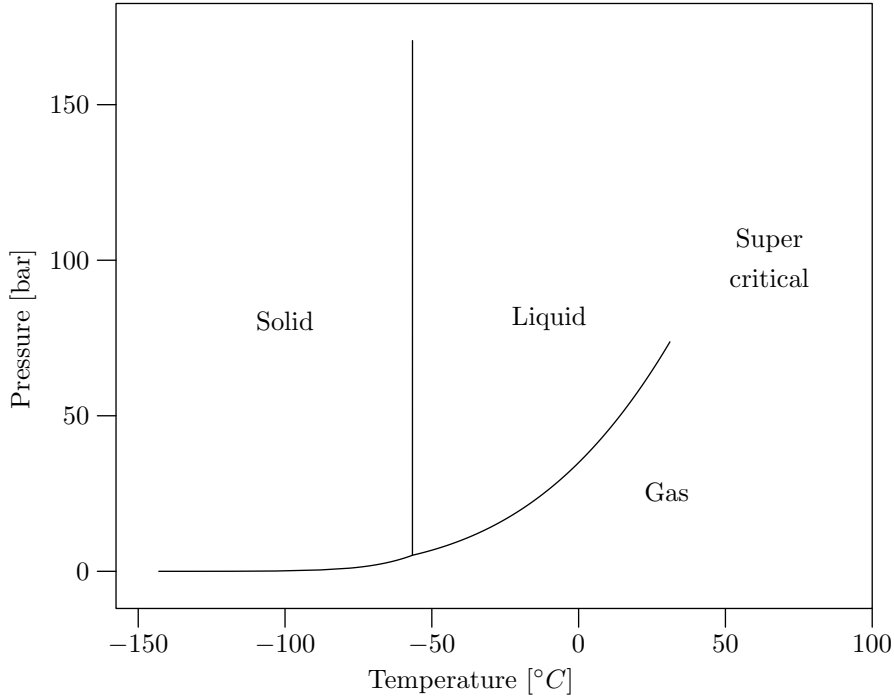


Figure A.1: Phase diagram for CO<sub>2</sub>.

Two points are known on both the vaporization and the sublimation curves, cf. table A.1, and  $\Delta\bar{H}$  can be determined to  $\Delta\bar{H}_{\text{vap}} = 16.6 \frac{\text{kJ}}{\text{mol}}$  and  $\Delta\bar{H}_{\text{sub}} = 26.7 \frac{\text{kJ}}{\text{mol}}$  respectively. It is hereby possible to produce two lines in the phase diagram for CO<sub>2</sub>. This is illustrated in figure A.1.

For the **melting** process equation (A.12) is integrated, this gives equation (A.16):

$$P_2 = P_1 + \frac{\Delta H_{\text{fus}}}{\Delta V_{\text{mfus}}} \cdot \ln \left( \frac{T_2}{T_1} \right) \quad (\text{A.16})$$

Since  $\Delta\bar{H}_{\text{sub}} = \Delta\bar{H}_{\text{fus}} + \Delta\bar{H}_{\text{vap}}$ ,  $\Delta\bar{H}_{\text{fus}}$  can be determined to  $10.1 \frac{\text{kJ}}{\text{mol}}$ . The maximum density it is possible to make in solid CO<sub>2</sub> is  $1.56 \frac{\text{g}}{\text{ml}}$ , hence a molar volume of  $\bar{V}_{\text{ms}} = 0.0282 \frac{\text{L}}{\text{mol}}$ . In article "Compatibility of silicone and carbon dioxide" in chapter 2 the density of liquid CO<sub>2</sub> at  $P = 900 \text{ bar}$  and  $T = -55^\circ\text{C}$  is  $1.30 \frac{\text{g}}{\text{ml}}$ , hence a molar volume of  $\bar{V}_{\text{ml}} = 0.0339 \frac{\text{L}}{\text{mol}}$ . This give a change in molar volume of  $\Delta\bar{V}_m = 0.00573 \frac{\text{L}}{\text{mol}}$ . Due to the small change in molar volume from liquid to solid CO<sub>2</sub> the line in the phase diagram is very steep. This is also shown in figure A.1.



## Appendix B

# Molecular Interaction

To determine the interactions from adhesion between two materials the microscopic molecular interaction forces are described. These forces also give rise to the phenomena cohesion which is the basic idea of solubility parameters. Therefore the thermodynamics supporting the solubility parameter aspect are included.

The interactions between the molecules in a liquid are called the cohesive forces [40]. These forces originate from the Van der Waals forces and are given by dispersion forces, dipole-dipole interactions, dipole-induced dipole interactions, electron donor-acceptor interactions (Lewis acid-base interactions) and hydrogen bonds between the molecules. The attraction interactions are dependent on the intermolecular distance in the power of  $-6$  [41, 42] and are described in the following.

**Dispersion forces:** Dispersions are electrons flickering between different positions creating fluctuations of partial charge [43]. This appears when two instantaneous dipoles correlate their directions, so that a positive partial charge on one molecule will appear close to a negative partial charge on another molecule [44].

**Dipole-dipole interactions:** A dipole originates from the difference in electronegativity. For molecules with more than two atoms the dipole moment is defined as the vector sum of all the dipoles in the molecule [45]. Furthermore these interactions have an orientating effect on molecules, one dipole tending to align the other into energetically favourable arrangements [46].

**Dipole-induced dipole interactions:** An induced dipole is made by the polarization of a molecule (polar or nonpolar) in the vicinity of a polar molecule [46]. In contrast to dispersion and dipole-dipole interactions, dipole-induced dipole interactions are unsymmetrical.

**Electron donor-acceptor interactions (Lewis acid-base interactions):** A Lewis acid is an electron pair acceptor and a Lewis base is an electron pair donor [47]. A Lewis acid-base complex is formed by an overlap between a filled electron orbital of sufficiently high energy in the donor molecule and a vacant empty orbital of sufficiently low energy in the acceptor molecule.

**Hydrogen bonds:** If the molecule contains atoms having higher electronegatives than that of hydrogen (e.g. N, O, and/or F) the molecule has the ability to make hydrogen bonds. This bonding is energetically close to chemical bonds which makes

the interaction strong [45]. The hydrogen bonding is in particular a lewis acid-base complex because the lewis definition of acid and base is an extension of the brønsted definition [46].

The energy required to vaporize a liquid at constant pressure and the energy to isothermal expand the gas phase to infinity equals the energy used to overcome the cohesive forces. The cohesive forces can thus be expressed by equation (B.1) [46].

$$\Delta E_c = \Delta E_{vap} + \Delta E_{inf} \quad (B.1)$$

↓

$$\Delta E_c = \Delta E_{vap} + \int_{V_{sat}}^{\infty} \left( \frac{\partial E}{\partial V_{M,g}} \right)_T dV_{M,g} \quad (B.2)$$

where:

$\Delta E_c$  is cohesive energy [J]

$\Delta E_{vap}$  is vaporization energy [J]

$\Delta E_{inf}$  is energy necessary to expand the saturated gas volume to infinite volume [J]

$V_{sat}$  is volume of the saturated gas [m<sup>3</sup>]

$V_{M,g}$  is molar volume in the gas phase  $\left[ \frac{\text{m}^3}{\text{mol}} \right]$

When one mol of liquid evaporates, the system does work on the surroundings as the gas expands ( $w_g$ ), this work is given by equation (B.3).

$$w_g = -P_{ex} V_{M,g} = -RT \quad (B.3)$$

where:

$P_{ex}$  is the external pressure [Pa]

$T$  is the absolute temperature [K]

$R$  is the gas constant  $\left[ \frac{\text{J}}{\text{mol K}} \right]$

As the liquid evaporates, the volume of the liquid is decreased. This can be regarded as work done on the system by the surroundings ( $w_{li}$ ), this work is given by equation (B.4).

$$w_{li} = P^* V_{M,li} \quad (B.4)$$

where:

$P^*$  is the saturated vapor pressure [Pa]

$V_{M,li}$  is the molar volume of the liquid  $\left[ \frac{\text{m}^3}{\text{mol}} \right]$

The evaporation of liquid results in a change in the enthalpy ( $\Delta H_{vap}$ ) because of the cohesive forces.  $\Delta E_{vap}$  is given by equation (B.5) [45].

$$\begin{aligned} \Delta E_{vap} &= \Delta H_{vap} + w_g + w_{li} \\ \Downarrow \\ \Delta E_{vap} &= \Delta H_{vap} - RT + P^* V_{M,li} \end{aligned} \quad (B.5)$$

For an isothermal expansion of an ideal gas  $\Delta E_{inf}$  is zero. This may not be the case for real gases because cohesive forces can still exist in the gas phase, i.e. there is an increase in  $\Delta H_{inf}$ . On basis of  $\Delta H_{inf}$ , equation (B.2), (B.4) and (B.5) can be subdivided into equation (B.6) [46].

$$\Delta E_c = \Delta H_{vap} - RT + P^* V_M + \Delta H_{inf} \quad (B.6)$$

At temperatures below the boiling point  $\Delta H_{inf} + P^*V_M \ll \Delta H_{vap} - RT$ . Hence  $\Delta H_{inf}$  and  $P^*V_M$  can be neglected and equation (B.6) leads to equation (B.7).

$$\Delta E_c = \Delta H_{vap} - RT \quad (\text{B.7})$$

This approximation is only valid if the external pressure is not too high. The consequence of a too high external pressure is that the calculated  $\Delta E_c$  becomes negative, e.g. at the critical point  $\Delta H_{vap}$  becomes zero. This is unacceptable because equation (B.6) indicates that  $\Delta E_c$  is positive.

Dividing  $\Delta E_c$  with  $V_M$  gives the cohesive energy density ( $c$ ) which is given by equation (B.8).

$$c_c = \frac{\Delta E_c}{V_M} = \delta_c^2 \quad (\text{B.8})$$

where:

$\delta_c$  is the total solubility parameter also called the Hildebrand solubility parameter  $\left[ \sqrt{\frac{\text{J}}{\text{cm}^3}} \right]$

The exchange energy density ( $A^{AB}$ ) is the change of the cohesive energy density associated with the mixing process of compound  $A$  and  $B$  [46].  $A^{AB}$  is given by equation (B.9).

$$A^{AB} = c^A + c^B - 2c^{AB} \quad (\text{B.9})$$

As indicated in equation (B.8)  $c$  can be described by the solubility parameters ( $\delta$ ). In the beginning of this chapter different cohesive forces and interactions have been described and  $c$  for the different interactions are given in equation (B.10) to (B.14) [46].

$$c_d = \delta_d^2 \quad (\text{B.10})$$

$$c_p = \delta_p^2 \quad (\text{B.11})$$

$$c_i = 2\delta_i\delta_d \quad (\text{B.12})$$

$$c_l = 2\delta_a\delta_b \quad (\text{B.13})$$

$$c_h = 2\delta_a\delta_b \quad (\text{B.14})$$

where the subscripts  $d$ ,  $p$ ,  $i$ ,  $l$ ,  $a$ ,  $b$  and  $h$  refer to dispersion, dipole-dipole, dipole-induced dipole, electron pair donor and acceptor, electron pair acceptor, electron pair donor and hydrogen bonding respectively.

For dispersion and dipole-dipole interactions  $c^{AB}$  is given by equation (B.15) and for dipole-induced dipole, Lewis acid-base and hydrogen bonding interactions  $c^{AB}$  is given by equation (B.15).

$$c^{AB} = \sqrt{c^A c^B} = \delta_i^A \delta_d^B + \delta_i^B \delta_d^A \quad (\text{B.15})$$

The reason for this difference is that for dispersion and dipole-dipole interactions the interaction forces of the two molecules is of the same mechanism and for dipole-induced dipole, Lewis acid-base and hydrogen bonding interactions the contribution is of different type, e.g. for dipole-induced dipole there is a difference in the contribution from the molecule with the permanent dipole compared to that of the molecule with the induced dipole [46].

Applying equation (B.9) to these interactions gives equation (B.16), (B.17), (B.18), (B.19) and (B.20) for the dispersion, dipole-dipole, dipole-induced dipole, Lewis acid-base and hydrogen bonding interactions respectively [46].

$$A_d^{AB} = (\delta_d^A - \delta_d^B)^2 \quad (\text{B.16})$$

$$A_p^{AB} = (\delta_p^A - \delta_p^B)^2 \quad (\text{B.17})$$

$$A_i^{AB} = 2(\delta_d^A - \delta_d^B)(\delta_i^A - \delta_i^B) \quad (\text{B.18})$$

$$A_l^{AB} = 2(\delta_a^A - \delta_a^B)(\delta_b^A - \delta_b^B) \quad (\text{B.19})$$

$$A_h^{AB} = 2(\delta_a^A - \delta_a^B)(\delta_b^A - \delta_b^B) \quad (\text{B.20})$$

It is seen from equation (B.19) and (B.20) that hydrogen bonding interactions are described by the Lewis acid-base interaction contribution. The reason for this is that the hydrogen bonding interactions are a particular type of Lewis acid-base interaction [46].

One of the assumptions central to the cohesion approach to interactions is that the various contributions are additive.  $A^{AB}$  is thereby given by equation (B.21) [46].

$$\begin{aligned} A_c^{AB} &= A_d^{AB} + A_p^{AB} + A_i^{AB} + A_{ab}^{AB} \\ &= (\delta_c^A)^2 + (\delta_c^B)^2 - 2\delta_d^A\delta_d^B - 2\delta_p^A\delta_p^B - 2\delta_i^A\delta_d^B - 2\delta_i^B\delta_d^A - 2\delta_a^A\delta_b^B \\ &\quad - 2\delta_a^B\delta_b^A \end{aligned} \quad (\text{B.21})$$

where  $\delta_c^2$  is given by equation (B.22) [46].

$$(\delta_c^A)^2 = (\delta_d^A)^2 + (\delta_p^A)^2 + 2\delta_i^A\delta_d^A + 2\delta_a^A\delta_b^A \quad (\text{B.22})$$

This interaction model can be applied to determine the miscibility of two or more compounds. Different approaches to this model has been taken resulting in different solubility systems. The main difference between these models is the types of interaction forces that are included in the system. Equation (B.22) is the basis for the different cohesion approaches.

## B.1 Solubility parameters

Solubility parameters give a systematic estimate for the compatibility between two compounds. These can be solvents as well as polymers. The basic idea of the parameters is that the cohesive energy is equal to the energy needed for vaporization. This energy is included in different interaction parameters such as for instance polar and non polar contributions. The solubility parameters do not encounter geometric aspects such as size and structure. These are important too and in general smaller  $V_m$  compounds are better solvents than compounds with larger ones. Solubility parameters for polymers do not change much with temperature where as those for liquids change rapidly [48].

### B.1.1 Hansen solubility parameters

Taking basis in equation (B.22) Hansen has ignored the dipole-induced dipole parameter ( $\delta_i$ ) because it does not improve significantly the solubility predictions.  $\delta_a$  and  $\delta_b$  are combined in a hydrogen bonding parameter  $\delta_h$ . This gives equation (B.23)[46].

$$\delta_c^2 = \delta_d^2 + \delta_p^2 + \delta_h^2 \quad (\text{B.23})$$

### B.1.1.1 Theoretical estimation of Hansen solubility parameters

Obtaining HSP can be done in three different ways, either by literature [46, 48], theoretically by group contribution calculations or experimentally by mixing the compound with different solvents.

Estimating HSP can theoretically be done by using a method based on chemical structure instead of estimating the parameters directly from the physical properties. The experience with the group contribution method is that reliable results are obtained for practical purposes when the molecules are simple and only contain one functional group [46].

When estimating HSP from knowledge about the chemical structure of a compound it is assumed that the contributions from the chemical groups are additive, i.e. if the structure of a compound is known, HSP can be calculated from tabulated group contribution values and from the molar volume of the compound.

$\delta_d$  can be estimated from equation (B.24) [46].

$$\delta_d = \frac{\sum_n F_{d,n}}{V_M} \quad (\text{B.24})$$

where:

$F_{d,n}$  is the  $n$ th group molar dispersion attraction constant listed in table B.1  $\left[ \sqrt{\frac{\text{Jcm}^3}{\text{mol}}} \right]$

$\delta_p$  can be estimated from equation (B.25) [46].

$$\delta_p = \frac{\sqrt{\sum_n (F_{p,n})^2}}{V_M} \quad (\text{B.25})$$

where:

$F_{p,n}$  is the  $n$ th group molar dipole-dipole attraction constant listed in table B.1  $\left[ \sqrt{\frac{\text{Jcm}^3}{\text{mol}}} \right]$

When more than one polar group is present, equation (B.25) must be corrected for the interaction of polar groups according to planes of symmetry. Hence if two identical polar groups are present in symmetrical positions,  $\delta_p$  calculated in equation (B.25) must be reduced by multiplying with a symmetry factor.

- 0.5 for one plane of symmetry.
- 0.25 for two planes of symmetry.
- 0 for more planes of symmetry.

$\delta_h$  can be estimated from equation (B.26) [46].

$$\delta_h = \sqrt{\sum_n \left( -\frac{E_{h,n}}{V_M} \right)} \quad (\text{B.26})$$

where:

$E_{h,n}$  is the contribution of hydrogen bonds to the molar cohesive energy listed in table B.1  $\left[ \sqrt{\frac{\text{J}}{\text{mol}}} \right]$

The values for  $F_{d,n}$ ,  $F_{p,n}$  and  $E_{h,n}$  are determined by homomorphology [46].

The group contribution values that have to be applied for the HSP and Hoy solubility approach respectively are listed in table B.1 [46].

Table B.1: Group contribution values for HSP and Hoy.

Group	HSP $F_d$ $\left[\frac{\sqrt{\text{J cm}^3}}{\text{mol}}\right]$	HSP $F_p$ $\left[\frac{\sqrt{\text{J cm}^3}}{\text{mol}}\right]$	HSP $E_h$ $\left[\sqrt{\frac{\text{J}}{\text{mol}}}\right]$	Hoy $F_c$ $\left[\frac{\sqrt{\text{J cm}^3}}{\text{mol}}\right]$	Hoy $F_p$ $\left[\frac{\sqrt{\text{J cm}^3}}{\text{mol}}\right]$	Hoy $^zV'$ $\left[\frac{\text{cm}^3}{\text{mol}}\right]$
-CH <sub>3</sub>	415.5	0.0	0.0	303.4	0.0	21.548
-CH <sub>2</sub> -	277.0	0.0	0.0	269.0	0.0	15.553
>CH-	92.0	0.0	0.0	175.9	0.0	9.557
>C<	-70.0	0.0	0.0	65.5	0.0	3.532
=CH <sub>2</sub>	400.0	0.0	0.0	258.8	66.9	19.173
=CH-	200.0	0.0	0.0	248.5	59.5	13.178
=C<	70.0	0.0	0.0	172.8	63.0	7.183
-O-	100.0	405.0	3900.0	235.2	216.0	6.462
>C=O	290.0	785.0	2650.0	538.0	525.7	17.265
-COO-	392.5	500.0	6100.0	668.1	524.1	23.728
-CHO	470.0	800.0	4500.0	598.6	531.6	23.261
-COOH	419.5	435.0	10750.0	564.8	415.6	26.102
-C=N	438.0	1085.0	2300.0	725.3	724.5	23.066
-S-	447.0	362.0	0.0	428.3	428.3	18.044
NO <sub>2</sub>	470.0	1045.0	1600.0	-	-	-
-NH <sub>2</sub>	280.0	610.0	7000.0	463.5	463.5	17.012
-NH-	151.5	207.5	3100.0	368.2	368.2	11.017
>N-	20.0	800.0	5000.0	125.0	125.0	12.569
PO <sub>4</sub>	740.0	1890.0	13000.0	-	-	-
-OH	206.0	505.0	19750.0	579.9	579.9	12.457
Ring6	1620.0	0.0	0.0	-48.0	61.0	-
Phenyl	1470.0	110.0	0.0	-	-	-
-Cl	450.0	580.0	400.0	422.8	310.9	19.504
-Br	550.0	610.0	2100.0	527.5	112.7	25.305
-I	650.0	665.0	4000.0	-	-	-
-F	220.0	460.0	0.0	84.5	73.2	11.200

### B.1.1.2 Experimental estimation of Hansen solubility parameters

The experimental approach to estimate HSP are thoroughly described in the article "Compatibility of silicone and carbon dioxide" in chapter 2. Based on 452 polymers with known HSP and  $Ra$  the average  $Ra$  is  $10.19 \sqrt{\text{MPa}}$  with a standard deviation of  $4.66 \sqrt{\text{MPa}}$ . As a rule of thumb a solvent is therefore assumed theoretically to dissolve the considered compound if  $Ra$  is less than approx.  $10 - 15 \sqrt{\text{MPa}}$ . In practice, however, this value is dependent on the molecular size and shape of both the solvent and the compound. Solvents with a low molecular weight ( $M$ ) have a greater ability to dissolve compounds than solvents with higher molecular weights with the same HSP.[48] In this work however, the Flory-Huggins model to determine miscibility is applied.

### B.1.2 Hoy's solubility parameters

In this section Hoy's approach to solubility parameters is described. Like Hansen, Hoy is considering dispersion forces, dipole-dipole interactions and hydrogen bonding interactions [46].

The value of the solubility parameters is determined by evaluating  $\delta_c$ . Then the aggregation number ( $\alpha_{agg}$ ) is determined according to equation (B.27).

$$\log(\alpha_{agg}) = 3.39066 \frac{T_b}{T_c} - 0.15848 - \log V_M \quad (\text{B.27})$$

where:

$T_b$  is the boiling point temperature [K]

$T_c$  is the critical temperature [K]

The ratio  $\frac{T_b}{T_c}$  may be estimated from equation (B.28).

$$\frac{T_b}{T_c} = 0.567 + \sum_n \Delta_{T,n} - \left( \sum_n \Delta_{T,n} \right)^2 \quad (\text{B.28})$$

where:

$\Delta_T$  is the critical temperature Lyderson group constant

Then  $\delta_h$  is given by equation (B.29).

$$\delta_h = \delta_c \sqrt{\frac{\alpha_{agg} - 1}{\alpha_{agg}}} \quad (\text{B.29})$$

Then  $\delta_p$  is given by equation (B.30).

$$\delta_p = \delta_c \sqrt{\frac{\sum_n F_{p,n}}{\alpha_{agg} \sum_n F_{c,n}}} \quad (\text{B.30})$$

where:

$F_c$  and  $F_p$  are Hoys group molar contributions  $\left[ \frac{\sqrt{\text{Jcm}^3}}{\text{mol}} \right]$  listed in table B.1

$\delta_d$  is given by equation (B.31).

$$\delta_d = \delta_c - \delta_p - \delta_h \quad (\text{B.31})$$

( $\delta_d$ ) for Hoy being evaluated by difference, may be considered less reliable than those of Hansen, which are evaluated directly by homomorph methods [46].

### B.1.3 Beerbower, Martin and Wu solubility parameters

Equation (B.22) is usually not applied because of its complexity (5 components). Beerbower, Martin and Wu (BMW) have developed an intermediate system (4 components). As in the Hansen approach the dipole-induced dipole parameters are ignored because they are not improving significantly the solubility predictions. Applying equation (B.22)  $\delta_c$  is given by equation (B.32) [46].

$$\begin{aligned} \delta_c^2 &= \delta_d^2 + \delta_p^2 + 2\delta_a\delta_b \\ \Downarrow \\ \delta_c^2 &= \delta_d^2 + \delta_p^2 + 2\delta_a\delta_b \end{aligned} \quad (\text{B.32})$$

The values for  $\delta_d$  and  $\delta_p$  are based on HSP.  $\delta_b$  can be determined from a spectroscopic proton-accepting parameter  $\beta$ .  $\delta_a$  is calculated from equation (B.32) [46]. The BMW approach is not used because of the lack of known parameters, i.e. not enough solvents have been tested by this method.

## Appendix C

### List of abbreviations

Table C.1: List of abbreviations

Code	Description	Unit
[HEMA]	Concentration of HEMA	[M]
[HFBA]	Concentration of HFBA	[M]
[I]	Initiator concentration	[M]
[M]	Monomer concentration	[M]
$[M]_t$	Concentration of monomer at time $t$	[M]
$\partial$	Partial derivative	[—]
$\partial[\text{HEMA}]$	Momentary molefraction of HEMA in copolymer	[—]
$\partial[\text{HFBA}]$	Momentary molefraction of HFBA in copolymer	[—]
$\alpha$	Thermal expansion coefficient	[K <sup>-1</sup> ]
$\alpha_{agg}$	Aggregation number	[—]
$a$	Electron pair acceptor	[—]
$A$	Pre-exponential factor	[—]
$A_i$	Data fit for $i$ 'th solvent	[—]
AIBN	2,2'-azobis(isobutyro-nitrile)	[—]
$A^{AB}$	Exchange energy density	[MPa]
$A_{\text{After water}}$	Peak integral in FT-IR	[—]
$A_{\text{Over night}}$	Peak integral in FT-IR	[—]
ATR	Attenuated total reflectance	[—]
ATRP	Atomic transfer free radical polymerization	[—]
$\beta$	Isothermal compressibility coefficient	[bar <sup>-1</sup> ]
$b$	Electron pair donor	[—]

*continues ...*

Table C.1: (continued)

Code	Description	Unit
$b_i$	Function of temperature	[—]
$B$	Bernoulian statistic parameter	[—]
BMA	Butyl methacrylate	[—]
$\chi$	Flory-Huggins interaction parameter	[—]
$c_c$	Cohesive energy density	[MPa]
$c_i$	Constant	[—]
$C$	Pre-exponential factor	[—]
CO <sub>2</sub>	Carbon dioxide	[—]
$C_{t,\text{silicone}}$	Total relative concentration of silicone oil in silicone elastomer at time $t$	[—]
$C_{t,x}$	Relative concentration at time $t$ and place $x$	[—]
$\delta$	Chemical shift	[ppm]
$\delta_c$	Hansen's total cohesive energy parameter	[ $\sqrt{\text{MPa}}$ ]
$\delta_d$	Hansen's dispersion parameter	[ $\sqrt{\text{MPa}}$ ]
$\delta_h$	Hansen's hydrogen bond parameter	[ $\sqrt{\text{MPa}}$ ]
$\delta_p$	Hansen's polar parameter	[ $\sqrt{\text{MPa}}$ ]
$\delta_{\alpha\beta}$	Delta function	[—]
$\Delta E_{\text{inf}}$	Energy necessary to expand a saturated gas volume to infinit volume	[J]
$\Delta E_{\text{vap}}$	Vaporization energy	[J]
$\Delta H_{\text{fus}}$	Enthalpy of melting	[J]
$\Delta H_{\text{sub}}$	Enthalpy of sublimation	[J]
$\Delta H_{\text{vap}}$	Enthalpy of vaporization	[J]
$\Delta T$	Critical temperature Lyderson group constant	[—]
$\Delta V^\ddagger$	Activation volume	[ $\frac{\text{L}}{\text{mol}}$ ]
$d$	Dispersion	[—]
$D$	Diffusion constant	[ $\frac{\text{m}^2}{\text{s}}$ ]
$D_{\text{CO}_2}$	Diffusion constant for silicone oil extraction in liquid CO <sub>2</sub>	[ $\frac{\text{m}^2}{\text{s}}$ ]
$D_{\text{heat}}$	Diffusion constant for silicone oil extraction by heat treatment at 200°C	[ $\frac{\text{m}^2}{\text{s}}$ ]

*continues ...*

Table C.1: (continued)

Code	Description	Unit
DEPDC	Diethyl peroxydicarbonate	[—]
DMF	Dimethyl formamide	[—]
DSC	Differential scanning chromatography	[—]
$\epsilon$	Interaction energy between two segments	[J]
$e$	Polar effect	[—]
$E_a$	Activation energy	$\left[\frac{\text{J}}{\text{mol}}\right]$
$E_{\alpha\beta}$	Deformation gradient tensor	[—]
$E_c$	Total cohesive energy	$\left[\frac{\text{J}}{\text{mol}}\right]$
$E_d$	Dispersion force contribution to cohesive energy	$\left[\frac{\text{J}}{\text{mol}}\right]$
$E_h$	Hydrogen bond contribution to cohesive energy	$\left[\frac{\text{J}}{\text{mol}}\right]$
$E_{h,n}$	Group contribution of hydrogen bond	$\left[\sqrt{\frac{\text{J}}{\text{mol}}}\right]$
$E_p$	Polar force contribution to cohesive energy	$\left[\frac{\text{J}}{\text{mol}}\right]$
Elastosil	Elastosil LR3003/10 shore A silicone	[—]
EoS	Equation of state	[—]
ESR	Electron spin resonance	[—]
$EWC$	Equilibrium water content	[%]
$f$	Initiator efficiency	[—]
$f_m(\phi)$	Free energy of mixing per lattice site	[—]
$F$	Hemholtz free energy	[J]
$F_{d,n}$	Group molar dispersion attraction constant	$\left[\sqrt{\frac{\text{J mL}}{\text{mol}}}\right]$
$F_{el}$	Elastic energy	[J]
$F_m$	Free energy of mixing	[J]
$F_{p,n}$	Group molar dipole-dipole attraction constant	$\left[\sqrt{\frac{\text{J mL}}{\text{mol}}}\right]$
FH	Flory-Huggins	[—]
FIB-SEM	Focused ion beam—scanning electron microscope	[—]
FT-IR	Fourier transform infrared spectroscopy	[—]
$G$	Gibb's free energy	[J]
GPC	Gel permeation chromatography	[—]
h	Heterotactic triad	[—]

*continues ...*

Table C.1: (continued)

Code	Description	Unit
$h$	Hydrogen bonding	[—]
$H$	Enthalpy	[J]
HCR	High consistency rubber	[—]
HEMA	2-hydroxyethyl methacrylate	[—]
HF	Hydrofluoric acid	[—]
HFBA	Heptafluorobutyl acrylate	[—]
HPLC	High performance liquid chromatography	[—]
HSP	Hansen's solubility parameters	[—]
HTV	High temperature vulcanization silicone	[—]
$i$	Isotactic triad	[—]
$i$	Dipole-induced dipole	[—]
$I_0$	Intensity of incident beam of light	[—]
$I_r$	Intensity of reflected beam of light	[—]
Int	Integral	[—]
IPN	Interpenetrating polymer network	[—]
IR	Infrared	[—]
$k$	Constant	[—]
$k_{11}$	Rate constant for homopropagation	$\left[\frac{1}{\text{M s}}\right]$
$k_{12}$	Rate constant for crosspropagation	$\left[\frac{1}{\text{M s}}\right]$
$k_{21}$	Rate constant for crosspropagation	$\left[\frac{1}{\text{M s}}\right]$
$k_{22}$	Rate constant for homopropagation	$\left[\frac{1}{\text{M s}}\right]$
$k_B$	Boltzmann constant	$\left[\frac{\text{J}}{\text{K}}\right]$
$k_d$	Decomposition rate coefficient	$[\text{s}^{-1}]$
$k_p$	Propagation rate coefficient	$\left[\frac{1}{\text{M s}}\right]$
$k_t$	Termination rate coefficient	$\left[\frac{1}{\text{M s}}\right]$
$k_u$	Bulk modulus	[bar]
$\lambda$	Wavelength	[nm]
$l$	Electron pair donor and acceptor	[—]
LSR	Liquid silicone rubber	[—]
$\mu$	Dipole moment	[Debye]

*continues ...*

Table C.1: (continued)

Code	Description	Unit
$m$	Mass	[g]
$m$	Meso diad	[—]
$m_0$	Initial mass	[g]
$m_t$	Mass at time $t$	[g]
$M_n$	Molecular weight by number	[kDa]
MEHQ	Monomethylether hydroquinone	[—]
$v_c$	Volume of lattice site	[L]
$n_c$	Number of partial chains in a gel	[—]
$n_i$	Refractive index of media $i$	[—]
$n_p$	Number of polymer molecules in mixture	[—]
$N$	Number of segments in each polymer molecule	[—]
NA	Not available	[—]
NMR	Nuclear magnetic resonance spectroscopy	[—]
NVP	N-vinyl pyrrolidone	[—]
$\omega_c$	Probability that a given lattice site is an entanglement	[—]
$\Omega$	Total number of lattice sites	[—]
$\phi$	Volume fraction	[—]
$\phi_0$	Initial volume fraction	[—]
$\phi_{0,\text{silicone}}$	Initial silicone oil content in silicone elastomer	[—]
$\phi_{0,\text{HEMA}}$	Initial molefraction of HEMA	[—]
$\phi_{0,\text{HFBA}}$	Initial molefraction of HFBA	[—]
$P$	Pressure	[bar]
$p$	Dipole-dipole	[—]
$P^*$	Saturated vapor pressure	[Pa]
$P_c$	Critical pressure	[bar]
PBMA	Poly(butyl methacrylate)	[—]
PDMS	Poly(dimethyl siloxane)	[—]
PHEMA	Poly(2-hydroxyethyl methacrylate)	[—]
PHEMA(EtGly)	PHEMA produced with ethylene glycol as cosolvent	[—]
PHEMA(EtOH)	PHEMA produced with ethanol as cosolvent	[—]
PHFBA	Poly(heptafluorobutyl acrylate)	[—]

*continues ...*

Table C.1: (continued)

Code	Description	Unit
PLP	Pulsed laser polymerization	[—]
PMMA	Poly(methyl methacrylate)	[—]
PMAA	Poly(methacrylic acid)	[—]
PVP	Poly(N-vinyl pyrrolidone)	[—]
PVT	Pressure volume temperature	[—]
$\partial q$	Heat exchange energy	[J]
$Q$	Intrinsic reactivity	[—]
$\rho$	Density	$\left[\frac{\text{g}}{\text{mL}}\right]$
$\rho'$	Reduced density	[—]
$r$	Racemic diad	[—]
$r_1$	Reactive ratio	[—]
$r_2$	Reactive ratio	[—]
$R$	Gas constant	$\left[\frac{\text{J}}{\text{mol K}}\right]$
$R_p$	Rate of polymerization	$\left[\frac{\text{M}}{\text{s}}\right]$
$R$	Radius in solubility sphere	$\left[\sqrt{\text{MPa}}\right]$
$R_a$	Solubility parameter distance between two materials	$\left[\sqrt{\text{MPa}}\right]$
RI	Refractive index	[—]
RMSE	Root mean square error	[—]
RTV	Room temperature vulcanization silicone	[—]
$\sigma$	Probability for meso diad	[—]
$s$	Syndiotactic triad	[—]
$S$	Entropy	$\left[\frac{\text{J}}{\text{K}}\right]$
scCO <sub>2</sub>	Supercritical carbon dioxide	[—]
SEC	Size exclusion chromatography	[—]
SG	Solubility grade	[—]
SP-PLP	Single pulsed—pulsed laser polymerization	[—]
$\theta$	Contact angle with water in ambient air	[°]
$t$	Time	[s]
$t_{\text{poly}}$	Polymerization time	[h:min]
$T'$	Reduced temperature	[—]

*continues ...*

Table C.1: (continued)

Code	Description	Unit
$T$	Temperature	[K]
$T_b$	Boiling temperature	[K]
$T_c$	Critical temperature	[K]
$T_g$	Glass transition temperature	[K]
$T_m$	Melting point	[K]
TLV	Threshold limit value	[ppm]
TTT	1,3,5-triallyl-1,3,5-triazine-2,4,6(1H,3H,5H)-trione	[—]
$u$	probability that a meso diad is followed by a racemic diad	[—]
$U$	Internal energy	[J]
UV	Ultraviolet	[—]
$\epsilon$	dielectric constant	[—]
$V$	Volume	[L]
$V_0$	Initial volume	[L]
$V_m$	Molar volume	$\left[\frac{\text{L}}{\text{mol}}\right]$
$V_{\text{sat}}$	Volume of saturated gas	[L]
$w$	Probability that a racemic diad is followed by a meso diad	[—]
$\partial w$	Work	[J]
WCA	Water contact angle	[—]
$x$	Distance	[m]
XPS	X-ray photoelectron spectroscopy	[—]
$z$	Lattice coordination number	[—]
$Z$	Parameter in EoS	[—]



# Bibliography

- [1] J. Karthausser. A method of producing an interpenetrating polymer network (ipn), the ipn and use thereof. *Patent*, WO2005/003237:1–35, 2005.
- [2] Joachim Karthausser, Maïke Benter, and Martin Alm. A method of producing a silicone rubber item and the product obtainable by the method. *Patent*, WO 2006/045320 A2:1–32, 2006.
- [3] Maïke Benter and Martin Alm. A method of coating a polymer surface with a polymer containing coating and an item comprising a polymer coated polymer. *Patent*, WO 2006/074666 A2:1–27, 2006.
- [4] Martin Alm, Maïke Benter, and Anne Marie Jensen. A method of producing an article comprising an interpenetrating polymer network (ipn) and an article comprising an ipn: I. *Patent*, Filed:1–32, 2006.
- [5] Martin Alm, Maïke Benter, and Anne Marie Jensen. A method of producing an article comprising an interpenetrating polymer network (ipn) and an article comprising an ipn: Ii. *Patent*, Filed:1–32, 2006.
- [6] Martin Alm. Compatibility between silicone and carbon dioxide. *Submitted to Journal of Supercritical Fluids, Not Published*, xx(xx):xx, 2007.
- [7] Martin Alm, Anne Marie Jensen, Maïke Benter, and Kjeld Schamburg. Free radical polymerization of 2-hydroxyethyl methacrylate in supercritical carbon dioxide. *Submitted to Macromolecules, Not Published*, xx(xx):xx, 2007.
- [8] Martin Alm, Harald Behl, and Kjeld Schamburg. Kinetics of the free radical polymerization of 2-hydroxyethyl methacrylate in supercritical carbon dioxide. *Not yet submitted*, xx(xx):xx, 2007.
- [9] André Colas and Jim Curtis. *Biomaterials science—An introduction to materials in medicine*, chapter Application of materials in medicine, biology, and artificial organs: Medical applications of silicone, pages 697–707. Elsevier Academic Press, 525 B Street, Suite 1900, San Diego, California 92101–4495, USA, 2nd edition, 2004.
- [10] Helmut Steinberger. Introduction to silicones. Lecture on silicones at Nanon’s premises, 2007.
- [11] Albert R. LeBoeuf. Hydrophilic silicone compounds and contact lenses containing polymers thereof. *Patent*, US004294974A, 1981.
- [12] Robert A. Janssen, Ellen M. Ajello, Richard D. Auten, Glenn S. Nomura, and Thomas E. Shank. Process for graft polymerization of surfaces of preformed substrates to modify surface properties. *Patent*, US005805264A, 1998.

## Bibliography

- [13] Douglas G. Vanderlaan, Ivan M. Nunez, and Marcie Hargiss. Silicone hydrogel polymers. *Patent*, US006020445, 2000.
- [14] Iupac. Iupac compendium of chemical terminology. <http://www.iupac.org/goldbook/I03117.pdf>, 2007.
- [15] Malcolm C. Stevens. *Polymer chemistry, an introduction*. Oxford university press, 198 Madison Avenue, New York 10016, 1999.
- [16] J. S. Turner and Y. L. Cheng. Preparation of pdms-pmma interpenetrating polymer network membranes using monomer immersion method. *Macromolecules*, 33:3714–3718, 2000.
- [17] Takashi Miyata, Jun-Ichi Higuchi, Hiroshi Okuno, and Tadashi Uragami. Preparation of polydimethylsiloxane/polystyrene interpenetrating polymer network membranes and permeation of aqueous ethanol solutions through the membranes by pervaporation. *Journal of applied polymer science*, 61:1315–1324, 1996.
- [18] Earth System Research Laboratory. Trends in atmospheric carbon dioxide - global. Internet: <http://www.esrl.noaa.gov/gmd/ccgg/trends/>, May 2007.
- [19] Paul A. Charpentier, Joseph M. DeSimone, and George W. Roberts. Decomposition of polymerisation initiators in supercritical co<sub>2</sub>: a novel approach to reaction kinetics using a cstr. *Chemical Engineering Science*, 55:5341–5349, 2000.
- [20] P. A. Charpentier, J. M. DeSimone, and G. W. Robert. Continuous precipitation polymerization of vinylidene fluoride in supercritical carbon dioxide: Modeling the rate of polymerization. *Industrial and Engineering Chemistry Product Research and Development*, 39(12):4588–4596, 2000.
- [21] Maartje F. Kemmere and Thierry Meyer. *Supercritical carbon dioxide - In polymer reaction engineering*. Wiley-VCH, Weinheim, Germany, 2005.
- [22] J. L. Kendall, D. A. Canelas, J. L. Young, and J. M. DeSimone. Polymerizations in supercritical carbon dioxide. *Chemical Review*, 99(2):543–564, 1999.
- [23] Eric J. Beckman. Supercritical and near-critical co<sub>2</sub> in green chemical synthesis and processing. *Journal of Supercritical Fluids*, 28:121–191, 2004.
- [24] Andrew I. Cooper. Polymer synthesis and processing using supercritical carbon dioxide. *Journal of Materials Chemistry*, 10:207–234, 2000.
- [25] Feng-Hsin Huang, Meng-Hui Li, Lloyd L. Lee, Kenneth E. Starling, and Frank T. H. Chung. An accurate equation of state for carbon dioxide. *Journal of Chemical Engineering of Japan*, 18(6):490–496, 1985.
- [26] Masao Doi. *Introduction to polymer physics*. Oxford science publications, Great Clarendon Street, Oxford ox2 6dp, New York, 2004.
- [27] WackerSilicones. Processing elastosil lr liquid silicone rubber. <http://www.wacker.com>, Hanns-Seidel-Platz 4, 81737 München, Germany, 2006.

## Bibliography

- [28] J. Crank and G. S. Park. *Diffusion in polymers*. Academic press inc., Berkeley Square House, Berkeley Square, London, 1968.
- [29] Zhibin Guan, J. R. Combes, Y. Z. Menciloglu, and J. M. DeSimone. Homogeneous free radical polymerizations in supercritical carbon dioxide: 2. thermal decomposition of 2,2'-azobis(isobutyronitrile). *Macromolecules*, 26:2663–2669, 1993.
- [30] William Z. Xu, Xinsheng Li, and Paul A. Charpentier. *insitu* atr-ft-ir study of the thermal decomposition of diethyl peroxydicarbonate in supercritical carbon dioxide. *Polymer*, 48:1219–1228, 2007.
- [31] Roland Fromme. Meeting between nanon and woehlk. Oral meeting, January 2006.
- [32] Hamerlik. List of 170 most popular contact lenses according to oxygen permeability values. [http://www.hamerlik.com/lens/contact\\_lenses\\_permeability.html](http://www.hamerlik.com/lens/contact_lenses_permeability.html), 2007.
- [33] Douglas A. Skoog, F. James Holler, and Timothy A. Nieman. *Principles of instrumental analysis*. Saunders College Publishing, London, 1998.
- [34] Franck R. Mayo and Frederick M. Lewis. Copolymerization. i. a basis for comparing the behavior of monomers in copolymerization; the copolymerization of styrene and methyl methacrylate. *Journal of the American Chemical Society*, 66:1594–1601, 1944.
- [35] Krzysztof Matyaszewski and Thomas P. Davis. *Handbook of radical polymerization*. Wiley-Interscience, John Wiley and sons, 605 third avenue, New York, USA, first edition, 2002.
- [36] David R. Lide. *Handbook of chemistry and physics*. CRC press, New York, 1997.
- [37] Sabine Beuermann and Michael Buback. *Supercritical carbon dioxide: in polymer reaction engineering*, chapter Kinetics of free-radical polymerization in homogeneous phase of supercritical carbon dioxide, pages 55–80. Wiley-VCH Verlag GmbH & Co. KgaA, Weinheim, Germany, 2005.
- [38] J. Brandrup and E. H. Immergut. *Polymer handbook*. Wiley-Interscience, John Wiley and sons, USA, third edition, 1989.
- [39] Raymond Chang. *Physical chemistry—for the chemical and biological sciences*. University science books, 55D Gate Five Road Sausalito California, 2000. Third edition.
- [40] Duncan J. Shaw. *Introduction to colloid and surface chemistry*. Butterworth-Heinemann, Linacre House Jordan Hill Oxford OX2 8DP, 1999.
- [41] Andrew R. Leach. *Molecular modelling - Principles and applications*. Prentice Hall, Edinburgh gate, Harlow, Essex CM20 2JE, England, 1996.
- [42] Lieng-Huang Lee. *Fundamentals of adhesion*. Plenum Pres, 233 Spring Street, New York, N.Y.10013, 1991.
- [43] Loretta Jones and Peter W. Atkins. *Chemistry molecules, matter and change*. Freeman, New York, 1997.
- [44] Peter W. Atkins. *The elements of physical chemistry*. Oxford University press, Walton Street Oxford OX 2 6DP, 1996.

## Bibliography

- [45] Peter W. Atkins. *Physical chemistry*. Oxford University press, Walton Street Oxford OX 2 6DP, 1994.
- [46] Allan F. M. Barton. *Handbook of solubility parameters and other cohesion parameters*. CRC press, Boca Raton Florida 33431, 1991.
- [47] Albert F. Cotton, Geoffrey Wilkinson, and Paul L. Gaus. *Basic inorganic chemistry*. John Wiley and sons, New York, 1995.
- [48] Charles M. Hansen. *Hansen solubility parameters-A users handbook*. CRC press, New York, 2000.